Title
JOSEPHSON JUNCTIONS AS MICROWAVE HETERODYNE DETECTORS

Author
Taur, Yuan.

Publication Date
1974-04-01

JOSEPHSON JUNCTIONS AS MICROWAVE HETERODYNE DETECTORS

Yuan Taur
(Ph.D. thesis)

April 1974

Prepared for the U. S. Atomic Energy Commission
under Contract W-7405-ENG-48

Table of Contents

JOSEPHSON JUNCTIONS AS MICROWAVE HETERODYNE DETECTORS

Yuan Taur

Inorganic Materials Research Division, Lawrence Berkeley Laboratory
and Department of Physics; University of California
Berkeley, California

ABSTRACT

The properties of point contact Josephson junctions operated as 36 GHz heterodyne detectors have been extensively studied. The measured performance is in good agreement with the theory developed for microwave coupling, conversion efficiency, and intrinsic noise based on the Resistively Shunted Junction model. A tunable cavity matching structure was designed to obtain good RF coupling to the point contact. By operating vanadium junctions at 1.4 K, we have achieved a single side band mixer noise temperature of 54 K (referred to the input) with a conversion gain of 1.35 and a signal bandwidth of the order of 1 GHz. This is significantly better than existing resistive mixers in this frequency range. We have also tried harmonic mixing, mixing in the presence of relaxation oscillation, and self local oscillator mixing with Josephson junctions, but the results are not as promising as fundamental mixing with an external local oscillator. Finally, two additional topics are discussed: a Josephson effect homodyne detector, and a proposed design for superconducting bolometers making use of the recently developed superconducting quantum interference devices.

I. INTRODUCTION

In 1962 a theory was developed by B. D. Josephson[1] for tunneling of supercurrents across a junction consisting of two bulk superconductors separated by a thin insulating layer approximately 10 Å thick. It was experimentally demonstrated later that the effects observed in such junctions exist in a variety of physical arrangements which have in common that two bulk superconductors are connected by a small region of weak superconductivity. There are three major kinds of superconducting weak links or Josephson junctions which are important for practical applications: (i) Tunnel junctions,[2] which comprise the geometry for which Josephson derived his original theory. (ii) Point contacts,[3] in which the junction is formed between two superconductors with one of them sharpened to a point. (iii) Constricted thin film bridges,[4,5] consisting of two superconductors connected by a narrow superconducting film with length and width of the order of one micron. It has been suggested that Josephson junctions have very good potential for being sensitive detectors of electromagnetic radiation in the millimeter-wave and far-infrared regions. We shall describe briefly the basic Josephson relations and the principle of detection.

In a bulk superconductor, the conduction electrons condense into a macroscopic quantum state which can be described by an equivalent wavefunction $\psi_o e^{i\phi}$, here $\phi=\phi(r,t)$ is a coherent phase factor which is a function of position and time. If two superconductors with phases

ϕ_1 and ϕ_2 are coupled by a weak link, the first Josephson relation states that the current flowing through the junction is related to the phase difference $\phi=\phi_1-\phi_2$ by

$$I(t) = I_c \sin\phi(t) \tag{1}$$

where I_c is the critical current of the junction determined by the material, temperature, and geometrical structure of the superconducting weak link. The second Josephson relation states that if a voltage V(t) is applied across the junction, the phase difference ϕ will change with time according to the relation

$$\frac{d\phi(t)}{dt} = \frac{2eV(t)}{\hbar} \tag{2}$$

The Josephson current described by Eqs. (1) and (2) arises from the transfer of electron pairs without energy loss from one side of the junction to the other.

To understand the use of Josephson junctions for detection and mixing, let us combine (1) and (2) to obtain a relation between the current through the junction and the voltage across it

$$I(t) = I_c \sin \left[\frac{2e}{\hbar} \int_o^t V(t')dt'\right] \tag{3}$$

This equation defines the characteristic of an ideal Josephson element. The most interesting result predicted by Eq. (3) is that when a constant voltage V_o is applied to the junction, an alternating current will flow at the Josephson frequency $\omega_o = 2eV_o/\hbar$. This means that Josephson junction is an active element which can convert DC power into AC and vice versa.

By differentiating Eq. (3), we can rewrite it in the following form:

$$V(t) = \frac{\hbar/2e}{\sqrt{I_c^{\,2} - I^2(t)}} \frac{dI(t)}{dt} \qquad (4)$$

This is the relation for a lossless inductor with non-linear inductance

$$L_J = \frac{\hbar/2e}{\sqrt{I_c^{\,2} - I^2(t)}} .$$

This kind of characteristic is very useful for high frequency device applications.

There are many different modes to operate Josephson junctions as radiation detectors. Among them are the broadband square law mode,[6] narrow-band regenerative mode,[7] linear heterodyne or homodyne mode,[8] etc. Since it is desirable in many applications to keep the frequency information of the detected signal, we are interested in building a heterodyne system using the non-linearity of Josephson junctions to mix a small signal with an external local oscillator and produce an output at a difference frequency where good quality amlifiers are available. Another possibility is to use the Josephson oscillation as an internal local oscillator, but since the intrinsic noise tends to broaden the linewidth of the Josephson oscillation,[9] this mode of operation is not as useful.

In order for a high frequency device to function efficiently, it must be well-coupled to the signal source. This is a rather difficult problem for Josephson junctions because their impedances are usually much lower than the impedance of the free space (377 ohms). Apart from practical problems, the impedance of a Josephson junction is limited by $R \lesssim \Delta/eI_c$[10] and I_c must be large enough to exceed the intrinsic noise in the junction. Among various kinds of Josephson junctions, we decided to make our device out of point contacts not only because they are easier to prepare and mount but also because their impedances are higher than those of constricted thin film bridges (low resistance) and tunnel junctions (low reactance). The signal frequency at which we operate our point contact junctions is 36 GHz, which was chosen for ease of making accurate microwave measurements.

In this thesis we shall describe the coupling of our point contact Josephson junctions to microwave fields, the conversion efficiency (or gain) of our 36 GHz mixer and its noise properties. All these experimental results are in excellent agreement with the theory.

II. EXPERIMENTAL SET-UP

A. Junction Preparation

1. Junction Material and Fabrication

We have used niobium, tantalum, and vanadium to make point contact Josephson junctions. They were formed by pressing a sharpened superconducting wire against the flat end of another superconducting wire. Both wires have diameters of 0.81 mm and were prepared with No. 600 emery papers. The tip was usually etched for a few seconds in a chemical solution to increase its sharpness. The etching solution for niobium consists of concentrated HNO_3, concentrated HF, and water mixed in equal volumes and the solution for tantalum is a mixture of 5 parts concentrated H_2SO_4, 2 parts concentrated HNO_3, and 2 parts concentrated HF. Vanadium wires were usually not etched. After being rinsed in distilled water and cleaned with acetone, the wires were either set aside in air for several days or heated on a hot plate to 200°C for 30 minutes to form an oxide layer. We also attempted to make junctions without the final oxidization procedure, but in general it was very difficult to adjust these clean wires to form junctions with desired characteristics.

2. Junction Mounting and Adjustment

Our point contact junctions were mounted in the middle of a standard-sized A-band niobium waveguide (0.71 cm × 0.36 cm ID) along the E-field direction as shown in Fig. 1. A clearance hole (diameter 1.32 mm) was drilled on the broad surface of the waveguide to introduce

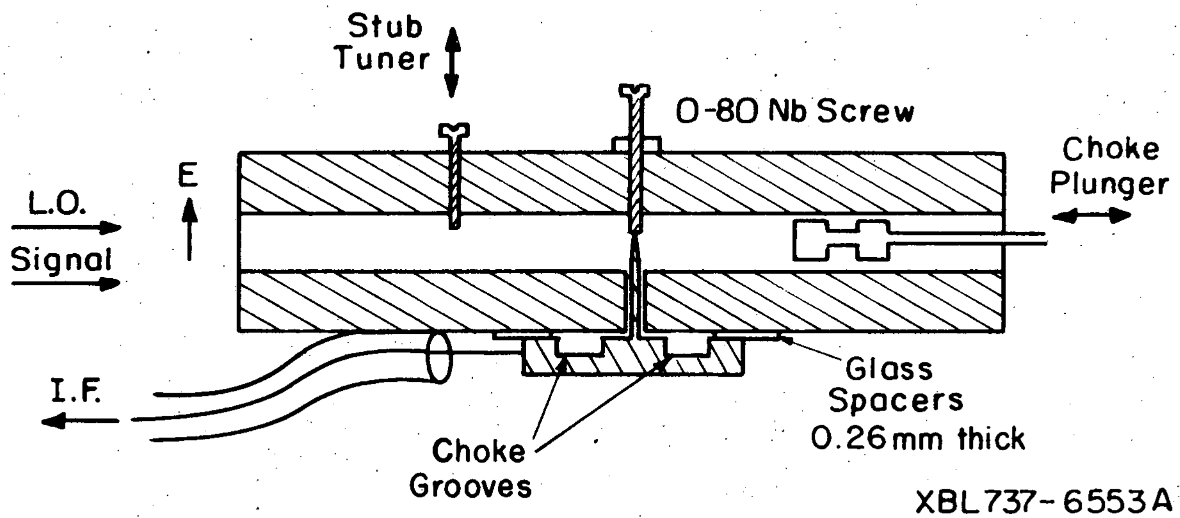

Fig. 1. Niobium waveguide assembly for a 36 GHz Josephson mixer.

the sharpened superconducting wire into the structure. The other end of this wire was threaded (000-120) and screwed into a niobium flange which was DC insulated from the waveguide by 0.25 mm thick glass spacers.

Most of our experiments were done with preadjusted niobium junctions using spacers made from a special glass[11] which has the same thermal expansion coefficient as that of the niobium. By monitoring the resistance on a scope, we were able to adjust the junction at room temperature with a 0-80 niobium screw and locknut, the whole structure was then sealed in helium exchange gas and cooled uniformly to 4.2 K. Junctions with resistance less than 1 ohm can be thermally cycled many times without significant changes in their I-V characteristics. However, high resistance junctions (10-20 ohms) tend to show open circuits when warmed up and need to be readjusted for the next run.

When tantalum or vanadium was used, the junctions were adjusted at liquid helium temperature. This was done by replacing the niobium screw with a 0-80 brass screw driven by a worm gear at the top of the cryostat. The junction was then formed between the tip and a short piece of tantalum or vanadium wire which was threaded (000-120) and screwed into the end of the brass screw. Junctions made this way were mechanically stable and often stayed unchanged for several hours, allowing plenty of time to make electrical measurements.

B. Microwave Circuit

1. Matching Structure

Since the characteristic impedance of a standard waveguide is much larger than that of a typical point contact, some impedance matching structure or cavity arrangement is necessary to achieve the best performance of the junction. For this purpose we put a conventional three-seetion choke plunger behind the junction and a stub tuner $(3/4)\lambda_g$ in front of the junction as shown in Fig. 1. The plunger is adjustable along the waveguide at low temperatures. The stub, which consists of a 000-120 brass screw, could be adjusted up and down by a worm gear when we dealt with preset-type junctions; but when the worm gear was used to adjust the junction, the stub tuner was preset at room temperature with a locknut. The performance of this microwave circuit will be discussed in Section IV and Appendix A.

The niobium waveguide shown in Fig. 1 was connected to the room temperature microwave system via a 90 cm length of stainless steel waveguide which gave 3 dB attenuation of the microwave power. A piece of wedge-shaped Eccosorb FR (Emerson and Cuming) was inserted into the low temperature end of the stainless steel waveguide as shown in Fig. 2 to reduce room temperature blackbody radiation. The attenuation of this cold attenuator was calibrated at liquid helium temperature to be (23 ± 0.5) dB.

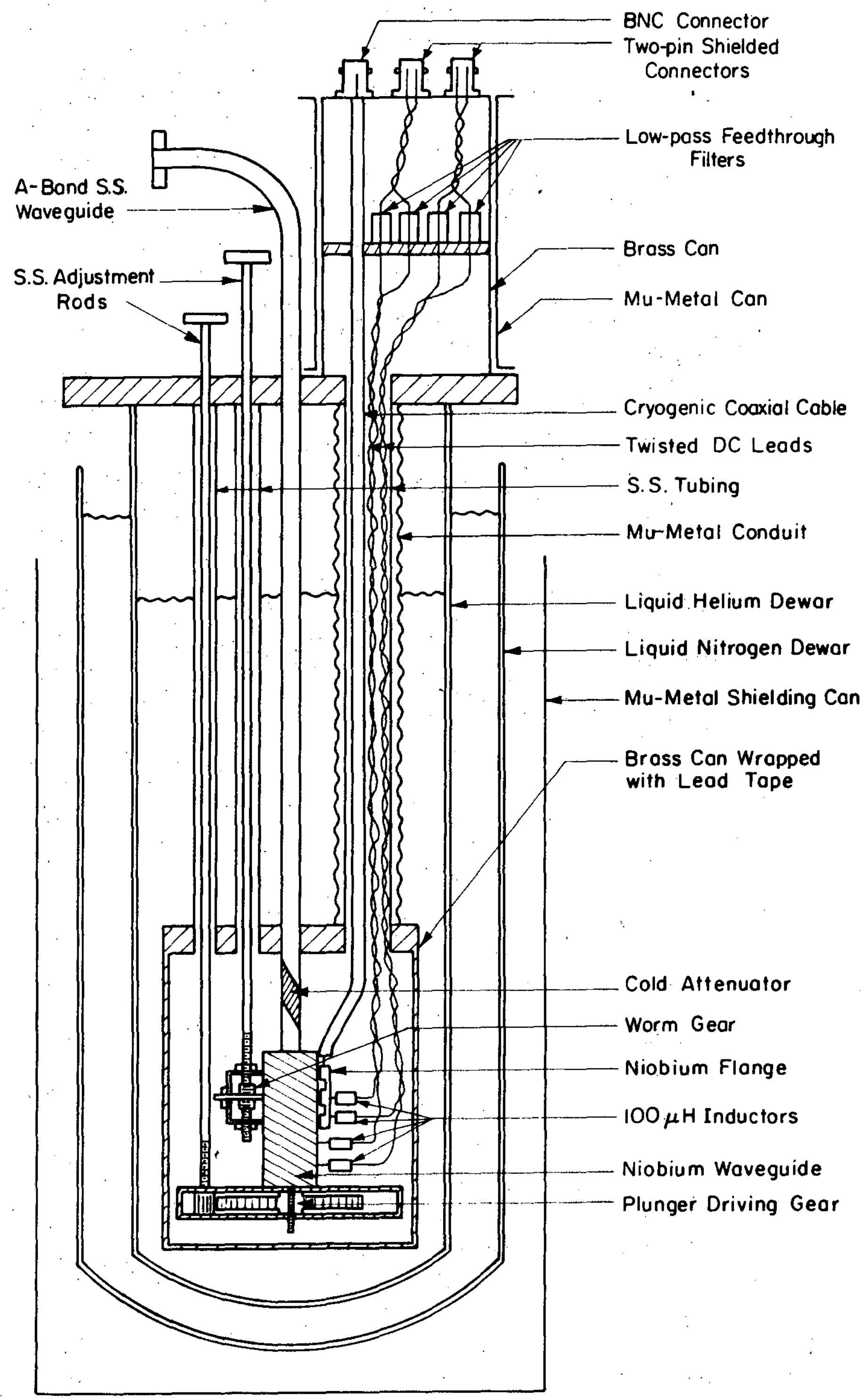

XBL743-5933

Fig. 2. Cross-sectional view of the dewar insert.

2. Microwave Sources

The microwave power was supplied by two oil-cooled klystron sources joined together with a 10 dB directional coupler. Their frequencies, measured by a wavemeter and crystal detector, were usually set at 36.00 GHz and 35.95 GHz respectively. Although no automatic frequency control unit was used, the klystron frequency drifts were less than 10 MHz/hour, which is good enough in our experiments. The output power of the klystrons was measured by an A-band thermistor connected to a power meter. All the attenuators were carefully calibrated so that we can determine the microwave power incident on the junction to an accuracy of 10 percent.

C. Electronics

1. DC Measurement

We measure the static I-V curve of the junction by a conventional four-lead technique with the waveguide, and thus one side of the junction, grounded. The intermediate frequency signal ($\approx$ 50 MHz) was isolated from the DC circuit by four 100 μH inductors, one in each lead. Two low-noise differential amplifiers with high common mode rejection (Burr-Brown Corp., model 3620) were used for current and voltage amplification. When it was desired to display junction characteristic on a scope, an audio frequency signal generator was transformer coupled to the driving circuit to avoid ground loops. In order to isolate the junction from radio wave pick-up, all the low frequency leads were carefully shielded and filtered as shown in Fig. 2. The insertion loss of the pi-section feedthrough filters at the top of the cryostat is 80 dB at 1 MHz and 20 dB at 25 kHz.

It is frequently desirable to DC bias the junction with a low impedance source. This was done by connecting a bias resistor and a current measuring resistor across the junction to form a loop with inductance of the order of 10 μH. These resistances were chosen to be small compared with the junction resistance.

2. Intermediate Frequency (IF) System

The IF signal (at 50 MHz) from the junction was coupled to our room temperature IF amplifiers via a cryogenic 50-ohm coaxial cable which gave negligible attenuation. Figure 3 shows a block diagram of our IF system. The IF amplifiers have a total gain of 75 dB and a bandwidth from 20 MHz to 100 MHz. Following the amplifiers we used either a Tektronix 1401A spectrum analyzer to read the signal power of a HP 411A RF voltmeter and a resonant bandpass filter (center frequency 50 MHz, $Q \approx 3$) to measure the noise power in a narrow bandwidth around 50 MHz.

The front end of our IF system is an Avantek UA142 broadband amplifier which has an input impedance of 50 ohms. The noise temperature T_{IF} of this amplifier when matched to a 50-ohm source is 110 K. This was measured by connecting a 50 ohm resistor at the input and reading the total noise power on the RF voltmeter when the temperature of the resistor was changed from 300 K to 77 K. Since the Johnson noise power of a resistor is proportional to its physical temperature, we can easily calculate T_{IF} by the formula $(T_{IF} + 300\text{ K})/(T_{IF} + 77\text{ K}) = P_N(300\text{ K})/P_N(77\text{ K})$.

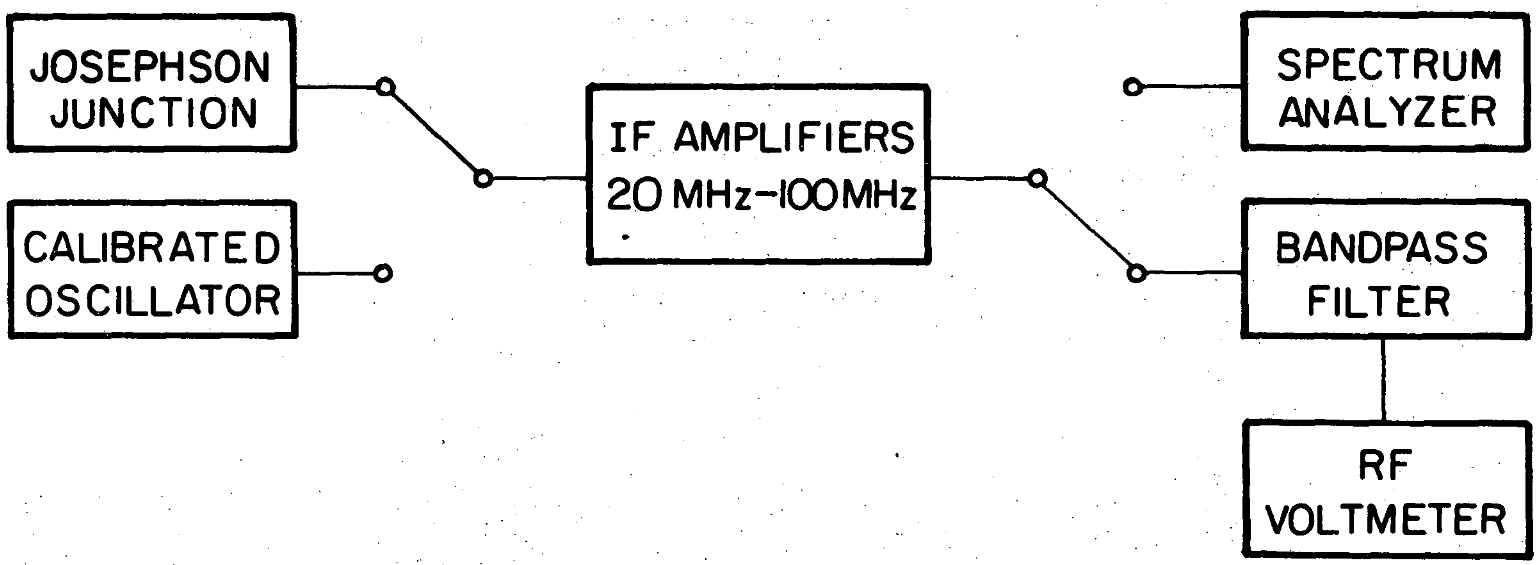

XBL 743-5916

Fig. 3. Block diagram for IF signal and noise measurement.

One could use an extension of this method to determine the IF coupling efficiency C_{IF} by measuring the Johnson noise from a normal junction in the resistive state. The details of this measurement will be described in Section V.B. For a 50-ohm resistive junction, we found that $C_{IF} = 0.9$ around 50 MHz. The deviation from perfect coupling is mainly caused by the shunt capacitance between the niobium flange and the niobium waveguide (≈ 10 pF).

D. Cryogenics

All of the experiments were carried out in a 5.1 cm ID glass dewar surrounded by a liquid nitrogen bath. The niobium waveguide assembly was immersed in liquid helium except when working with preadjusted niobium junctions. It takes 2 to 3 liters of liquid helium to cool down the apparatus and fill the dewar. The holding time is more than 24 hours when operated at 4.2 K and 10 hours when pumped to 1.3 K.

We regulated the temperature of the pumped helium using a throttled pumping valve for gross control and a thermometer bridge[12] for fine control. The bridge used a 150 ohm Allen-Bradley carbon resistor as thermometer and a 200 ohm metal film resistor as heater. Both resistors were glued onto the niobium waveguide with No. 2850 GT Stycast. When the waveguide structure is sealed in helium exchange gas, it is possible to operate the niobium junctions above 4.2 K to investigate their properties close to the transition temperature.

III. JUNCTION MODEL

A. Resistively Shunted Junction (RSJ) Model

It was proposed by McCumber[13] that the static I-V curves of point contact Josephson junctions can be understood by an equivalent circuit which consists of an ideal Josephson element shunted by a resistor R and a capacitor C. He defined a dimensionless parameter $\beta_c \equiv (2e/\hbar)R^2CI_c$ and showed that hysteresis will appear on the junction I-V curve if $\beta_c \gtrsim 0.7$. Hysteretic junctions often show switching characteristics and cannot be DC biased at low voltages. Therefore, almost all of our experiments were done with hysteresis-free point contact junctions, implying $\beta_c \lesssim 0.7$. For such point contacts, it seems to be reasonable to neglect the effect of the shunt capacitance and treat the junction as an ideal Josephson element with a purely resistive shunt.

Recent experiments[14] have shown the existence of a phase modulated quasiparticle ($\cos\phi$) current in different kinds of Josephson junctions. However, it was demonstrated[15] that such a current causes very little change in the predicted junction properties used for heterodyne detection. Therefore we can neglect this term in our model to simplify the calculations.

All of our experimental results were compared with the predictions of the RSJ model. In sections IIIB and IIIC we consider the static I-V curves of the junction driven by current sources and the variation of RF induced steps with RF amplitude. In section IV a theory is developed based on the RSJ model for junctions tightly coupled to microwave fields. The mixing and noise properties of a resistively shunted junction will be discussed in sections V and VI.

B. Static I-V Curves without RF

If a resistively shunted junction is driven by a DC current I_{DC}, the differential equation which governs the time dependence of the junction phase is simply

$$\frac{\hbar}{2eR}\frac{d\phi}{dt} + I_c \sin\phi = I_{DC} \tag{5}$$

This equation can be solved analytically for $\phi(t)$. Experimentally, it is easiest to measure the static I-V curve of the junction, i.e. a relation between I_{DC} and $V_{DC} \equiv \langle V(t) \rangle = \frac{\hbar}{2e} \langle \frac{d\phi}{dt} \rangle$. In this case, the RSJ model predicts a hyperbolic I-V curve

$$V_{DC} = \begin{cases} 0 & \text{if } I_{DC} \leqslant I_c \\ R(I_{DC}^2 - I_c^{\,2})^{1/2} & \text{if } I_{DC} > I_c \end{cases} \tag{6}$$

In the limit of $I_{DC} \gg I_c$, this I-V curve approaches an asymptotic slope 1/R.

In Fig. 4 we compare one of our typical I-V curves, obtained from low impedance niobium junctions, with the predictions of Eq. (6). We can fit the low voltage region of the experimental curve to a hyperbola, but the value of R required for the fit is less than the asymptotic resistance R_N of the junction at high voltages. If we draw a hyperbola

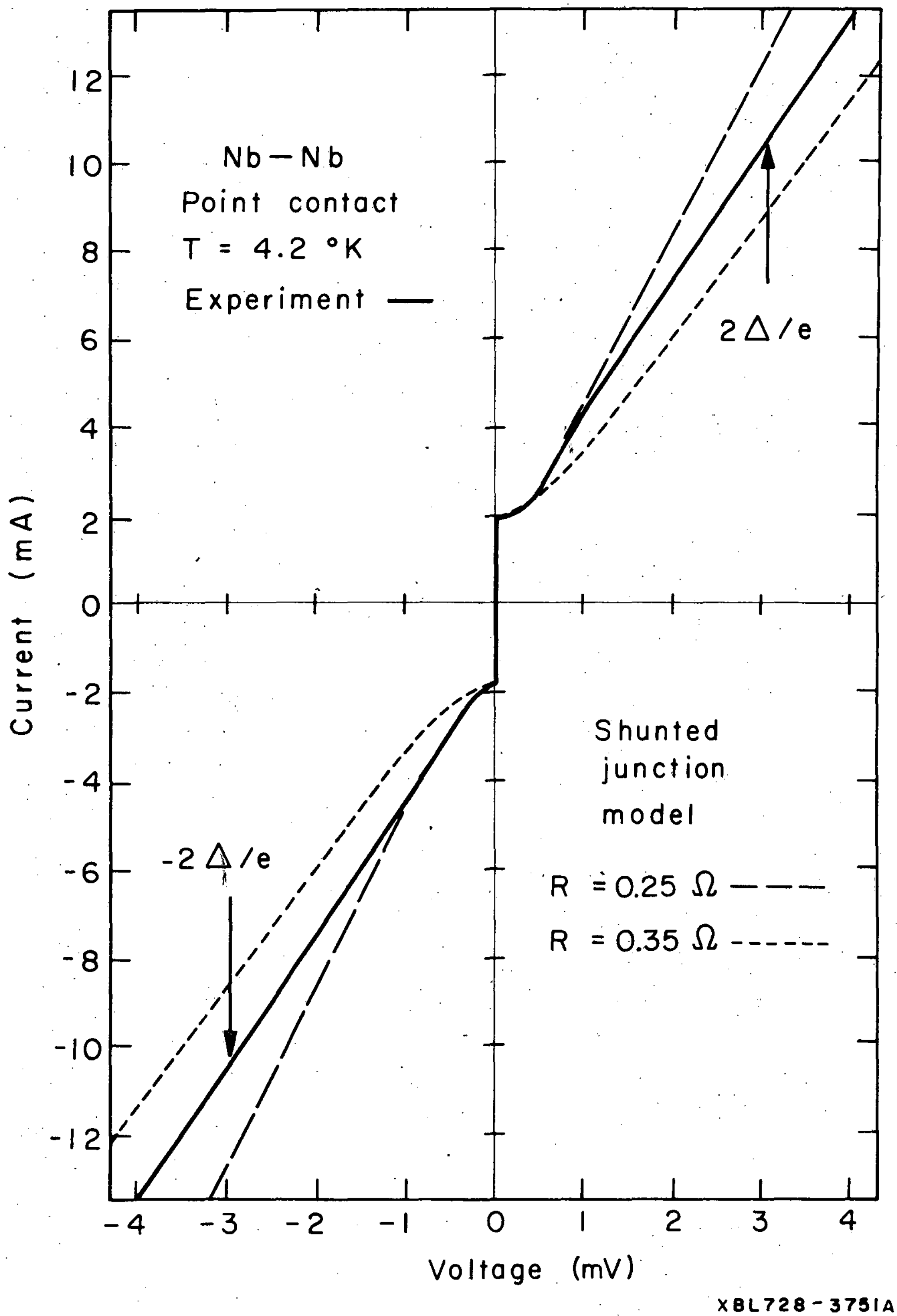

Fig. 4. Static I-V curve without RF.

with asymptotic slope $R^{-1} = R_N^{-1}$, it falls below the entire experimental curve. Either heating or phase slip effects might explain this discrepancy.

For hysteresis-free junctions, static I-V curves measured with a constant DC voltage bias source, i.e. with source resistance much smaller than R_N, are similar to those with a constant current source. The equivalent circuit should thus contain a series inductance in the case of voltage bias to account for the absence of negative resistance.

C. Step Height Variations with RF

It is well known that if an RF signal is applied to a Josephson junction, the zero-voltage current of the junction will be suppressed while constant-voltage steps appear on the junction I-V curve at $V_{DC} = n\hbar\omega_{RF}/2e$. It will be discussed in Section V that this effect is of ultimate importance in determining the performance of a high frequency Josephson mixer. In this section we shall consider the variation of these current steps with the power of the RF signal applied to the junction.

1. Normalized Frequency

In the absence of microwave matching networks, the RF source impedance is high compared with the junction shunt resistance R, therefore it acts like a constant current source to the junction and we have

$$\frac{\hbar}{2eR}\frac{d\phi}{dt} + I_c \sin\phi = I_{DC} + I_{RF} \sin \omega_{RF} t \tag{7}$$

This equation can be written in terms of the normalized currents $\alpha_{DC} = I_{DC}/I_c$, $\alpha_{RF} = I_{RF}/I_c$ and time $\tau = (2eRI_c/\hbar)t$ as

$$\frac{d\phi}{d\tau} + \sin\phi = \alpha_{DC} + \alpha_{RF}\sin\Omega\tau \tag{8}$$

where $\Omega \equiv \hbar\omega_{RF}/2eRI_c$ is called the "normalized frequency" which determines the important features of the RF response of the junction.

It follows from Eq. (8) that constant voltage steps appear on the junction I-V curve at voltages given by the Josephson relation $V_{DC} = n\hbar\omega_{RF}/2e = n\Omega RI_c$. Using a perturbation method, Kanter[16] solved Eq. (8) in the limit of $\alpha_{RF} \ll 1$ for the sensitivity of a resistively shunted junction operated as a square-law detector. For finite RF currents Eq. (8) has no analytic solutions. Russer[17] has used an analog computer to solve this case and show that the dependence of the step heights on RF current in Eq. (8) differs significantly from the Bessel function dependence predicted in Josephson's theory assuming constant voltage sources. In cooperation with F. Auracher, we have used a digital computer to calculate a series of I-V curves from Eq. (8) for different values of the normalized RF current and the normalized frequency Ω.

2. Comparison of Experimental Results with Theory

In order to make comparison with the results predicted by the current source model, our experiments were carried out without the plunger and stub. Instead, a matched load was placed behind the point contact so that the junction sees the waveguide impedance which is much larger than the junction resistance R.

In Fig. 5(a) we show a series of experimental I-V curves measured for different values of the incident RF power P_{RF} using a preadjusted niobium point contact at 4.2 K with $\Omega = 0.16$. It is a common practice to estimate the height of steps from data which are rounded by noise by fitting the region between steps to a straight line of finite slope. When this is done we obtain the estimated heights of the zeroth and first steps plotted against $\sqrt{P_{RF}}$ ($\propto \alpha_{RF}$) in Fig. 5(b). To make comparisons with the predictions of the noise free RSJ model, we calibrate the horizontal scale of the data by the value of α_{RF} at the first zero of the zero voltage step. The value of the shunt resistance R which was used in this fit is the one required to fit the low voltage region of the static I-V curve in the absence of RF. The fit is very good despite the crude method used to obtain the points from the measured I-V curves. Similar fits[18,19] for thin film bridges have shown less good agreement. In particular, there is a characteristic drop in the height of the aeroth step as α_{RF} approaches zero known as Dayem effect, which does not appear in our point contact data.

Comparisons similar to those shown in Fig. 5 are given in Fig. 6 for a higher pressure niobium point contact operated at 8 K with a normalized frequency $\Omega = 1.67$. Both theory and experiment give a step height dependence which is closer to Bessel functions for large Ω. The agreement between theory and experiment, however, is much less good than for small Ω. The fit is obtained only over a small range

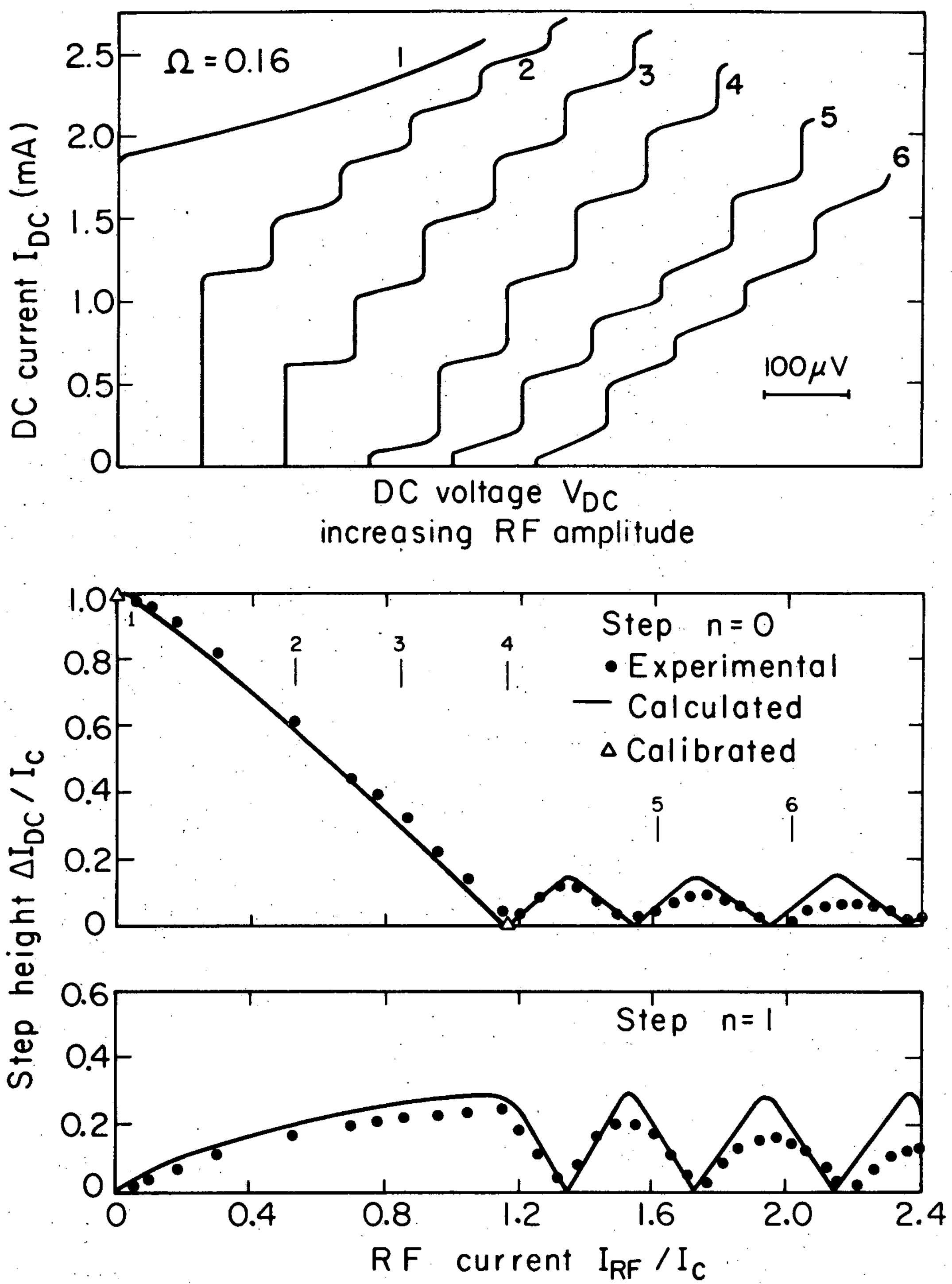

XBL728-3744

Fig. 5. Static I-V curves and step height variations with RF amplitude for a small normalized frequency.

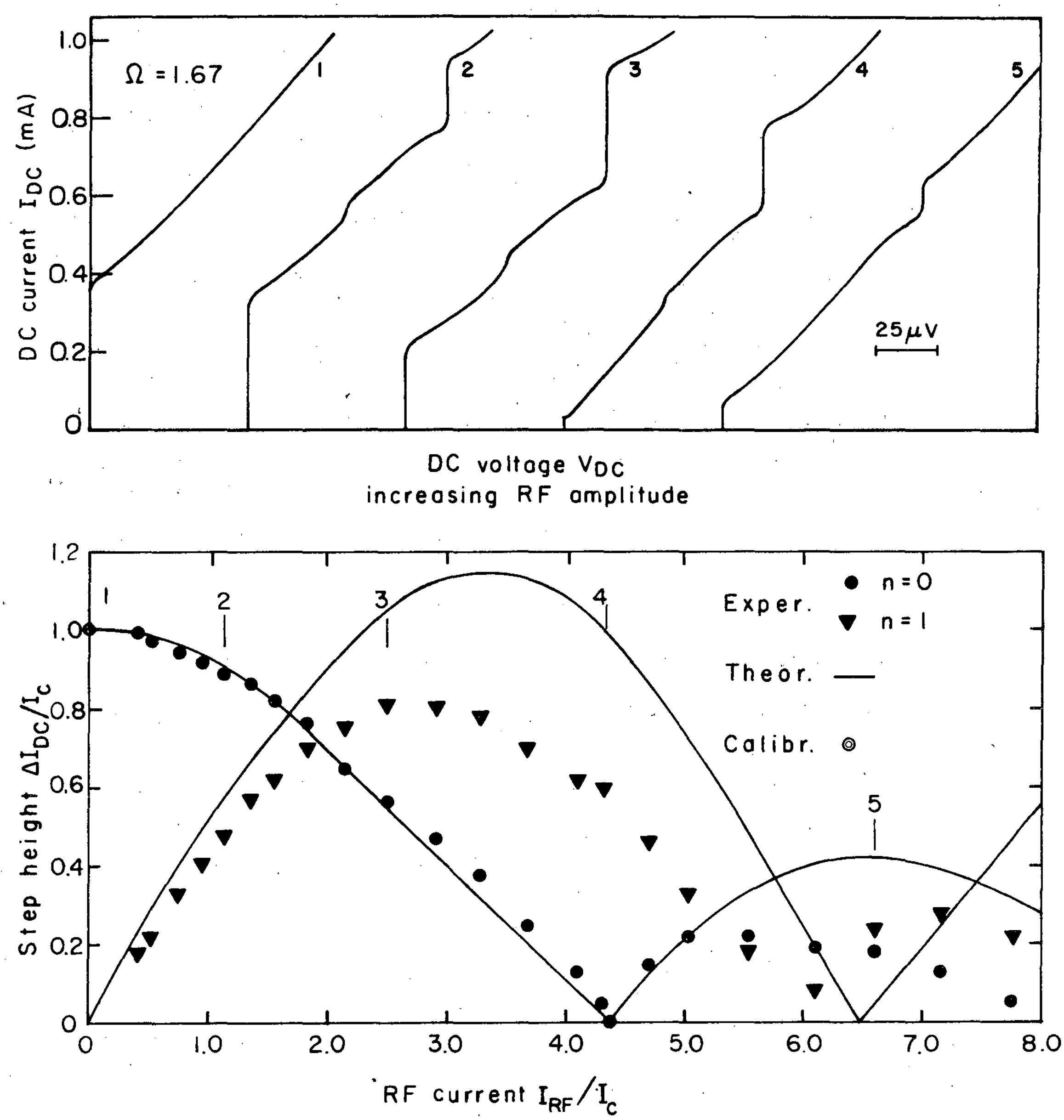

XBL 728-1455

Fig. 6. Static I-V curves and step height variations with RF amplitude for a large normalized frequency.

of experimental parameters. Even after careful corrections are made for noise rounding, the height of the first step relative to I_c is less than the predicted value.

D. Temperature and RF Power Dependence of the Shunt Resistance

In our experiments, we have also examined the temperature and RF power dependences of the junction shunt resistance. In Figs.7, 8 we show two series of junction I-V curves taken for different values of temperature and microwave power. It is clear that the asymptotic resistance of the junction is insensitive to both parameters. This suggests that there is no significant tunneling contribution to the junction current for otherwise we would expect a strong RF power dependence of the shunt resistance arising from photon assisted quasiparticle tunneling[20] with a smeared energy gap.

Energy gap structures, which appear as a bump on junction I-V curves at $V_{DC} = \pm 2\Delta_{Nb}(T)/e$, were often observed for high resistance ($R \gtrsim 20$ ohms) point contacts but not for low resistance point contacts such as the one shown in Fig. 4. However, for our purpose to operate the junction as a device at 36 GHz, we are only interested in the junction behavior at voltages much lower than the energy gap, where our oxidized point contacts can be closely described by the RSJ model.

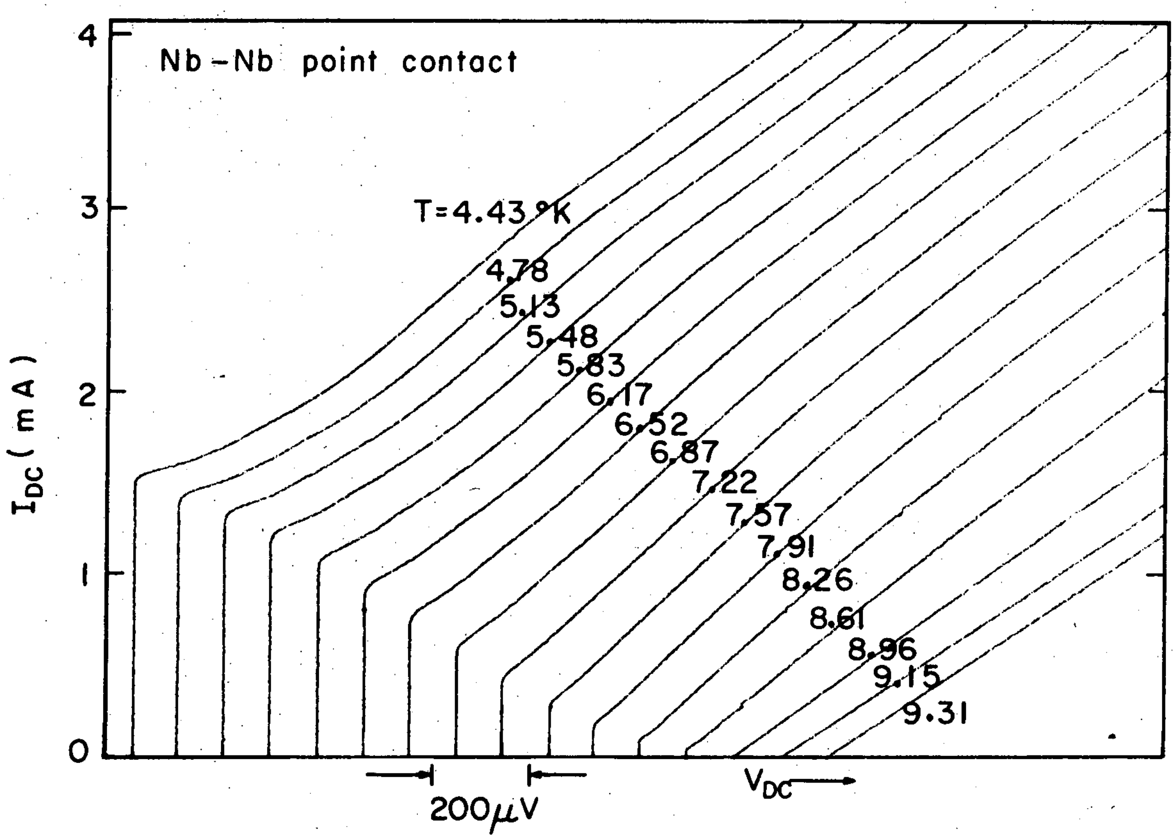

XBL728 - 3741

Fig. 7. Temperature dependence of the static I-V curve.

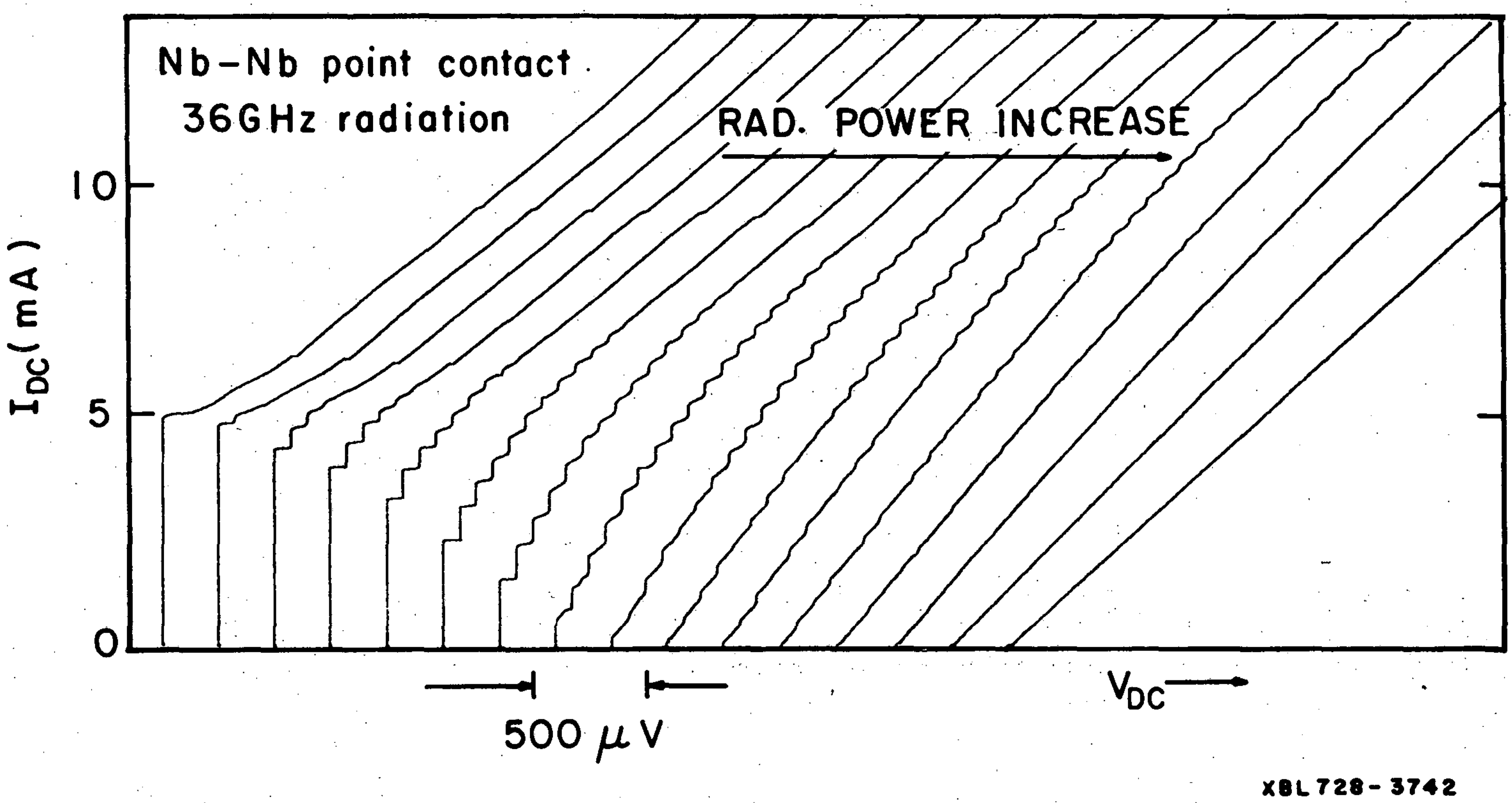

Fig. 8. Microwave power dependence of the static I-V curve.

IV. MICROWAVE POWER COUPLING

A. Theory of RF Power Coupling to a Josephson Junction

1. Definition of the Problem

In order to construct a high frequency Josephson effect device with good performance, it is necessary to couple the junction efficiently to the radiation source which usually has an impedance much higher than the junction resistance. F. Auracher and T. Van Duzer[21] used a digital computer to calculate the RF impedance of a resistively shunted Josephson junction by applying an RF current $i_{RF} \sin \omega_{RF} t$ to the junction and measuring the Fourier components of the junction voltage at ω_{RF}. They plotted the real and imaginary parts of the junction impedance, which determines the reflection and absorption of the incident RF power on the junction, as functions of the DC bias current. However, this is not exactly the information we need to design the coupling circuit for a Josephson junction mixer. In fact, the RF impedance they obtained is a strong function of i_{RF} and DC bias current, and under certain conditions the real part of this RF impedance becomes negative, which implies that the concept of matching to a Josephson junction is not adequate.

We approach this problem in a different way by considering how to find an appropriate RF source impedance which maximizes the junction response for a given amount of signal power. In principle, the condition for the optimum RF power coupling to a Josephson junction depends on the kind of device it serves. In our case to operate the junction as a heterodyne receiver with an external local oscillator, it is desirable to maximize the variation of the zero-voltage step height I_o for a given change of the microwave power (this will be discussed in Section V. A.). From Figs. 5 and 6, this maximum variation occurs in the first period when I_o is suppressed to about 0.1 to 0.5 of its original value I_c. In this range I_o changes linearly with I_{RF}, i.e. $\Delta I_o \propto \Delta(P_{RF}{}^{1/2})$. Experimentally, we found that it is usually better to operate with I_o in the upper part of this range to minimize the effect of noise rounding which may degrade the performance of the device. Therefore, we define the dimensionless coupling parameter

$$\alpha^2 \equiv \left\{ \frac{\partial I_o}{\partial[(8P_{RF}/R)^{1/2}]} \right\}^2_{I_o = I_c/2} \tag{9}$$

where the derivative is evaluated at an RF level such that $I_o = I_c/2$ in the first period.

The parameter α^2 depends mainly upon the junction normalized frequency Ω and the normalized RF source impedance R_S/R. In the next section we shall describe a method to maximize α^2 for a given junction in the case of broad band coupling and plot the resultant α^2_{opt} as a function of Ω. We can then define the RF power coupling efficiency to a junction with normalized frequency Ω as

$$C_{RF} \equiv \frac{\alpha^2_{exp}(\Omega,\ R_S/R)}{\alpha^2_{opt}\ (\Omega)} \leqslant 1 \tag{10}$$

2. The Case of Broad Band Coupling

In the case of broad band coupling, the junction is connected to an RF source with source resistance R_S at all frequencies as shown in Fig. 9(a). This is equivalent to the circuit shown in Fig. 9(b), where the junction with a shunt resistance $R_{eff} = RR_S/(R+R_S)$ is driven by an RF current source. The effective normalized frequency of the junction is then $\Omega_{eff} = \hbar\omega_{RF}/2eR_{eff}I_c$. By definition $P_{RF} = R_S I_{RF}^2/8$, therefore Eq. (9) becomes

$$\alpha^2 = \frac{R}{R_S}\left(\frac{\partial I_o}{\partial I_{RF}}\right)^2_{I_o=I_c/2}$$

$$= \left(\frac{\Omega_{eff}}{\Omega} - 1\right)\left(\frac{\partial I_o}{\partial I_{RF}}\right)^2_{I_o=I_c/2} \tag{11}$$

Here $[(\partial I_o/\partial I_{RF})^2]_{I_o=I_c/2}$ is a function of Ω_{eff} only and has been calculated, for a resistively shunted junction, by many authors[22,23] using either digital or analog computers. The result is shown in Fig. 10 with the asymptotic behavior

$$\left(\frac{\partial I_o}{\partial I_{RF}}\right)^2_{I_o=I_c/2} \longrightarrow \begin{cases} 1 & \Omega_{eff} \ll 1 \\ (0.58/\Omega_{eff})^2 & \Omega_{eff} \gg 1 \end{cases} \tag{12}$$

For a given Ω, α^2 can be maximized by graphical methods for the range $\Omega < \Omega_{eff} < \infty$. Since $\alpha^2 = 0$ when $\Omega_{eff} = \Omega$ (RF current source) or $\Omega_{eff} \rightarrow \infty$ (RF voltage source), it always has a peak at some finite

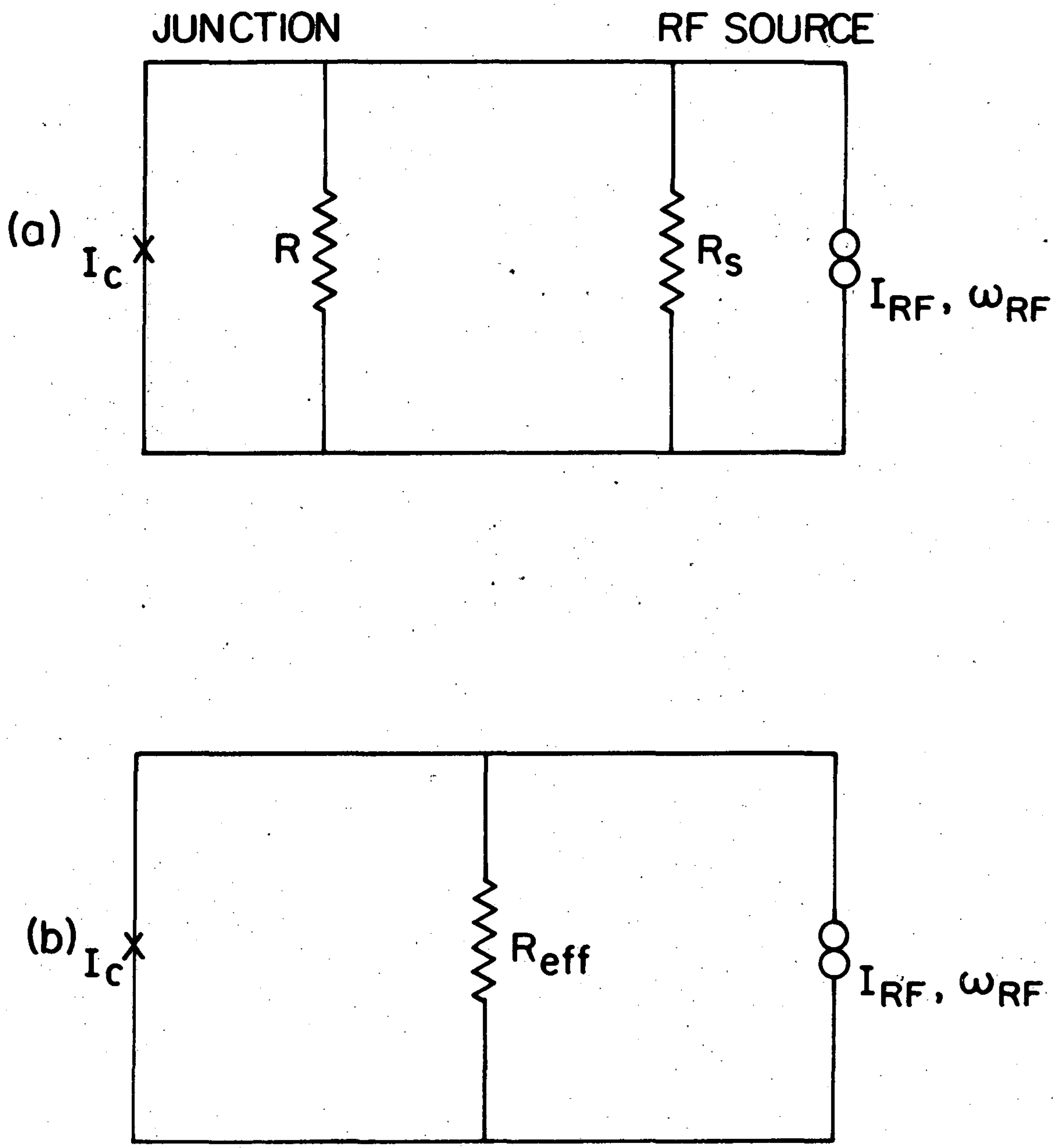

XBL 743-5918

Fig. 9. Equivalent circuits for broadband RF coupling.

value of Ω_{eff}. An example is given in Fig. 10 for the case $\Omega = 0.5$, where we found $\alpha^2_{opt} = 0.22$ at $\Omega_{eff} = 1.2$, i.e. $(R_S/R)_{opt} = 0.7$. Using this method we obtain α^2_{opt} and $(R_S/R)_{opt}$ as functions of Ω shown in Fig. 11. The asymptotic behavior of these quantities can be found from (12) to be

$$\alpha^2_{opt} \sim 0.25/\Omega, \qquad (R_S/R)_{opt} \sim 1.67\Omega \qquad \Omega \ll 1 \tag{13}$$

$$\alpha^2_{opt} \sim 0.08/\Omega^2, \qquad (R_S/R)_{opt} \sim 1 \qquad \Omega \gg 1 \tag{14}$$

We see from Fig. 11 that for small Ω the RF source resistance required to achieve the optimum values of α^2 can be much smaller than the junction resistance R. This means that it is even harder to obtain optimum coupling to junctions with low normalized frequencies.

3. <u>The Case of Resonant Coupling</u>

As mentioned before, we used a plunger and stub to resonantly reduce the microwave source impedance. This implies that the junction sees a low impedance only at frequencies close to the resonant frequency ω_c, which was made equal to the RF signal frequency. The equivalent circuit for resonant coupling is shown in Fig. 12, which was solved by J. Claassen[24] using a Hamilton-type[25] Josephson junction simulator. The result of his calculation is plotted in Fig. 13 as curves of $\alpha^2(\Omega{=}0.5,\ \Omega_{eff})$ and $\alpha^2(\Omega{=}0.2,\ \Omega_{eff})$ versus Ω_{eff} for the case of resonant coupling with an unloaded $Q \equiv \omega_c L/R_S \approx 10$.

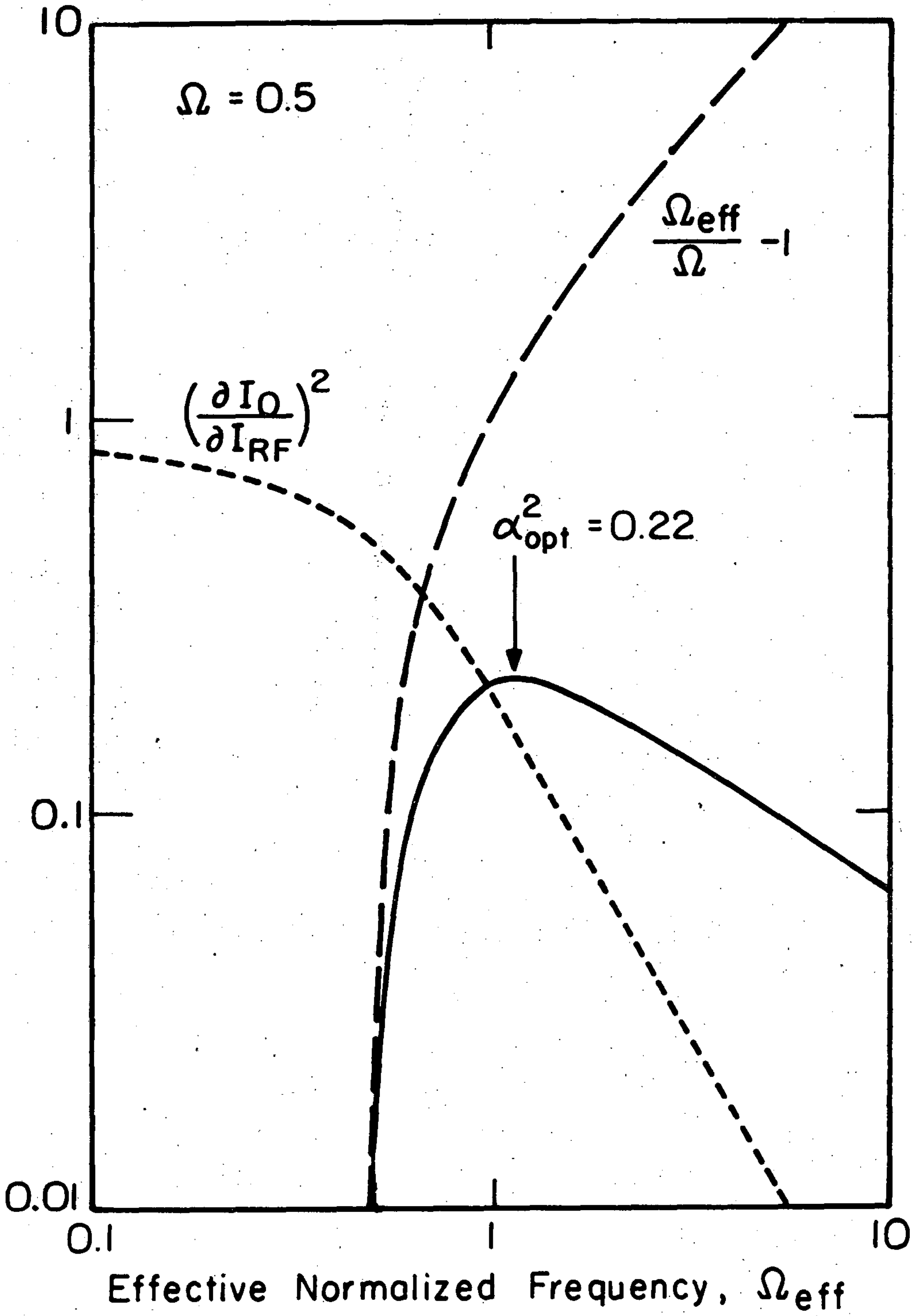

Fig. 10. Optimization of the coupling parameter; the solid curve gives $\alpha^2(\Omega{=}0.5,\ \Omega_{eff})$.

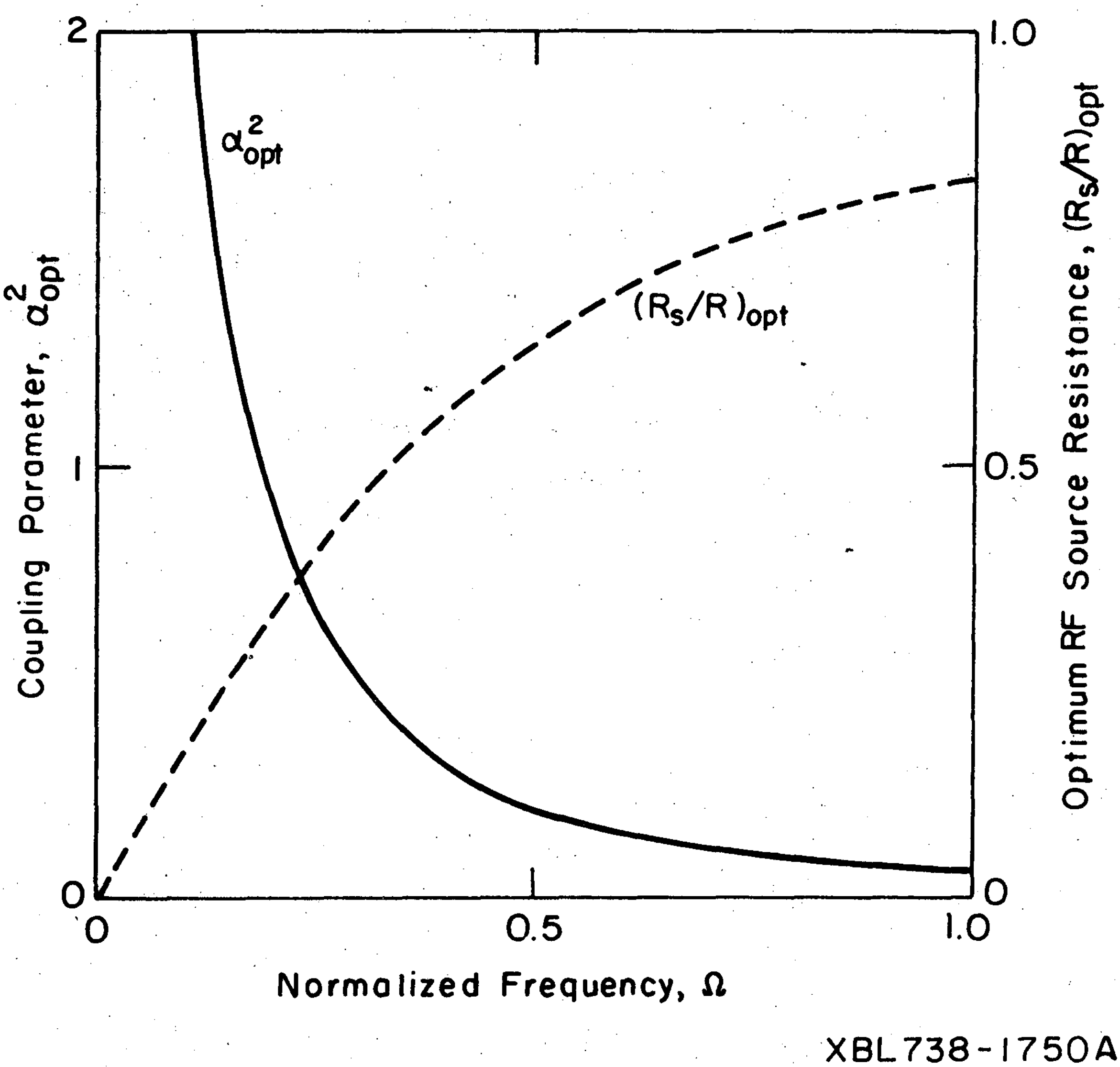

Fig. 11. Optimum coupling parameter and the corresponding RF source resistance computed from the RSJ model for broadband coupling.

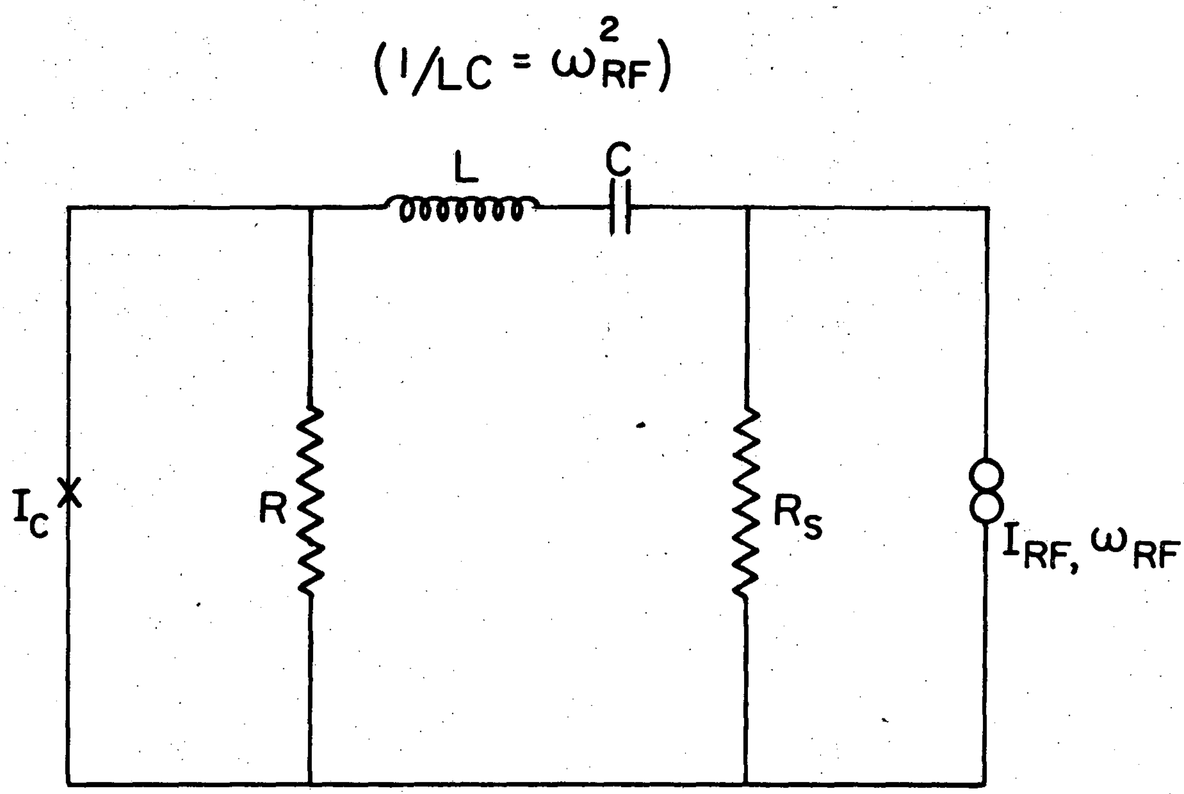

XBL 743-5914

Fig. 12. Equivalent circuit for resonant RF coupling.

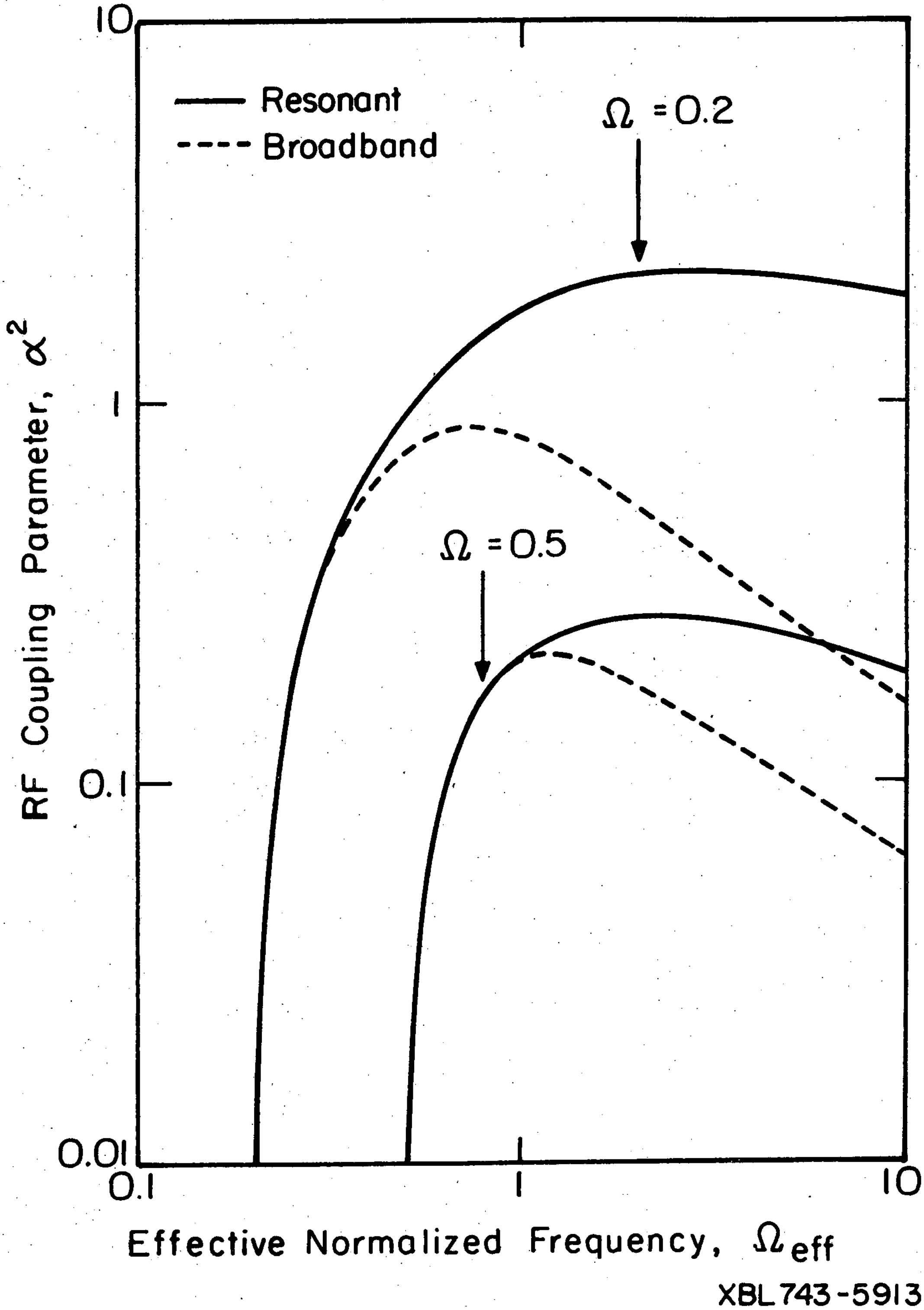

Fig. 13. Comparison of $\alpha^2(\Omega_{eff})$ for the case of resonant coupling to that of broadband coupling.

By comparing the resonant curves in Fig. 13 to the corresponding curves for broad band coupling, we found that they agree with each other when $\Omega_{eff} \leqslant 2\Omega$(i.e. $R_S \gtrsim R$). But for $\Omega_{eff} \gg \Omega$(i.e $R_S \ll R$), the curves for resonant coupling start to deviate from the ones for broad band coupling and reach slightly larger values of α^2_{opt}. This is more pronounced in the case Ω=0.2. However, it is very difficult to achieve the situation $R_S \ll R$ or $\Omega_{eff} \gg \Omega$ experimentally since the microwave source resistance before the impedance transformation is much greater than R, and we almost always operate in the regime $R_S \gtrsim R$ where there is no essential difference between resonant and broad band coupling. We also learned from the simulator that adding noise to the RSJ model has little or no effect on α^2_{opt}.

Therefore we conclude that as far as experimental interest is concerned, the basic result of resonant coupling is the same as that of broad band coupling. Then we can use Eq. (10) with the values of $\alpha^2_{opt}(\Omega)$ given in Fig. 11 to estimate how good a coupling we have achieved with the plunger and stub.

B. Microwave Cavity

1. Microwave Equivalent Circuit

The microwave equivalent circuit of the matching structure is shown in Fig. 14(a) for the TE_{10} mode which is the only allowed mode of propagation in the niobium waveguide. Here the junction is represented by an ideal Josephson element shunted by a constant resistor R as usual and X_L is the inductive reactance of the superconducting

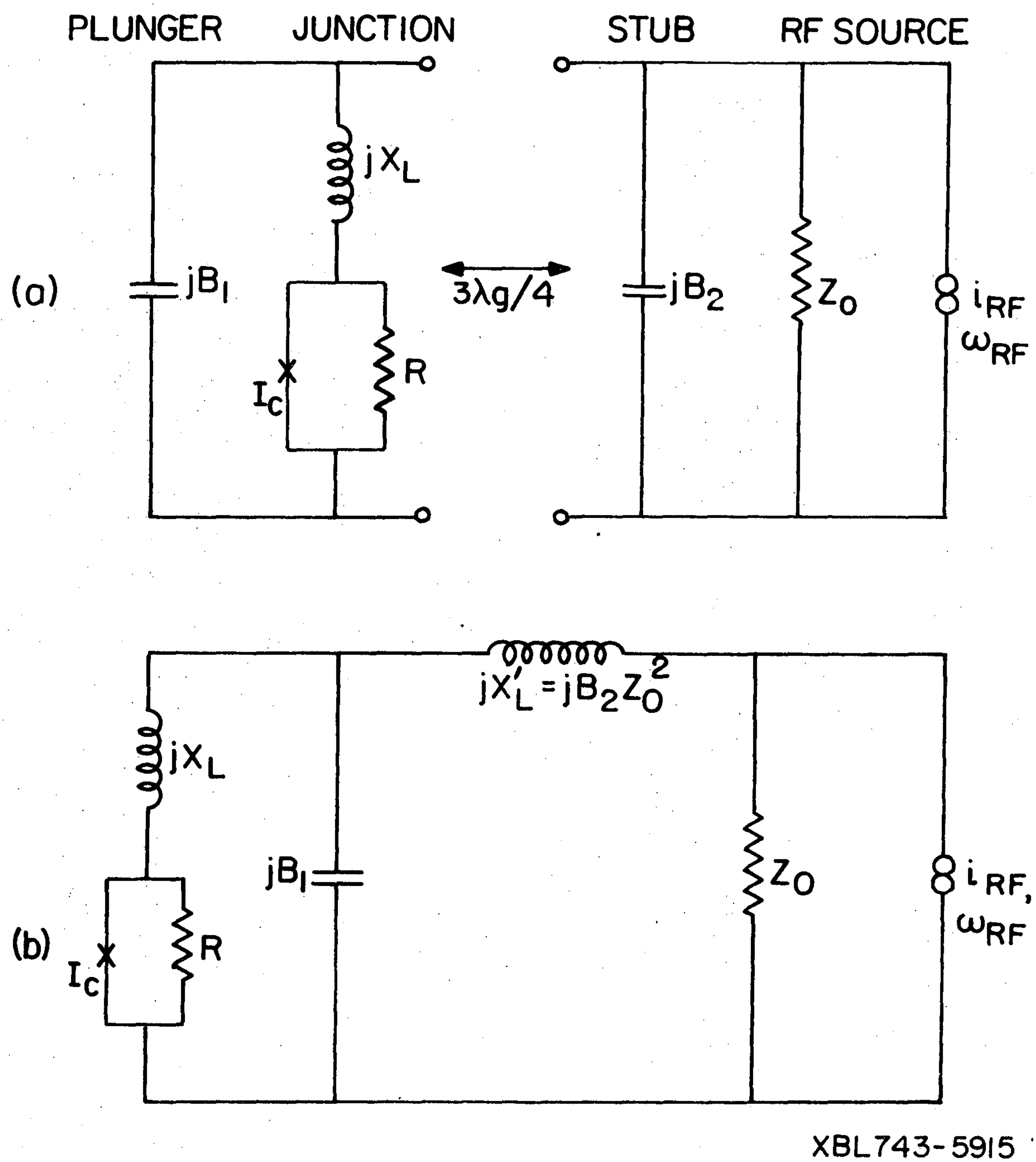

Fig. 14. Microwave equivalent circuits of the resonant cavity; the $3\lambda_g/4$ section between the stub and junction has a characteristic impedance Z_o.

wires in series with the junction, in our case, $X_L \approx 50 - 100$ ohms.[26] The effect of the plunger is described by a shunt susceptance B_1. In principle, B_1 can take any real values from $-\infty$ to $+\infty$, but in order to cancel jX_L, B_1 is always made to be positive, i.e. capacitive. The stub tuner, placed at $3\lambda_g/4$ in front of the junction, is represented by a capacitive susceptance B_2 which can be varied from 0 to $+\infty$ as the stub moves into the waveguide to some resonant position[27] before it reaches the far wall of the waveguide. Finally, the microwave source is represented by Z_o and i_{RF} where $Z_o = 450$ ohms.

We can transform the impedance at the stub through the distance $3\lambda_g/4$ to the junction and obtain the circuit in Fig. 14(b). Here the stub is converted into an inductor jX_L' in series with the source. It will be shown in Appendix A that one can always vary B_1 and B_2 (or X_L') such that the junction sees an RF source with a real source impedance R_S which can take any value much smaller than Z_o at the RF signal frequency as shown in Fig. 12, where $R_S I_{RF}^2 = Z_o i_{RF}^2$ by power conservation. In principle, for a given junction with normalized frequency Ω and shunt resistance $R \ll Z_o$, two adjustments are sufficient to eliminate the imaginary part of the source impedance and bring the real part R_s to $(R_s)_{opt}$.

2. Loss in the Cavity

In Fig. 14 we have neglected other losses in the cavity besides the junction shunt resistance R. These include the skin depth loss on the waveguide walls and the microwave leakage out of the hole containing the superconducting wire (the plunger and stub are practically lossless). The skin depth loss can be characterized by a resistance $(\alpha'\ell)Z_o$[27] in the microwave equivalent circuit of the junction, where α' is the attenuation constant per unit length and $\ell \approx 1$ cm is the length of the cavity. For our superconducting niobium waveguide at 4.2 K, $(\alpha'\ell)Z_o < 0.1$ ohm, which is much smaller than typical junction resistances and therefore is not important at all. However, our measurement showed that the microwave leakage from a niobium flange without choke grooves is equivalent to a resistance about 20 ohms in series with the junction, which seriously limits the performance of the matching circuit especially for low impedance junctions. With proper design of a choke flange (presented in Appendix A), we were able to reflect a microwave short circuit to the plane where the wire enters the waveguide. This reduces the leakage resistance to less than one ohm so that it can be neglected for junctions with $R \gtrsim 10$ ohms. (An alternative way to solve the leakage problem is to use multi-section coaxial chokes with similar properties.)

C. Experimental Results

1. Coupling Parameter Without Matching Structure

In our experiments we obtained the parameter α^2 from its definition Eq. (9) by measuring the change of I_o with respect to the RF power P_{RF} incident on the junction. Here we use a power meter to read the absolute microwave power at room temperature and then make corrections for the cold attenuator (23 dB) and the loss in the stainless steel waveguide (3 dB) to get P_{RF}.

When the plunger is replaced by a matched load and if no stub tuner is used, the junction is essentially driven by an RF current source since both R and X_L are much smaller than Z_o. The relation between the RF current I_{RF} flowing through the junction and P_{RF} is then $P_{RF} = (1/8)Z_o I_{RF}^2$. Therefore we have

$$\alpha^2 = \frac{R}{Z_o}\left(\frac{\partial I_o}{\partial I_{RF}}\right)^2_{I_o=I_c/2} \tag{15}$$

where $[(\partial I_o/\partial I_{RF})^2]_{I_o=I_c/2}$ is known as a function of the normalized frequency Ω of the junction.

For a given junction with R and Ω, we can calculate $(R/Z_o)\times [(\partial I_o/\partial I_{RF})^2]_{I_o=I_c/2}$ and compare it with the experimentally measured value of α^2. We found that the agreement is very good to within $\pm$ 10% for junctions with $R \leqslant 20$ ohms and $\Omega \leqslant 0.3$. This mainly checks our calibrations of the microwave power and the attenuators. Since absolute power measurement is very difficult for small microwave signals ($\leqslant 1$ μW) at frequencies higher than 100 GHz, we suggest that, by fabricating junctions with larger RI_c products, this method can be used to calibrate the output power of such high frequency sources.

2. <u>Coupling Parameter with Matching Structure</u>

When a good junction is obtained, we apply enough microwave power to suppress the zero-voltage current by an appreciable amount. Then we adjust the plunger and stub to enhance the effect of the microwave signal, that is, to minimize I_o until the optimum positions are found. Our experience showed that α^2 is not as sensitive to the stub as to the plunger. In fact, as will be discussed in Appendix A, with high impedance junctions, one can achieve fairly good coupling even without the stub. This allows us, without affecting the performance of the matching circuit too much, to preset the stub tuner at room temperature when the stub adjustment rod is used to adjust the junction at low temperatures. However the plunger adjustment at low temperatures is always important, this can be seen in Fig. 15 where we plot the coupling parameter α^2_{exp} against plunger position for a typical junction.

The maximized coupling parameter α^2 was measured and compared to the values of α^2_{opt} predicted by the RSJ model in Fig. 11. We found that with the preset stub and a good choke flange, an RF coupling efficiency ($C_{RF} \equiv \alpha^2_{exp}/\alpha^2_{opt}$) better than 0.75 can be achieved for junctions with $R \gtrsim 10$ ohms and $\Omega \gtrsim 0.2$. Typical examples are given in Table 1. This important result confirms our coupling theory and microwave circuit analysis.

For junctions with $R \approx 5$ ohms, it is necessary to have the stub adjustable at low temperature to obtain an RF coupling over 80%. At even lower resistance levels ($R < 2$ ohms), the coupling efficiency becomes smaller because the loss due to the residual microwave leakage starts to be comparable with the junction loss.

We have also examined the bandwidth of our matching circuit by tunning the Klystron frequency away from the resonance and obtaining plots for C_{RF} versus RF frequency shown in Fig. 16 for two different junctions. As expected, the bandwidth of the coupling curve increases with the resistance R of the junction; typically, $B \approx 1.8$ GHz and

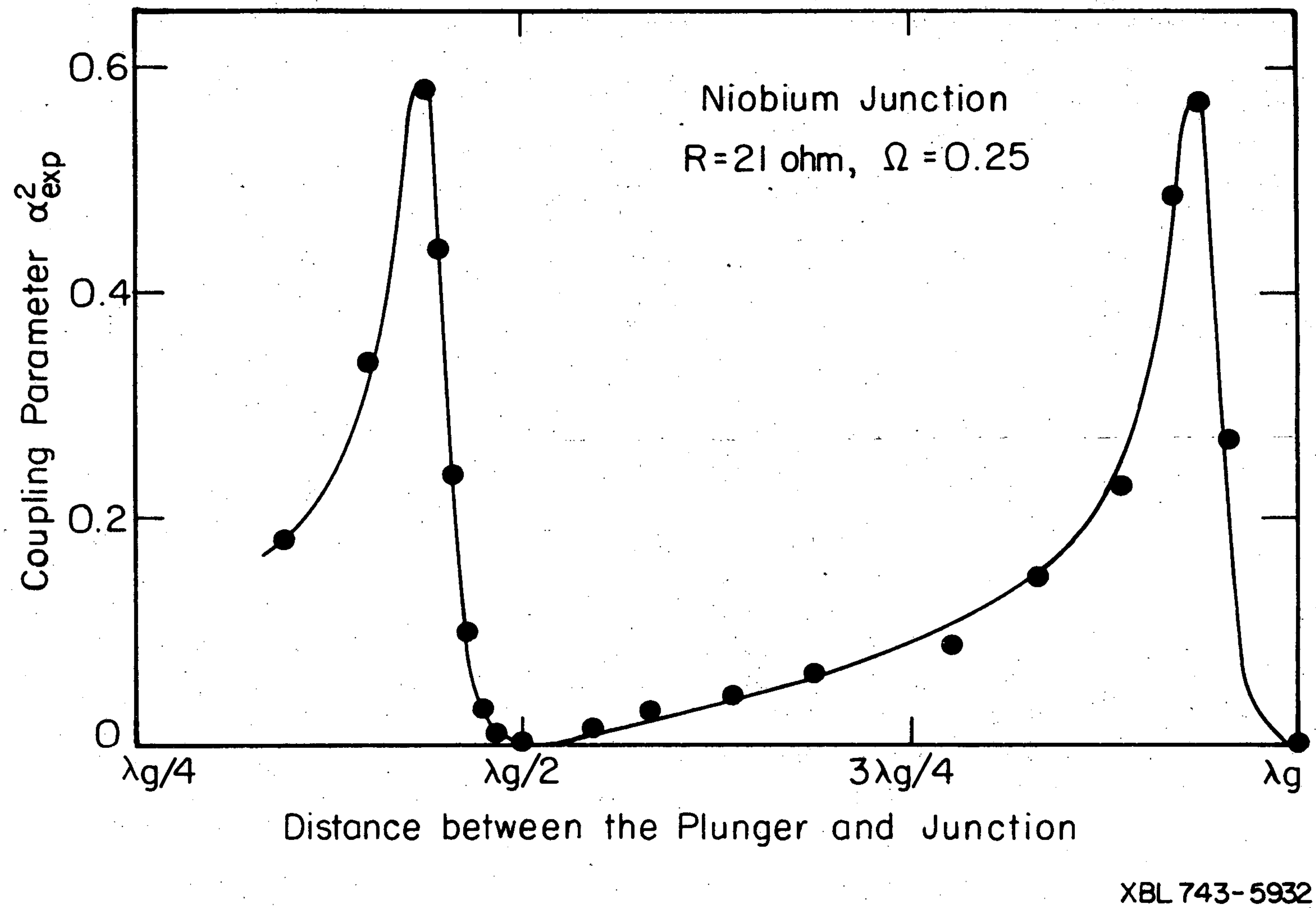

Fig. 15. Measured RF coupling parameter versus plunger position; the variation repeats itself for each interval of $\lambda_g/2$.

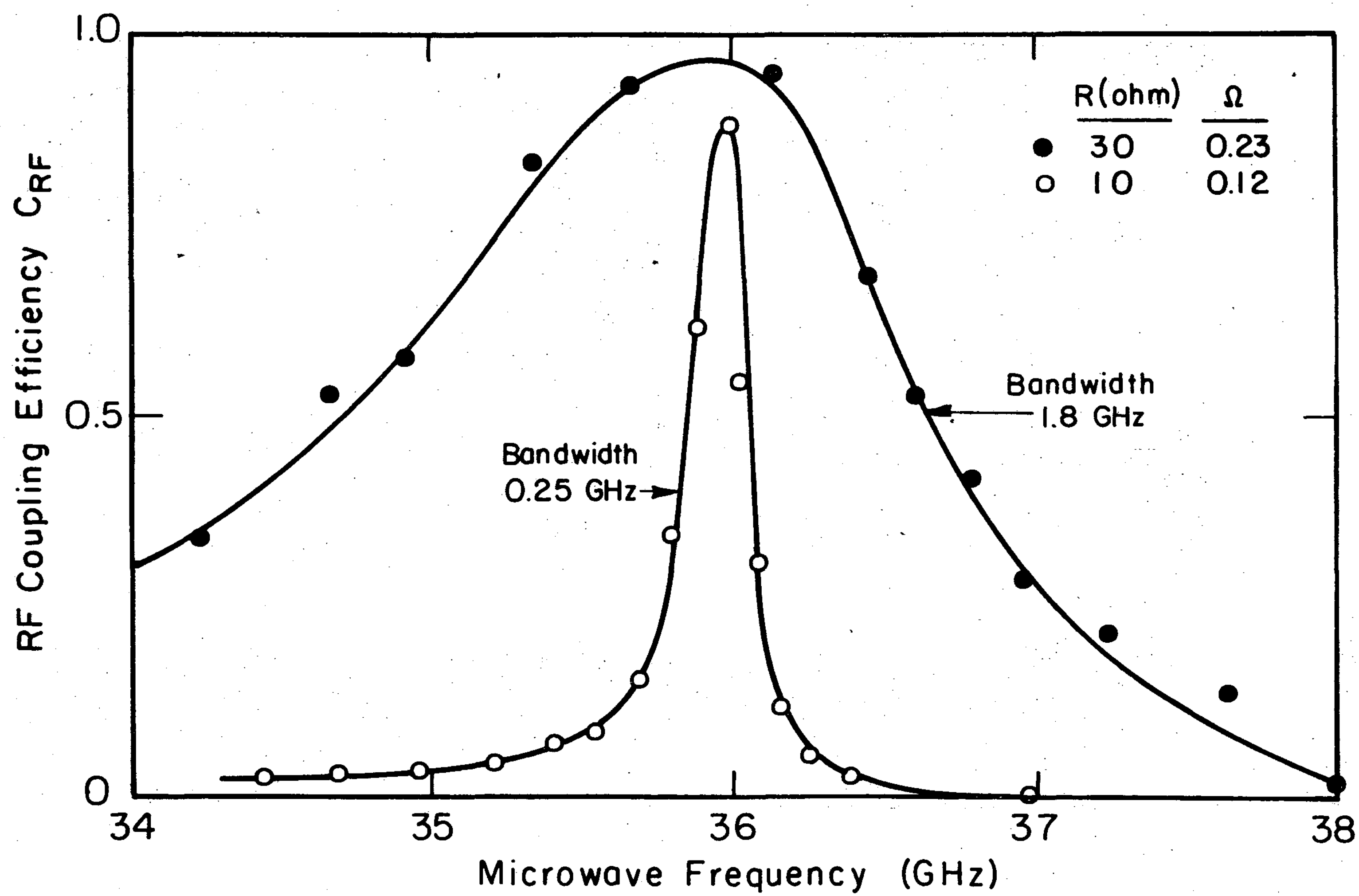

XBL743-5935

Fig. 16. Microwave coupling bandwidth for two niobium junctions at 4.2 K; the plunger and stub have been adjusted to maximize C_{RF} at 36.0 GHz.

$Q \approx 20$ for a 30-ohm junction. The dependence of the bandwidth on R will be discussed in Appendix A.

3. I - V Curves of Well-coupled Junctions

When a junction is resonantly coupled to microwave fields, it sees an RF impedance R_S comparable to its shunt resistance R at the resonant frequency ω_c. Therefore, when the junction is biased at a DC voltage corresponding to ω_c, an appreciable fraction of the AC Josephson current will flow in R_S and excite the cavity. This produces a current step on the junction I - V curve at $V_{DC} = \pm \hbar\omega_c/2e$ known as cavity mode step.[28,29] This structure was only occasionally observed for our well-coupled junctions. One of the reasons is that the noise can easily wipe out those cavity mode steps if they are small, especially for small normalized frequencies.

Figure 17 shows a series of I - V curves of one of our junctions which had pronounced cavity mode steps. These curves were measured for different plunger positions without applied microwaves. The first cavity mode step occurs at voltage equal to $\hbar\omega_c/2e$ as expected and its position changes with the plunger. But the second cavity mode step appears at a fixed voltage slightly less than $2 \times \hbar\omega_c/2e$. This is probably due to some unexpected higher order modes whose resonant frequency is not sensitive to the plunger. We do not fully understand all the details of these cavity induced steps, but we know from the data that the resonant frequency ω_c of the cavity can be tuned by adjusting the plunger.

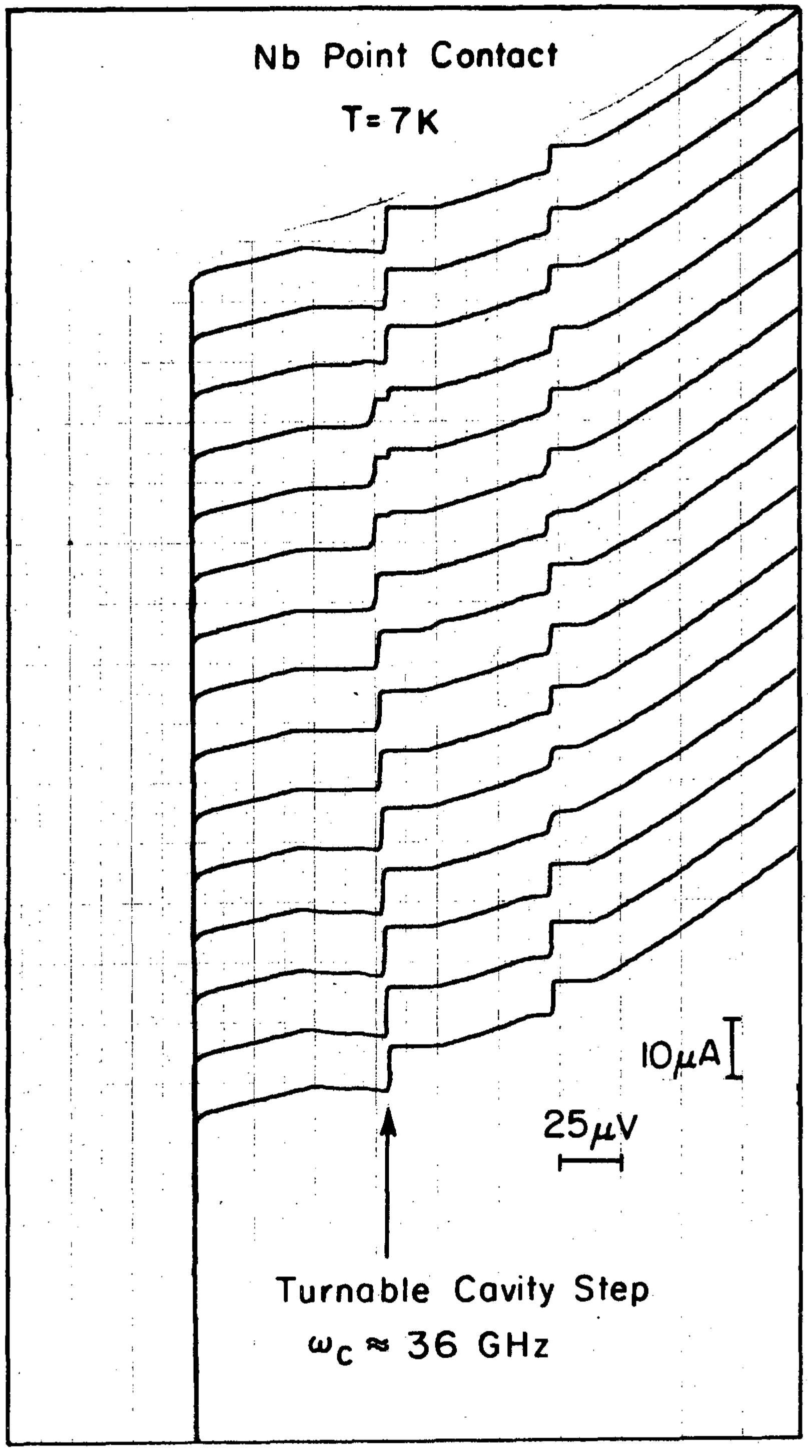

XBL743-5934

Fig. 17. Tunable cavity mode step; the distance between the plunger positions for the first and last curves is $\lambda_g/2$.

Another effect of the coupling circuit on the static I - V curve is observed when we apply microwaves to well-coupled junctions. This is shown in Fig. 18 where we fix the resonant frequency ω_c and vary ω_{RF} in the vicinity of ω_c to examine the change in the shape of the I-V curves. We believe that such changes occur mainly because the imaginary part of the RF impedance seen by the junction alternates its sign from inductive to capacitive near the resonant frequency. Such pronounced effects are not always seen, they show up only when the normalized frequency of the junction is less than 0.3 and the RF source resistance at resonance is smaller than R. John Claassen was able to reproduce very similar curves shown in Fig. 19 using the junction simulator described before, showing that the effect we observed is in good agreement with the RSJ model.

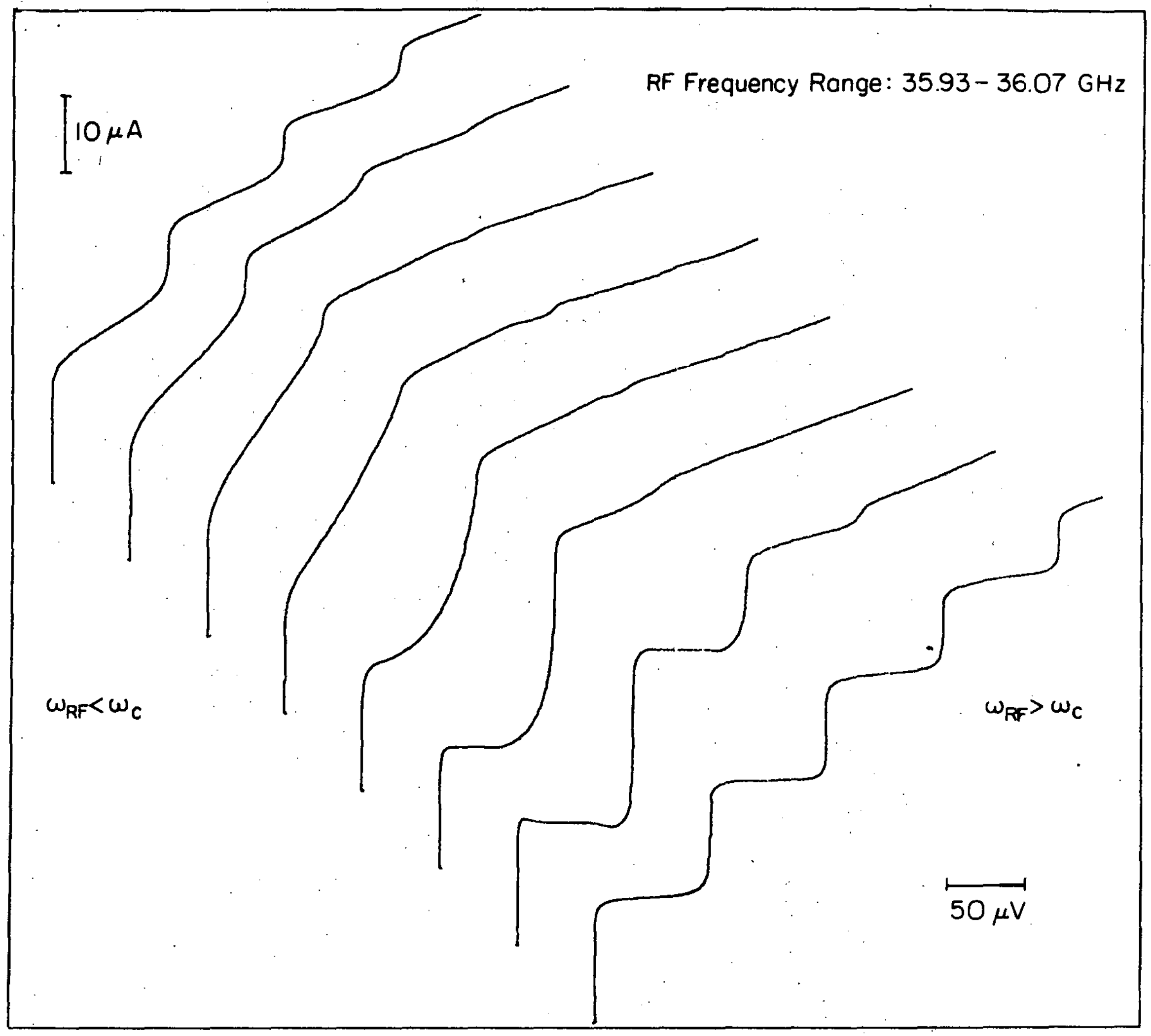

XBL 738-1756

Fig. 18. Change in the I-V curve of a resonantly coupled junction as ω_{RF} is varied relative to ω_c; the RF level was adjusted to produce the same depression of the zero-voltage current in each case, and was minimum for the fourth curve from the left, where $\omega_{RF} = \omega_c$.

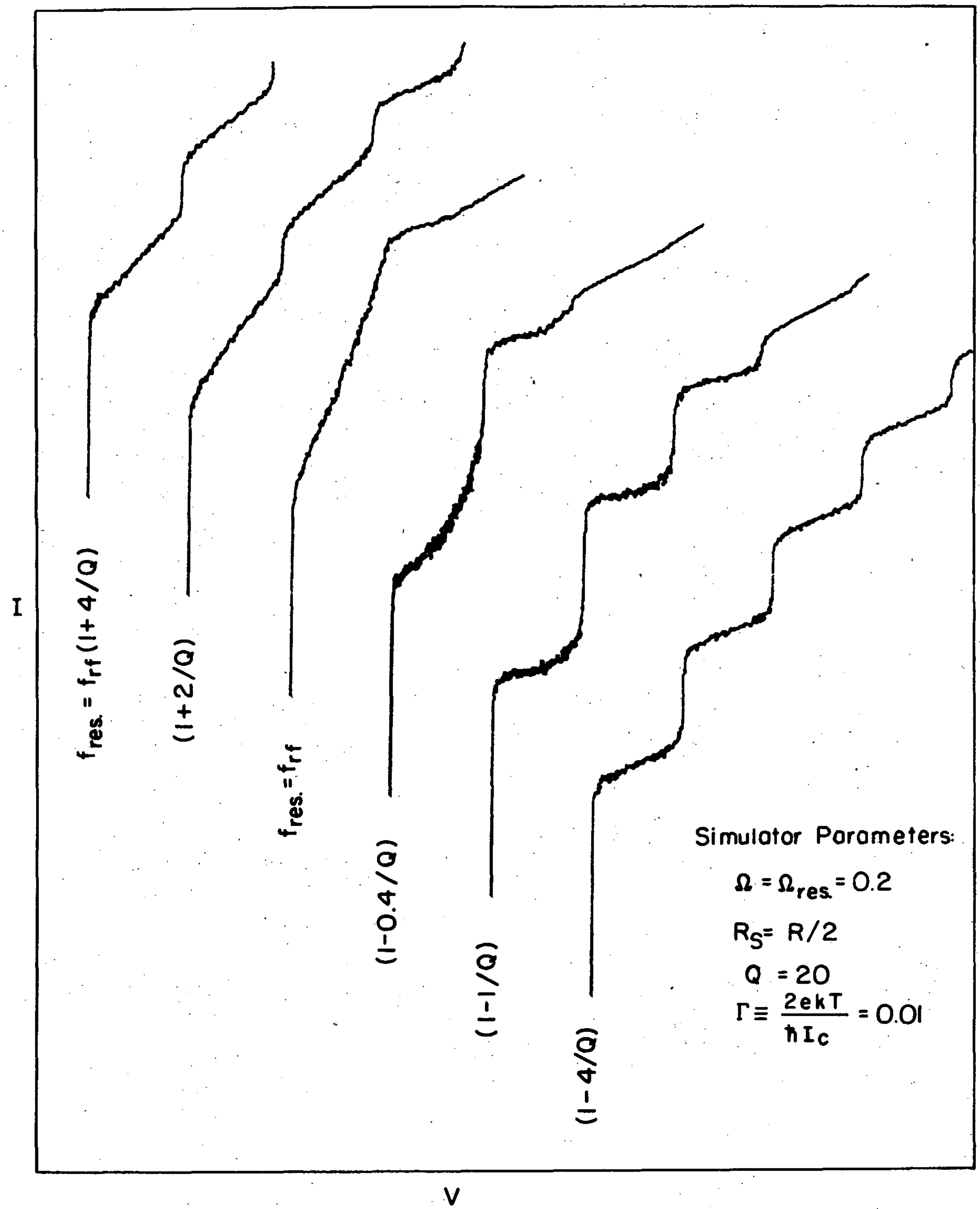

XBL738-1749

Fig. 19. Analog simulation for conditions similar to those of Fig. 18; the parameter Γ characterizes the amount of noise that has been introduced into the simulator to represent Johnson noise in the shunt resistor.

V. FUNDAMENTAL MIXING

A. Theory of a Josephson Effect Mixer

1. Current Source Model

The theory of a resistively shunted Josephson junction operated as a mixer with external local oscillator (LO) was first studied extensively by F. Auracher and T. Van Duzer.[30] Since the experimental result of our 36 GHz point contact mixer will be compared with this theory, we shall describe their model briefly.

Consider the simplest case where the junction is driven by two RF current sources with amplitudes I_{LO}, I_S and frequencies ω_{LO}, ω_S respectively as indicated in Fig. 20(a). The assumptions which were usually made for practical mixers are $|\omega_{IF}| \equiv |\omega_S - \omega_{LO}| \ll \omega_{LO} \approx \omega_S$ and $I_S \ll I_{LO}$, i.e. large frequency ratio and small signal limit. The total RF current flowing through the junction can then be written as

$$I_{LO} \sin \omega_{LO} t + I_S \sin (\omega_s t + \theta)$$

$$\approx [I_{LO} + I_S \cos(\omega_{IF} t + \theta)] \sin[\omega_{LO} t + \frac{I_S}{I_{LO}} \sin(\omega_{IF} t + \theta)] \qquad (16)$$

where we have neglected higher order terms such as $(I_S/I_{LO})^2$.

In the final expression, the phase of the LO current is modulated slowly at a frequency $\omega_{IF} \ll \omega_{LO}$ with a very small amplitude I_S/I_{LO}. Therefore we can neglect this phase modulation and consider the junction driven by an RF current which is amplitude modulated at ω_{IF} by the small signal I_S. This causes the junction I-V curve to move up and

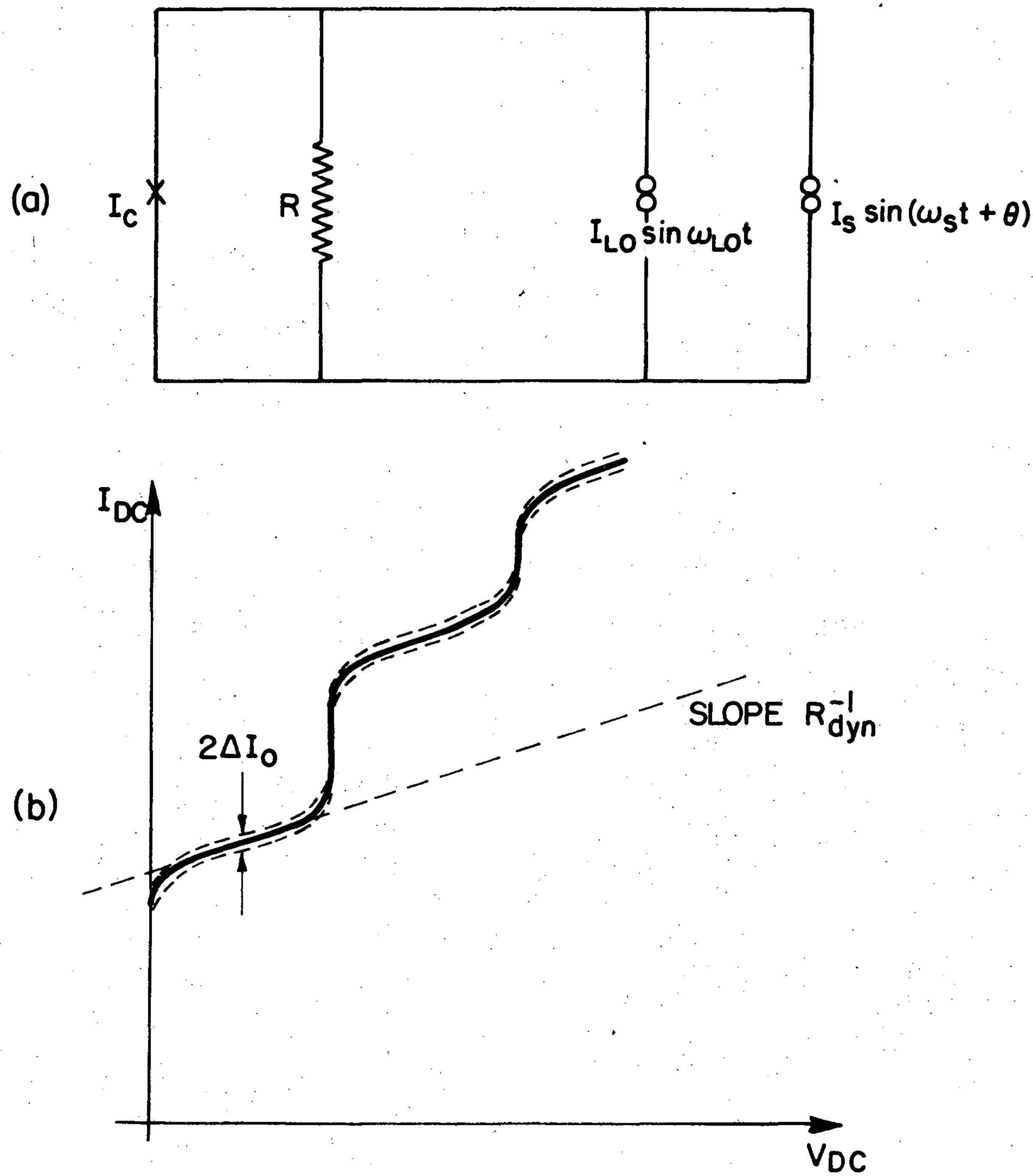

XBL 743-5931

Fig. 20. Equivalent circuit and schematic I-V curve for fundamental mixing with RF current sources.

down at frequency ω_{IF} as illustrated in Fig. 20(b). At bias voltages where the Josephson frequency is much higher than ω_{IF}, the IF response of the junction can be found from a pair of DC I-V curves taken for RF currents with amplitudes $I_{LO}+I_S$ and $I_{LO}-I_S$ respectively.

If the junction is DC biased between the zeroth and first steps, the amplitude of the IF voltage across the junction is $V_{IF} = R_{dyn}\Delta I_o$. Here $R_{dyn} = dV_{DC}/dI_{DC}$ is the inverse slope of the I-V curve at the bias point and $\Delta I_o = I_S|\partial I_o/\partial I_{LO}|$ is the amount of the zero-voltage step modulated by the signal current. We have discussed in Section IV.A that the best value of I_{LO} which gives a large value of $|\partial I_o/\partial I_{LO}|$ is such that I_o is suppressed to approximately $I_c/2$. Under this condition we have

$$V_{IF} = R_{dyn}\ I_S \left|\frac{\partial I_o}{\partial I_{LO}}\right|_{I_o=I_c/2} \tag{17}$$

In principle, one can also bias the junction between higher order steps and obtain IF voltages related to $|\partial I_1/\partial I_{LO}|$, $|\partial I_2/\partial I_{LO}|$ etc. But it was found experimentally that the results are not as good because higher order steps are generally small and rounded by noise. Consequently, we shall restrict ourselves to the situation where the junction is biased between the zeroth and first steps.

F. Auracher and T. Van Duzer[22,30] checked their model by using a digital computer to solve the exact equation

$$\frac{\hbar}{2eR}\frac{d\phi}{dt} + I_c \sin\phi = I_{DC} + I_{LO}\sin\omega_{LO}t + I_S \sin(\omega_S t + \theta) \tag{18}$$

for V(t). Then they computed the Fourier component of V(t) at ω_{IF} for a wide range of parameters and found good agreement with Eq. (17). This confirms the simple current modulation model and allows us to calculate the IF voltage from Eq. (17).

2. An Expression for the Conversion Efficiency

The most important quantity in a practical mixer is the over-all conversion efficiency η defined by

$$\eta = \frac{\text{the amount of IF power delivered to the IF amplifier}}{\text{the amount of RF power available from the signal source}} \tag{19}$$

In order to find an expression for η in a Josephson effect mixer, we have to assume a finite RF source resistance R_S as shown in Fig. 21(a), where $P_S = R_S I_S{}^2/8$ and $P_{LO} = R_S I_{LO}{}^2/8$ respectively. The IF load has no effect on this circuit since it is practically isolated from the junction at RF frequencies.

In Fig. 21(b) we show the IF equivalent circuit of the junction with V_{IF} given by Eq. (17). In this circuit the IF source resistance of the junction is simply R_{dyn} since we are working with intermediate frequencies much lower than the Josephson frequency. The available IF power from the junction is then $P_{IF} = V_{IF}{}^2/8R_{dyn} = (1/8)R_{dyn} I_S{}^2 \times \left[(\partial I_o/\partial I_{LO})^2\right]_{I_o = I_c/2}$. Supposing C_{IF} is the coupling efficiency between the junction and the IF amplifier, we have

$$\begin{aligned} \eta &= \frac{C_{IF} P_{IF}}{P_S} = C_{IF} \frac{R_{dyn}}{R_S} \left(\frac{\partial I_o}{\partial I_{LO}}\right)^2_{I_o = I_c/2} \\ &= C_{IF} \frac{R_{dyn}}{R} \left\{\frac{\partial I_o}{\partial[(8P_{LO}/R)^{1/2}]}\right\}^2_{I_o = I_c/2} = C_{IF} \frac{R_{dyn}}{R} \alpha^2(\Omega, R_S/R) \end{aligned} \tag{20}$$

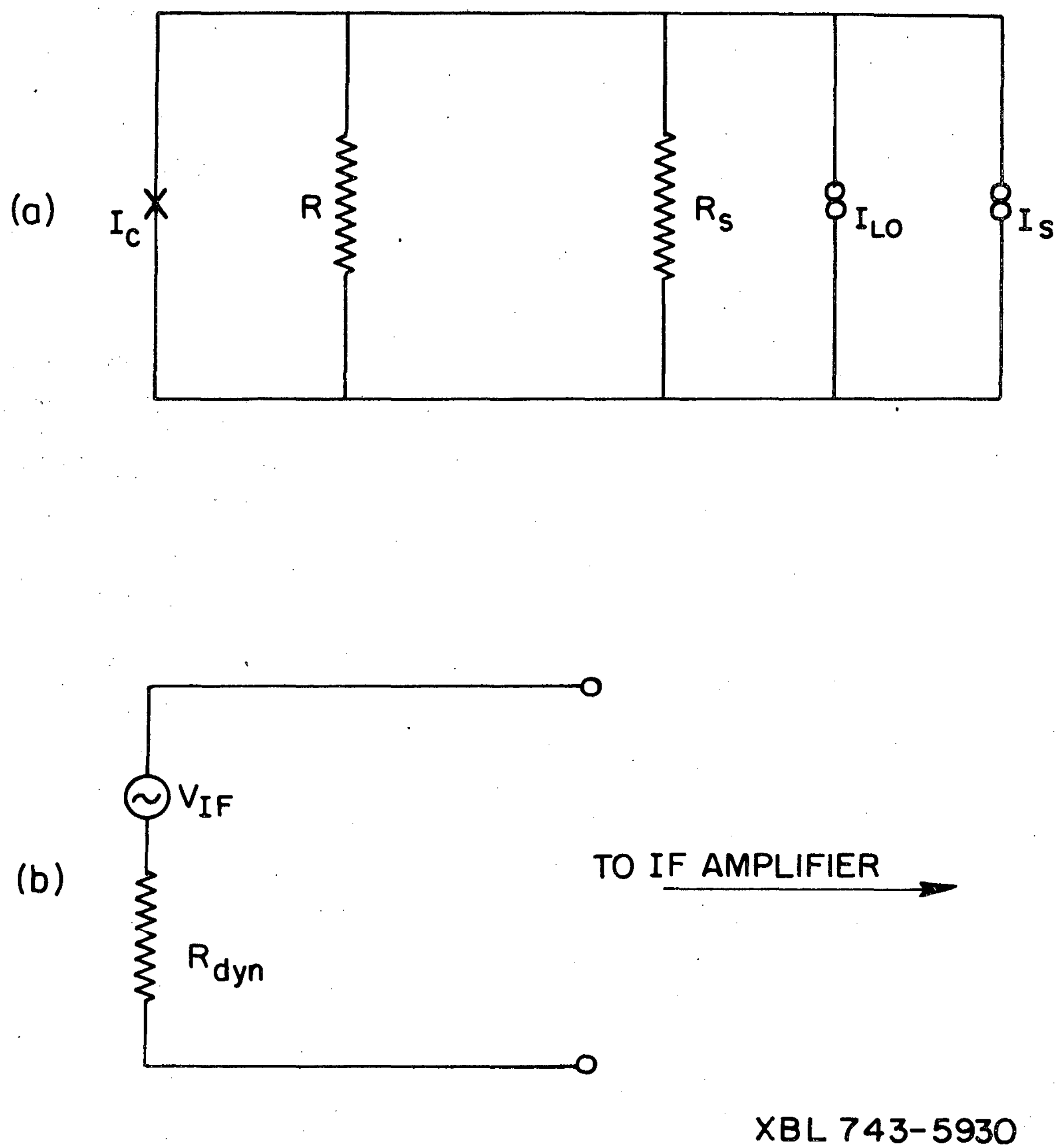

Fig. 21. The RF and IF equivalent circuits of a Josephson mixer for the case of broadband RF coupling.

Here the factor R_{dyn}/R is a strong function of the junction noise; while α^2, the RF coupling parameter described in Section IV, is independent of noise. This equation expresses η in terms of experimentally measurable quantities and is very important in predicting the performance of a Josephson mixer. It is implicitly stated in Eq. (20) that η is not sensitive to the frequency ratio ω_{IF}/ω_S.

Although Eq. (20) is derived mainly for the case of broadband RF coupling, it should also be valid when the junction is coupled to RF sources via a resonant circuit. This has been confirmed by J. Claassen[31] using the Josephson junction simulator to show that Eq. (20) gives the correct answer if Q of the resonant coupling is sufficiently low that the source impedance of the LO seen by the junction is the same as that of the signal, i.e. $Q < \omega_S/\omega_{IF} \approx 1000$, which is always the case in our experiments. He also verified the IF equivalent circuit in Fig. 21(b) by measuring IF voltages across the junction in the presence of several different IF loads.

B. Experimental Procedure

1. Measurement of IF Power and Coupling Efficiency

In order to calculate the experimental value of conversion efficiency, we have to measure the amount of IF signal power delivered to the amplifier. This is done by displaying the amplified IF signal at 50 MHz on a spectrum analyzer with scales calibrated by a matched Wavetek oscillator as shown in Fig. 3. In Fig. 22 we show a pair of

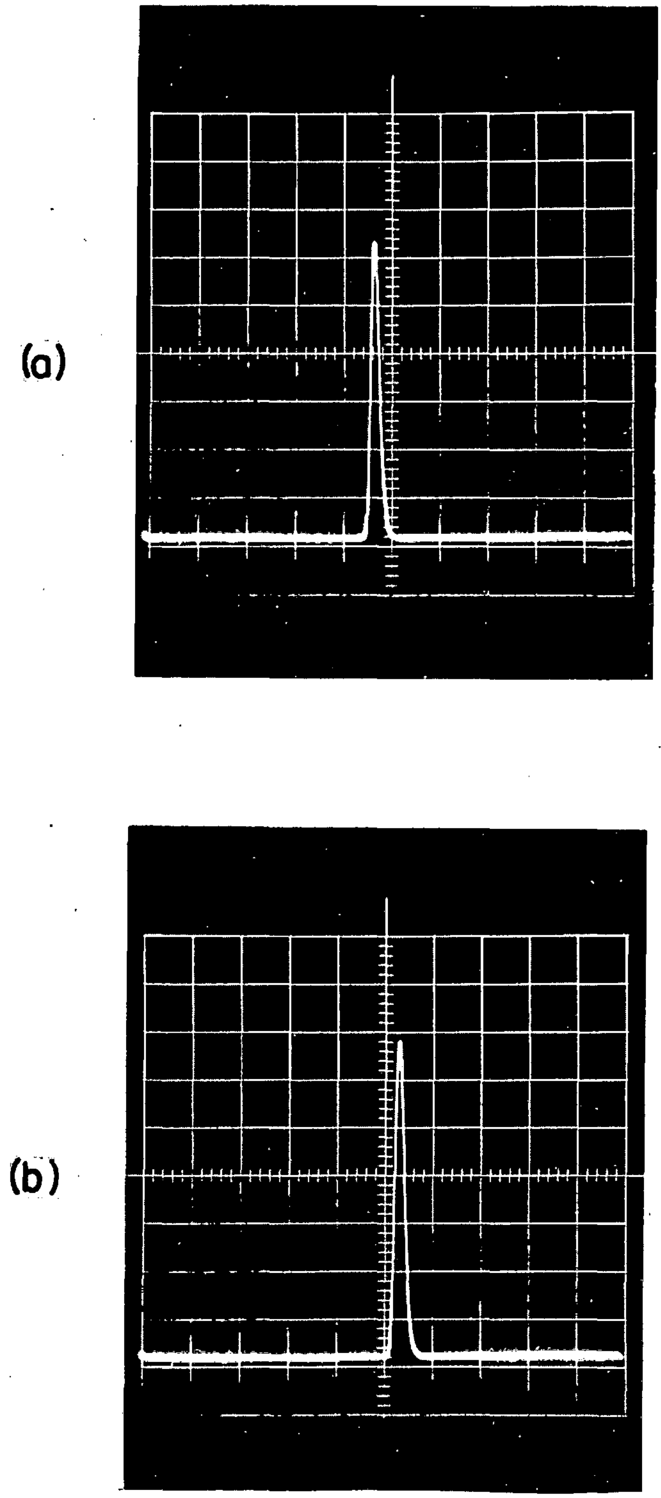

XBB 743-2050

Fig. 22. Spectrum analyzer display of (a) IF signal from the junction and (b) calibrated signal from the Wavetek oscillator; the apparent linewidths of both signals are limited by the resolution bandwidth to be 100 kHz (the horizontal scale of both displays is 500 kHz/div).

pictures for both the real IF signal and the signal (10^{-12} W refer to the input of the amplifier) from the Wavetek oscillator. Since the resolution bandwidth of the spectrum analyzer is set (100 kHz in most cases) to be larger than the actual linewidths of both signals, we can determine the amount of IF power from its height on the display.

The coupling efficiency C_{IF} is defined as the amount of IF signal power coupled to the amplifier divided by the available IF power from the junction. It depends upon the IF resistance R_{dyn} of the junction. In order to measure C_{IF} we keep the IF configuration (such as cables, connectors, etc.) unchanged but replace the superconducting wires with copper wires to form metal to metal point contact which we assume behaves as an ordinary resistor with Johnson noise (this will be discussed in Section VI.A). Since the available noise power from a Johnson noise resistor is simply kTB, C_{IF} can be determined by measuring the coupled Johnson noise power within a bandwidth of 50 MHz ± 10 MHz from the resistive point contact. To subtract off the amplifier noise contribution, we vary the junction temperature from 300 K to 77 K and compare the difference in the coupled noise power (P_j) to that of a matched load (P_m) immediately in front of the IF amplifier. Using the formula $C_{IF} = [P_j(300\text{ K})-P_j(77\text{ K})]/[P_m(300\text{ K})-P_m(77\text{ K})]$ (the denominator is a measure of k(300 K-77 K)B), we obtain IF coupling efficiencies for a range of junction resistance shown in Fig. 23.

In our experiments, the IF source resistance R_{dyn} of the junction is usually within the range of 20 to 90 ohms. Figure 23 shows that C_{IF} is between 0.8 and 0.9 in this range.

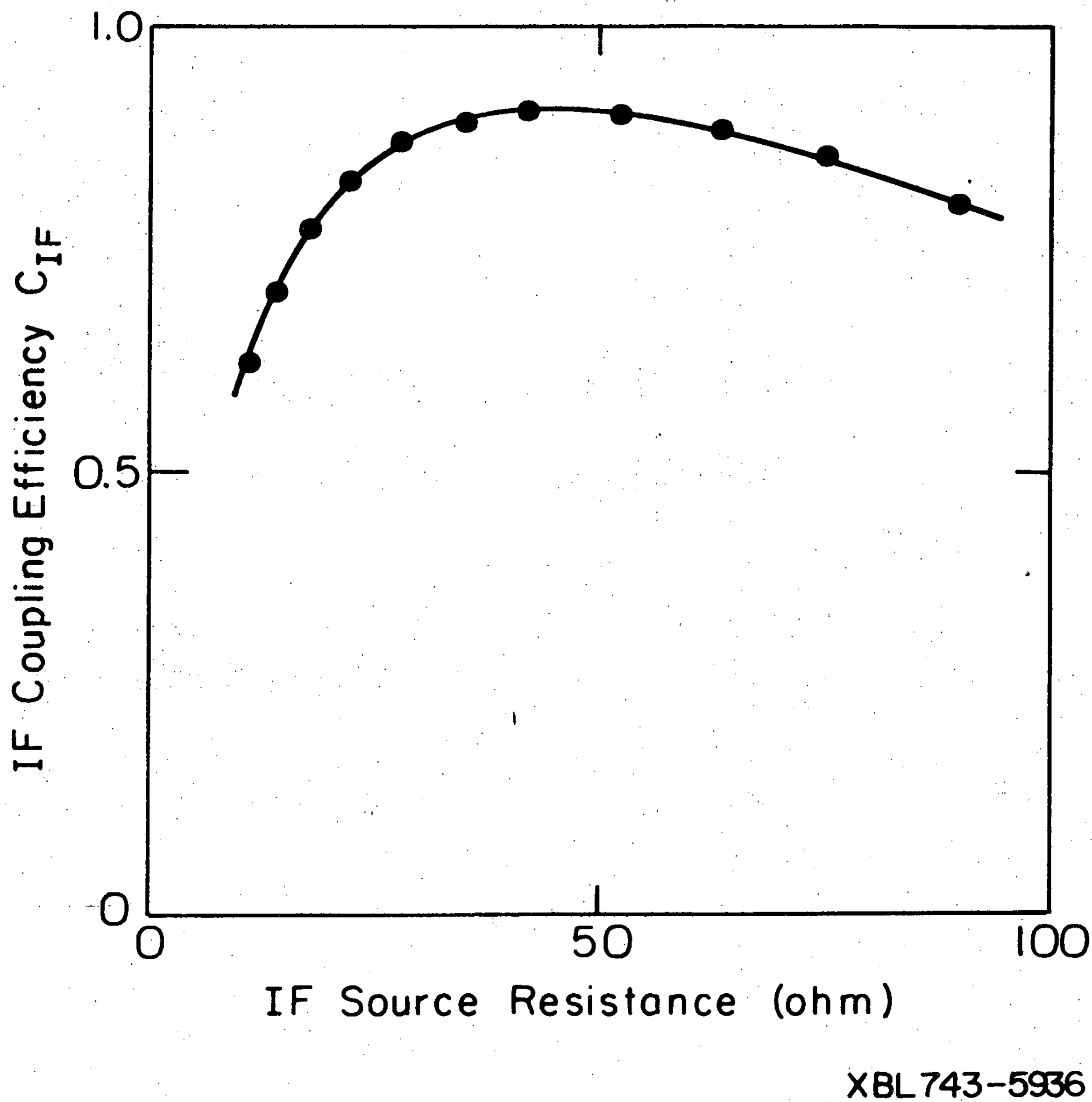

Fig. 23. Measured values of the IF coupling efficiency as a function of source resistance.

2. The Kind of Junctions Used for Mixing

It was mentioned in Section IV that we were able to achieve very good RF coupling for junctions with $R \gtrsim 10$ ohms and the bandwidth of the RF coupling increases with R. In practice, there is an upper limit for R of the order of 50 ohms due to mechanical instabilities. Therefore, most of our mixing data were obtained from junctions with resistances in the range of 10 to 50 ohms.

In order to obtain large values of α^2, it is desirable to work with junctions having small normalized frequencies, i.e., large RI_c products. However, junctions with large RI_c ($< \Delta/e$) are more likely to show hysteresis and cannot be biased between lower order steps. To avoid this problem we control the temperature and thus the critical current of the junction such that there is no hysteresis on the I - V curve. For niobium point contacts we often operate at temperatures above 4.2 K and the smallest normalized frequency achieved without hysteresis is approximately 0.2. Vanadium point contacts can be operated down to 1.4 K without hysteresis, with normalized frequencies typically in the range from 0.3 to 0.4.

Another parameter in Eq. (20) is the normalized dynamical resistance at the bias point. Since the portions of the I - V curve near the steps are always rounded by noise, it is best to bias the junction midway between the zeroth and first steps.

C. Experimental Results

1. Conversion Efficiency (Gain)

In Table I we summarize the mixing data of several well-coupled junctions, where η_{exp} is the conversion efficiency obtained by taking ratios of the measured IF and RF powers. Other parameters such as R_{dyn}, C_{IF}, and α^2_{exp} are independently determined from the junction I-V curves. It was found that η_{exp} agrees very well with the prediction of Eq. (20) and is insensitive to the sign and magnitude of $\omega_{IF} = \omega_S - \omega_{LO}$ as long as both the RF and the IF coupling efficiencies stay constant (this will be discussed later). This shows that Auracher-Van Duzer's mixing model can be applied to our point contact junctions.

The dependence of η_{exp} on bias voltages is shown in Fig. 24. As expected, large values of IF output were observed midway between induced steps where R_{dyn} reaches its maximum and the highest peak occurs between the zeroth and first steps. We also found that η_{exp} is not very sensitive to the amount of LO power applied as long as the zero-voltage current is suppressed to about 0.2 to 0.5 of its original value I_c in the first period, which corresponds to a local oscillator power level of $0.1\ RI_c^2 \approx 10^{-9}$ W. In this range both α^2 and R_{dyn}/R are nearly constant, as described in Section IV. A.

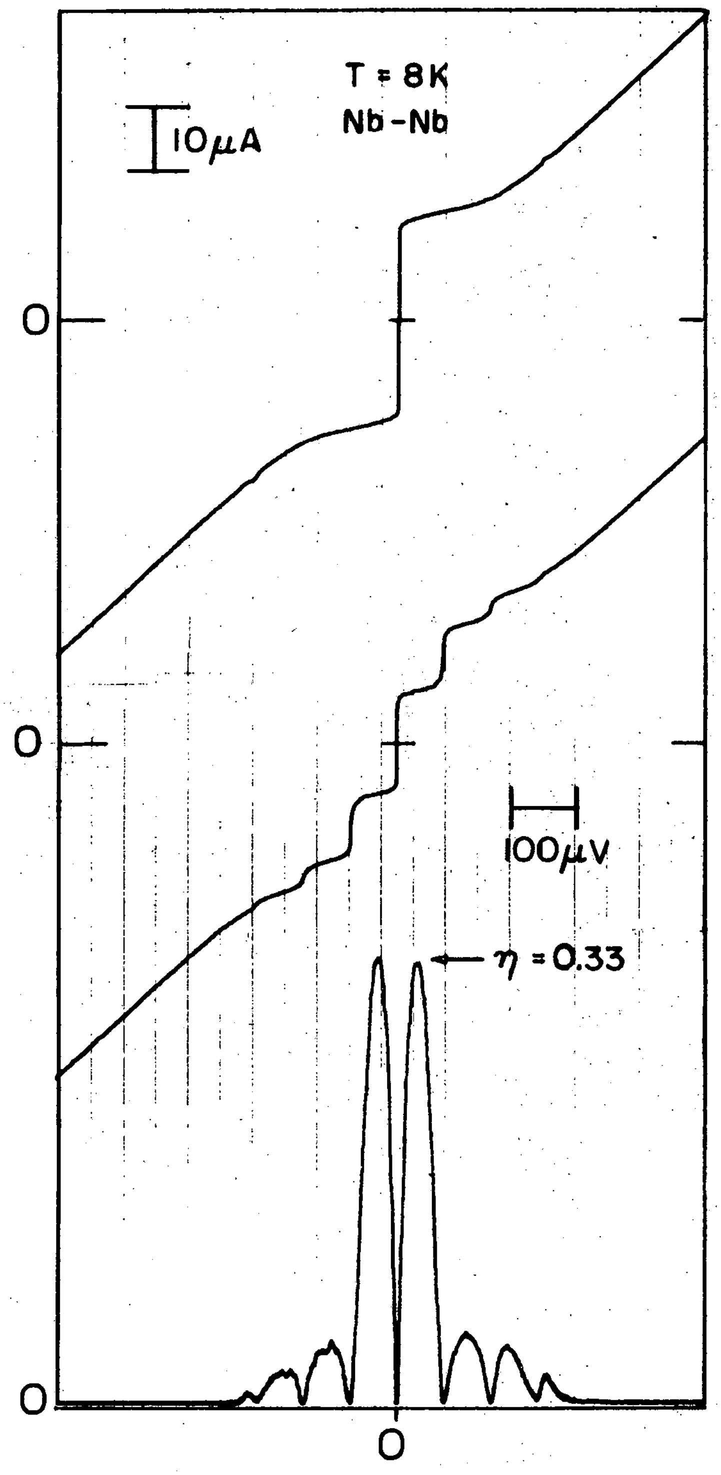

XBL 743-5917

Fig. 24. Static I-V curves for P_{LO}=0 and $P_{LO}\approx 10^{-9}$ W and conversion efficiency for fundamental mixing as a function of bias voltage.

2. Discussion of Conversion Gain

Values of η_{exp} greater than unity have been observed in our experiments whenever the product $C_{IF}(R_{dyn}/R)\alpha^2_{exp}$ is larger than one; a typical example is given in Fig. 25. In this case η should be called the conversion "gain". We shall discuss this interesting result obtained from junctions with positive IF resistance.

It is well known that the conversion efficiency of a non-linear reactance down-converter is limited by the frequency ratio ω_{IF}/ω_S if $\omega_S > \omega_{LO}$. This result is derived from the Manley-Rowe relations[32] under the assumption that power exchange only takes place at frequencies ω_{LO}, ω_S, and ω_{IF}. However, this assumption is not valid in Josephson point contacts since the shunt resistof allows power dissipation at all frequencies. Consequently, the Manley-Rowe relations do not set any upper limit for the conversion efficiency of our Josephson effect mixer.

Apart from the possibility of obtaining conversion gain, Josephson junctions aperated in our mixing mode are very similar to resistive mixers[33] since the conversion efficiency is observed to be insensitive to the sign and magnitude of $\omega_{IF} = \omega_S - \omega_{LO}$. Perhaps the best way to explain the conversion gain is to attribute it to the ratio of the junction IF resistance R_{dyn} to the RF resistance $(R_S)_{opt}$, which is always larger than one. For junctions with small normalized frequencies, the amplitude of the IF current is equal to that of the signal current and conversion gains up to $R_{dyn}/(R_S)_{opt}$ can be achieved. This can be seen by estimating the maximum value of η in the limit of $\Omega \ll 1$:

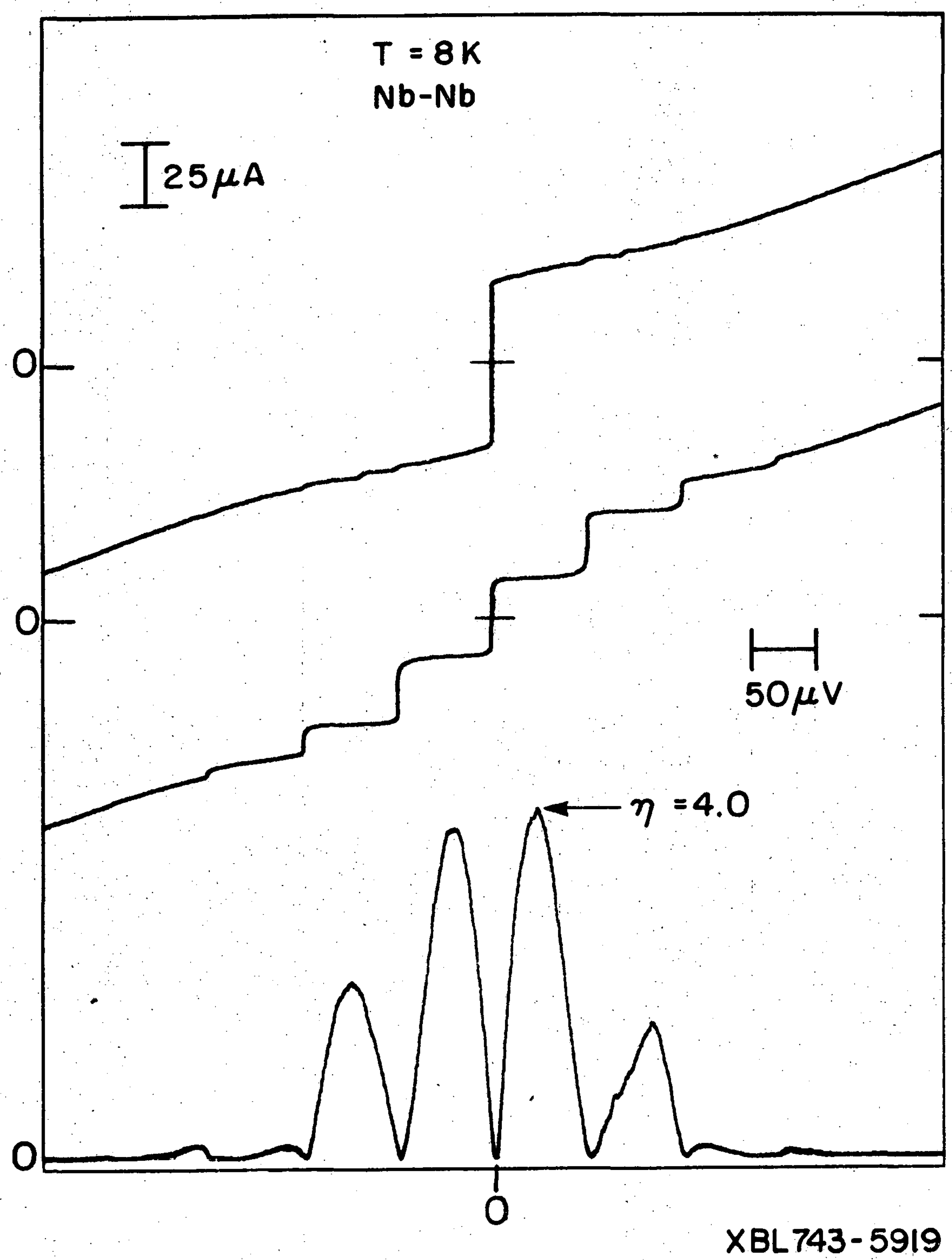

Fig. 25. Data similar to those in Fig. 24, but with conversion gain.

$$\eta_{max} = \alpha^2_{opt} \frac{R_{dyn}}{R} \approx \frac{0.25}{\Omega} \frac{R_{dyn}}{R} \lesssim \frac{R_{dyn}}{(R_S)_{opt}} \tag{21}$$

Here we have used Eq. (13) for α^2_{opt} and $(R_S)_{opt}/R$. At larger normalized frequencies however, part of the signal current flows in the shunt resistor and the amount of IF current is reduced. Therefore, it is less likely to obtain conversion gain from junctions with $\Omega \gtrsim 0.5$ although the resistance ratio $R_{dyn}/(R_S)_{opt}$ can still be large for such junctions.

3. Bandwidth and Dynamic Range

The bandwidth of our mixer can be limited by either the IF or the RF coupling circuit. The upper limit of the intermediate frequency is set by the capacitance between the niobium flange and waveguide to be $1/(2\pi \times 50$ ohm $\times$ 10 pF) $\approx$ 300 MHz. This number should be multiplied by two to be compared with the full RF coupling bandwidth. In Fig. 26 we plot the measured conversion efficiency versus $\omega_{IF} = \omega_S - \omega_{LO}$ for a niobium junction, which has a mixing bandwidth limited by the IF coupling to approximately 600 MHz. The asymmetry of the curve around $\omega_{IF} = 0$, however, is caused by the RF coupling circuit (see Fig. 16).

The dynamic range of a Josephson mixer is expected to be proportional to the product RI_c^2 of the junction. In Fig. 27 we plot the IF output power against RF signal power, both in normalized units, for two well-coupled junctions. The response is linear in the small signal limit as it should be and becomes saturated at a power level

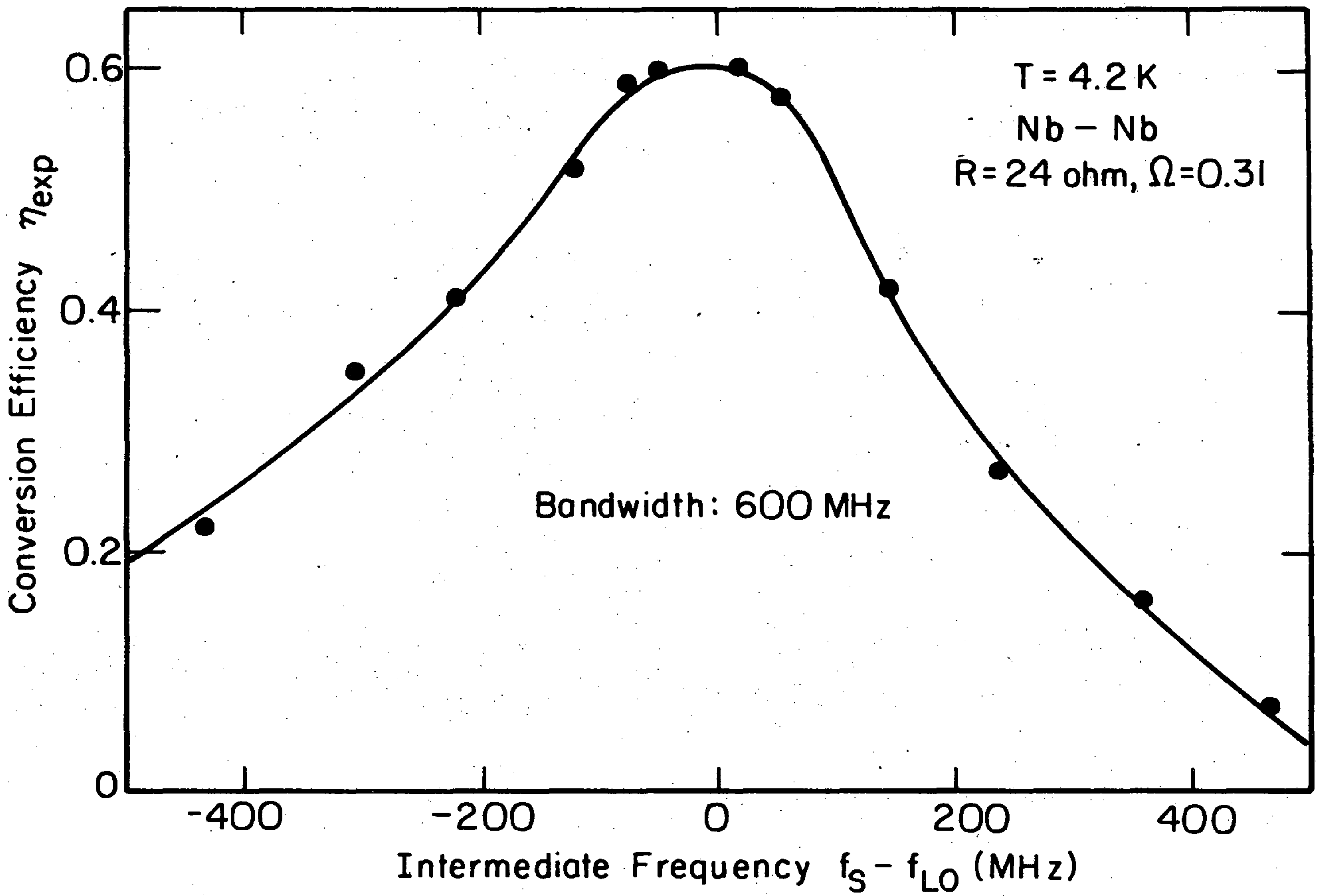

XBL 743-5937

Fig. 26. Bandwidth of a Josephson junction mixer; data obtained with f_{LO}, P_{LO}, and V_{DC} unchanged.

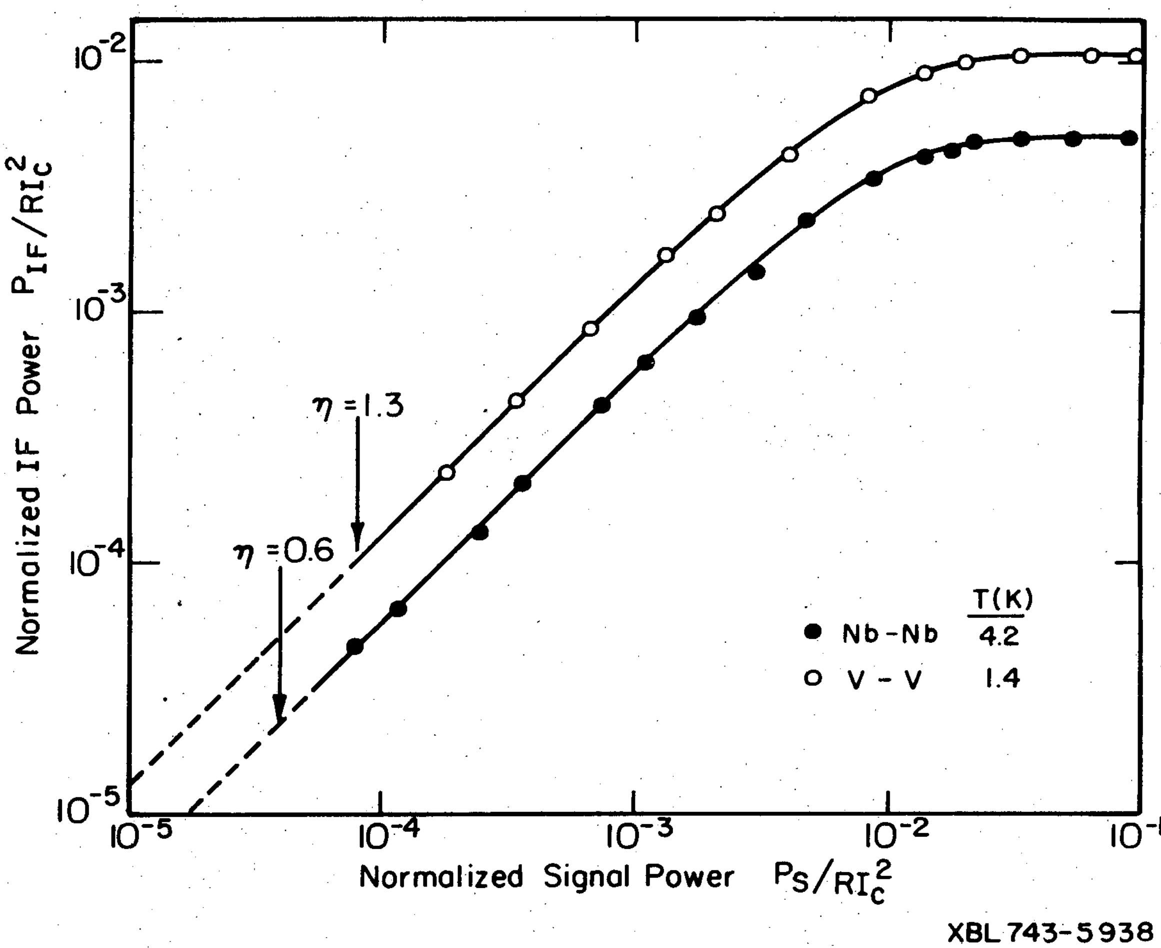

Fig. 27. Dynamical range of mixing; the product RI_c^2 is 4.8 nW for the solid circles and 2.1 nW for the open circles.

approximately equal to 0.01 RI_c^2 . This number is typically of the order of 10^{-10} W, compared with a noise limit approximately 10^{-17} W for a resolution bandwidth of 100 kHz and a postdetection bandwidth of 1 kHz (typical numbers for the spectrum analyzer we used).

VI. JUNCTION NOISE

A. Noise Measurement

1. Noise Temperature of a Josephson Junction

The sensitivity of a Josephson device is mainly limited by the intrinsic noise in the junction. We are interested in studying the noise properties of a point contact junction in the intermediate frequency range--which is much lower than the LO frequency or the Josephson frequency. Analytical calculation of this problem is very difficult because the local oscillator and Josephson oscillation can mix the junction noise in complicated ways. We shall develop a model to treat this problem assuming that the Johnson noise of the shunt resistor is the only source of noise in our point contacts.

The circuit of a resistively shunted Josephson junction including Johnson noise is shown in Fig. 28(a) where T is the ambient temperature of the junction and i_n is the Johnson noise current, which has a white spectrum up to frequencies higher than all other frequencies of interest. Since R_{dyn} is the resistance of the junction at frequencies much lower than the Josephson frequency, the low-frequency noise equivalent circuit of the junction can be drawn as in Fig. 28(b). Here I_n represents the amount of current noise in the limit of zero frequency and we define a dimensionless noise parameter β to be the ratio of this low-frequency noise current to the original Johnson noise current of the shunt resistor.

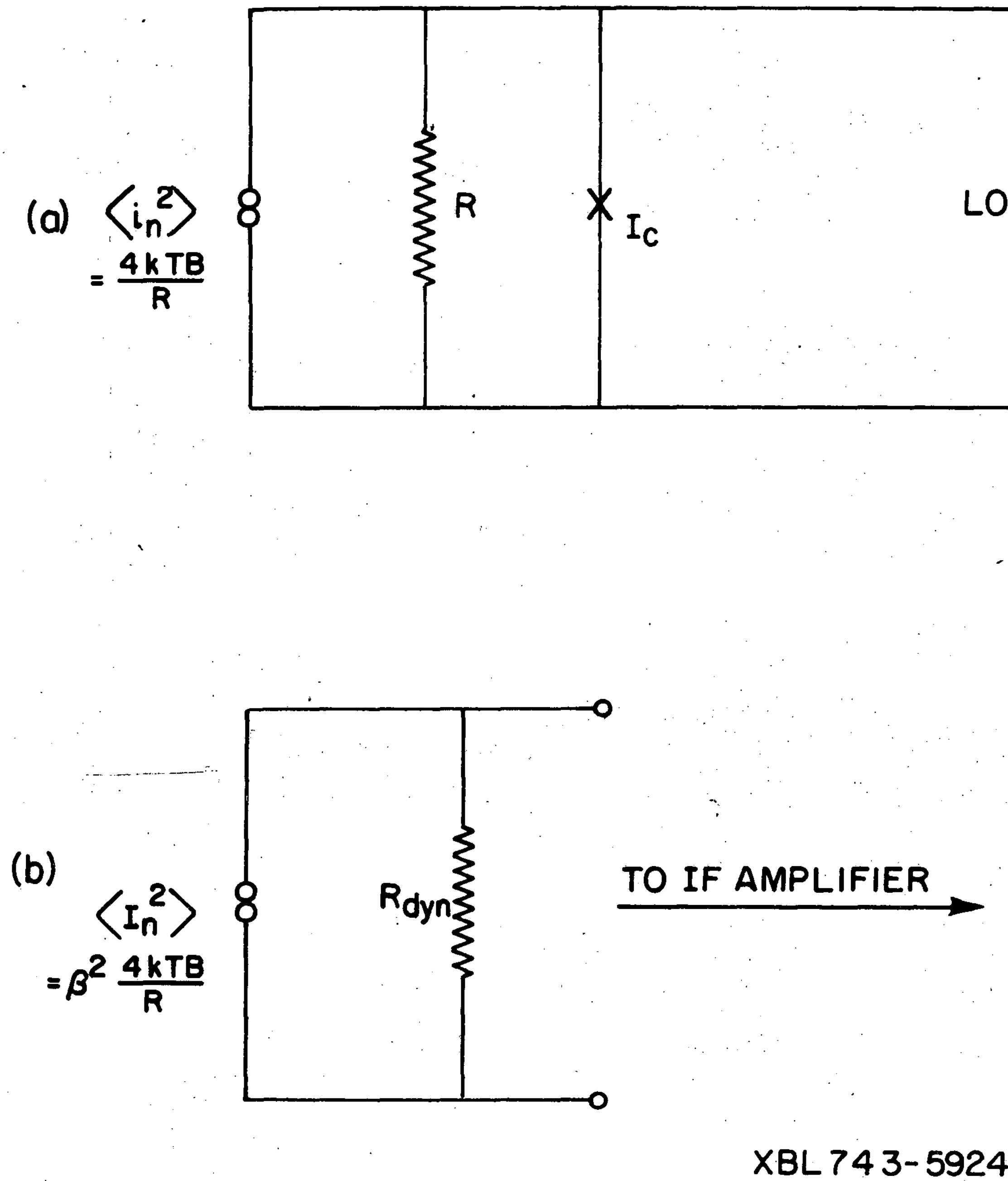

Fig. 28. Noise equivalent circuits of a resistively shunted Josephson junction with Johnson noise.

It is obvious that the noise parameter β must be greater than unity since 4kTB/R is the least amount of low-frequency noise one would expect in a Josephson junction with shunt resistance R. In fact, β is a very complicated function of all junction parameters and it can be enhanced appreciably over unity by various mixing processes or the presence of resonant circuit and shunt capacitance.

In Fig. 28(b) the available low-frequency noise power from the junction is $(1/4)\ R_{dyn} \langle I_n^2 \rangle = k(\beta^2\ (R_{dyn}/R)T)B$. Therefore we can define an effective low-frequency noise temperature for the junction as

$$T_N \equiv \beta^2 (R_{dyn}/R)T \tag{22}$$

In this representation, the low-frequency noise properties of a Josephson junction are equivalent to the Johnson noise of a resistor with resistance R_{dyn} at temperature T_N.

2. Calibration of IF Amplifier Noise

In addition to the shielding arrangement shown in Fig. 2, our noise measurements were performed in a basement room to avoid pick-up noise. As described in Section II.C, we measure the junction noise using an IF power meter whose output is proportional to the amplified noise power within a bandwidth around 50 MHz determined by the bandpass filter in front of it. The total noise power P_N consists of noise from the junction and noise contributed by the front end of the IF amplifiers (110 K at 50 ohms). It can be written as

$$P_N = f(R_{dyn}) + g(R_{dyn})T_N \tag{23}$$

Here $g(R_{dyn})$ is proportional to the IF coupling efficiency C_{IF} which depends upon the low frequency junction resistance R_{dyn}; and $f(R_{dyn})$ is proportional to the IF amplifier noise which is the sum of a constant term representing amplifier noise in the matched case and the amount of amplifier noise reflected by the junction.

In order to obtain T_N, we must calibrate functions f and g for a range of possible values of R_{dyn}. This was done by using the copper point contact junction described in Section V.B, which we assume has a noise temperature equal to its physical temperature T. At three different temperatures (300 K, 77 K, and 4.2 K) we adjust the resistance R_g of the copper point contact to different values between 10 and 100 ohms and measure the total noise power P_N. The results of these noise calibrations are shown as three curves in Fig. 29 and we can deduce functions f and g from any two of them.

We checked our method by plotting P_N versus T for several different values of R_g shown in Fig. 30. The data points lie on straight lines as they should within an experimental error of ± 5 K. This makes us believe that there is no other source of noise in our copper point contacts besides Johnson noise. Furthermore, we have done these noise measurements several times and the results are all consistent, which implies that the RF pick-up noise is negligible in our system.

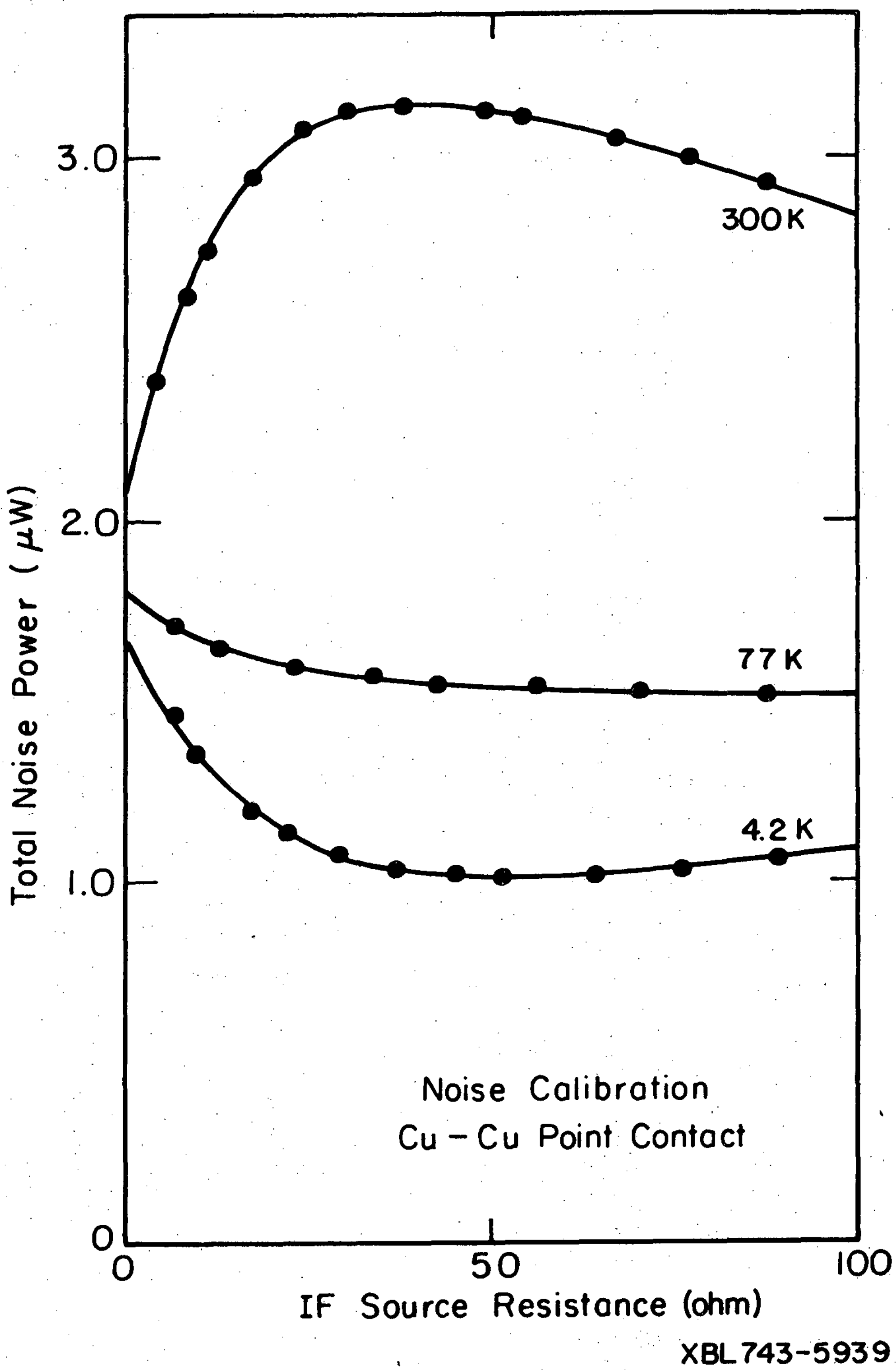

Fig. 29. Data used to calibrate the IF amplifier noise contribution; the amplifier noise is minimum for a source resistance of 50 ohms.

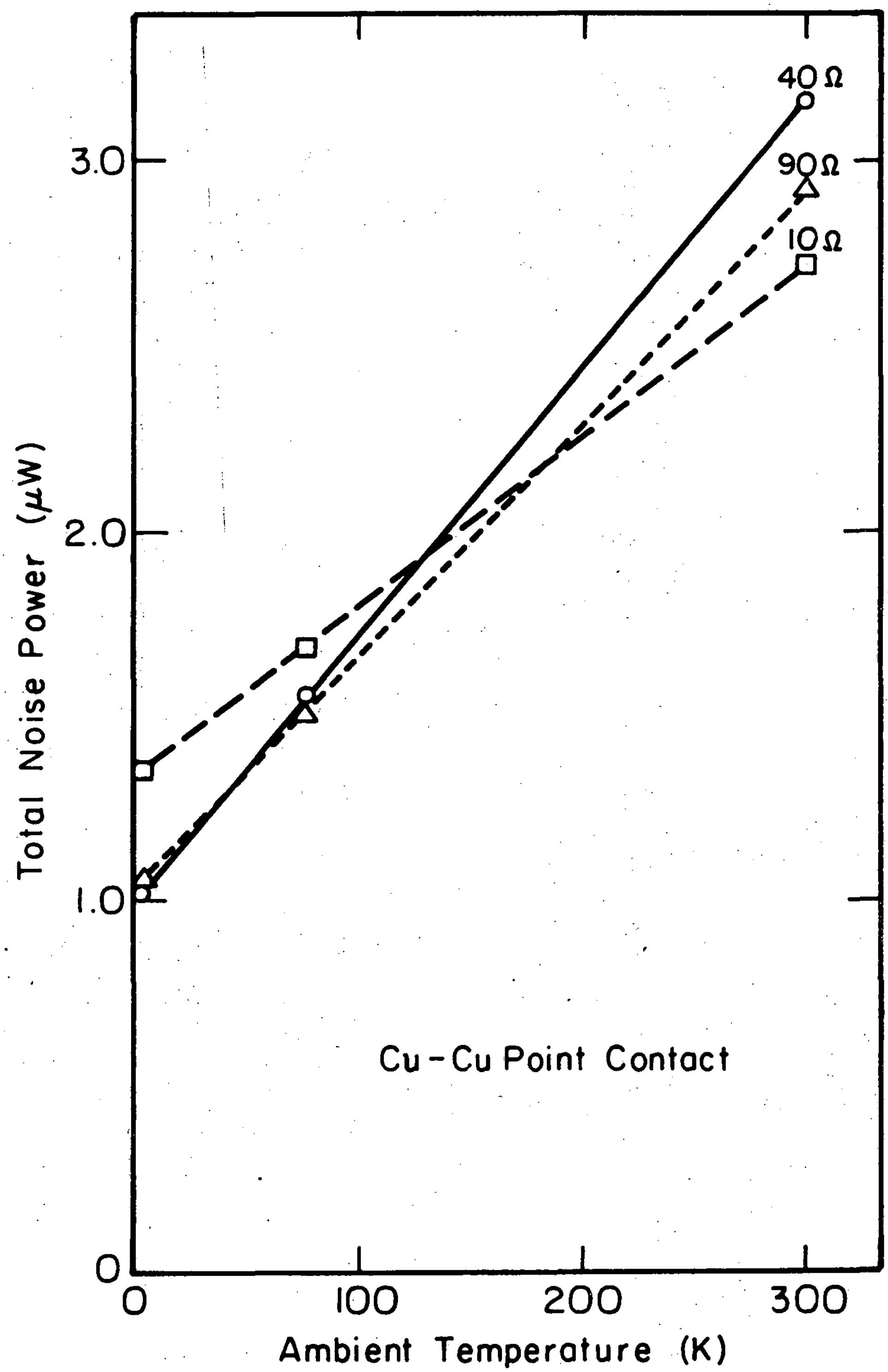

Fig. 30. Total noise power versus temperature of various source resistances, obtained from Fig. 29; the slope of each line is proportional to the IF coupling efficiency for the corresponding IF source resistance.

With the information of f and g we can determine the effective noise temperature T_N of a point contact Josephson junction by measuring the total noise power P_N and the dynamic resistance R_{dyn} at the bias point. For convenience our data will be presented in the form of the dimensionless noise parameter β^2 which is related to T_N by Eq. (22).

3. Experimental Results and Comparison with Theory

In order to make comparisons with theory, our data in this section were obtained without the matching structure. The complete equation which describes a resistively shunted junction with Johnson noise is then

$$\frac{d\phi}{d\tau} + \sin\phi = \alpha_{DC} + \alpha_{RF} \sin \Omega\tau + \alpha_n(\tau) \tag{24}$$

This is written in normalized units as in Eq. (8). In this equation $\alpha_n(\tau)$ represents Johnson noise current which has a correlation function $\langle \alpha_n(\tau)\alpha_n(\tau') \rangle = 2\Gamma\delta(\tau-\tau')$. Here $\Gamma \equiv 2ekT/\hbar I_c$ is a dimensionless parameter which specifies the relative magnitude of Johnson noise in a Josephson junction and determines the amount of noise rounding[34] on the I - V curve. The noise parameter β is proportional to the voltage fluctuations in the zero frequency limit and depends upon α_{DC}, α_{RF}, Ω, and Γ. J. Claassen[31] has used his Josephson junction simulator to solve Eq. (24) for β^2 under various circumstances. His results will be compared with our experimental data.

In Fig. 31 we show the measured values of β^2 at different bias voltages with and without microwaves for a niobium junction at 8 K, together with its static I - V curves. As expected β^2 approaches

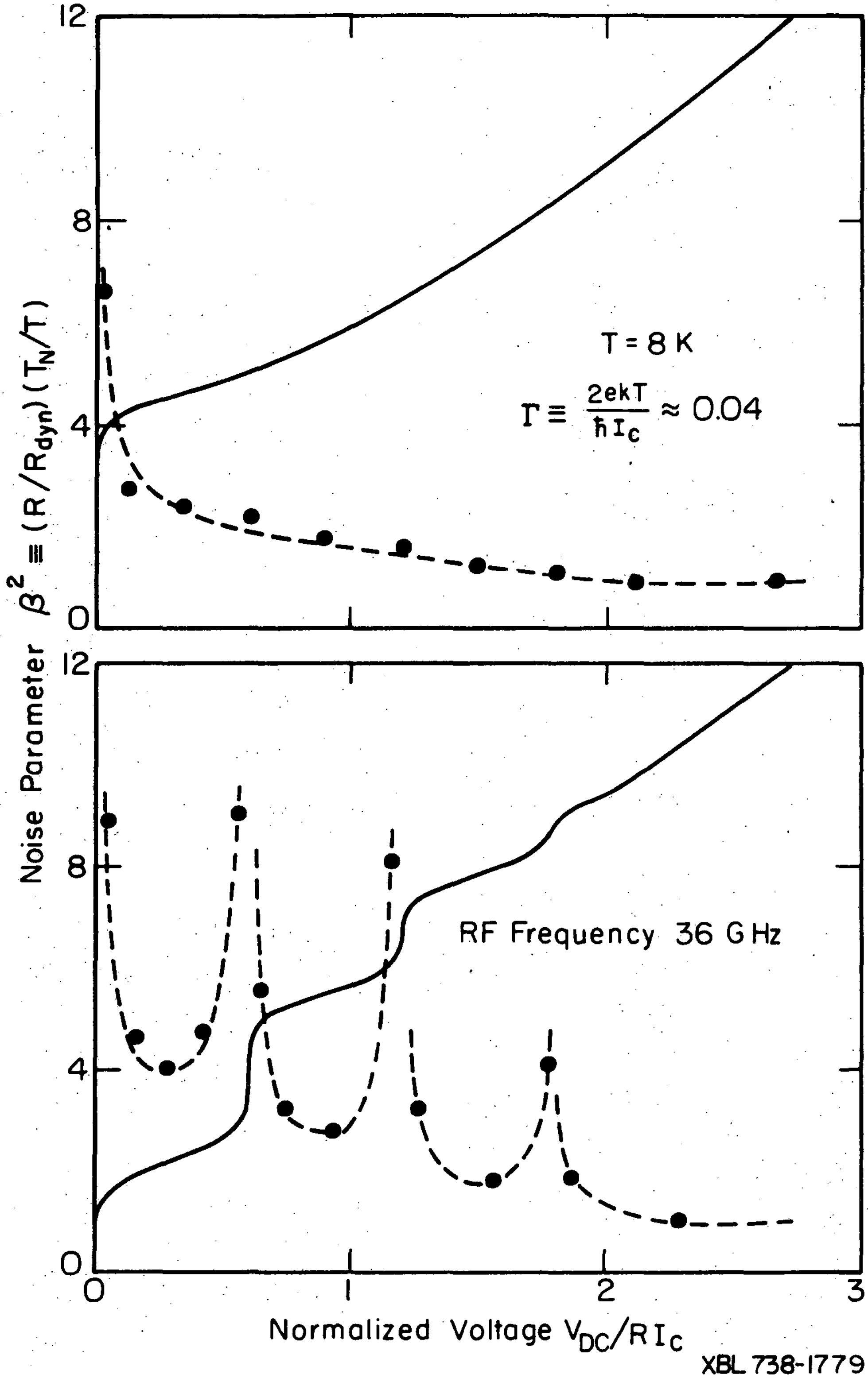

Fig. 31. Noise parameter β^2 measured as a function of bias voltage for $P_{LO}=0$ and $P_{LO}\neq 0$ (RF current source) with the corresponding I-V curves.

unity at large bias voltages where the junction is equivalent to a resistor with resistance R at temperature T (this is another evidence showing that pick-up noise is negligible). However, β^2 increases sharply when the junction is biased close to the zero-voltage step where the I - V curve shows severe rounding. We believe that this is caused by non-linear interactions between Johnson noise and AC Josephson currents which convert a large amount of high frequency noise to low frequency noise. Similar behavior of β^2 is observed near microwave induced steps where the applied RF current also takes part in the mixing processes. The data in Fig. 31 are compared with the result of the junction simulator shown in Fig. 32, which was obtained by using similar values of Ω and Γ. The agreement is very good both in shapes of the curves and in magnitudes of β^2.

In our mixing experiments, we are particularly interested in the values of β^2 at a bias voltage midway between the zeroth and first steps when I_o is suppressed by the applied RF to approximately $I_c/2$. We shall refer to the noise parameter under these conditions as $\beta_o{}^2$. Using the simulator, J. Claassen has calculated $\beta_o{}^2$ for the case of constant current RF source. The results are plotted as functions of Ω for two values of Γ spanning the typical experimental range in Fig. 33, where it can be seen that $\beta_o{}^2$ is not sensitive to Γ as long as the RF induced steps are not too severely rounded by noise (at $\Gamma = 0.04$ the step structure is almost completely suppressed for $\Omega < 0.2$). At large normalized frequencies the calculation predicts that $\beta_o{}^2$ approaches unity; however, at small normalized frequencies $\beta_o{}^2$ can be appreciably greater than one.

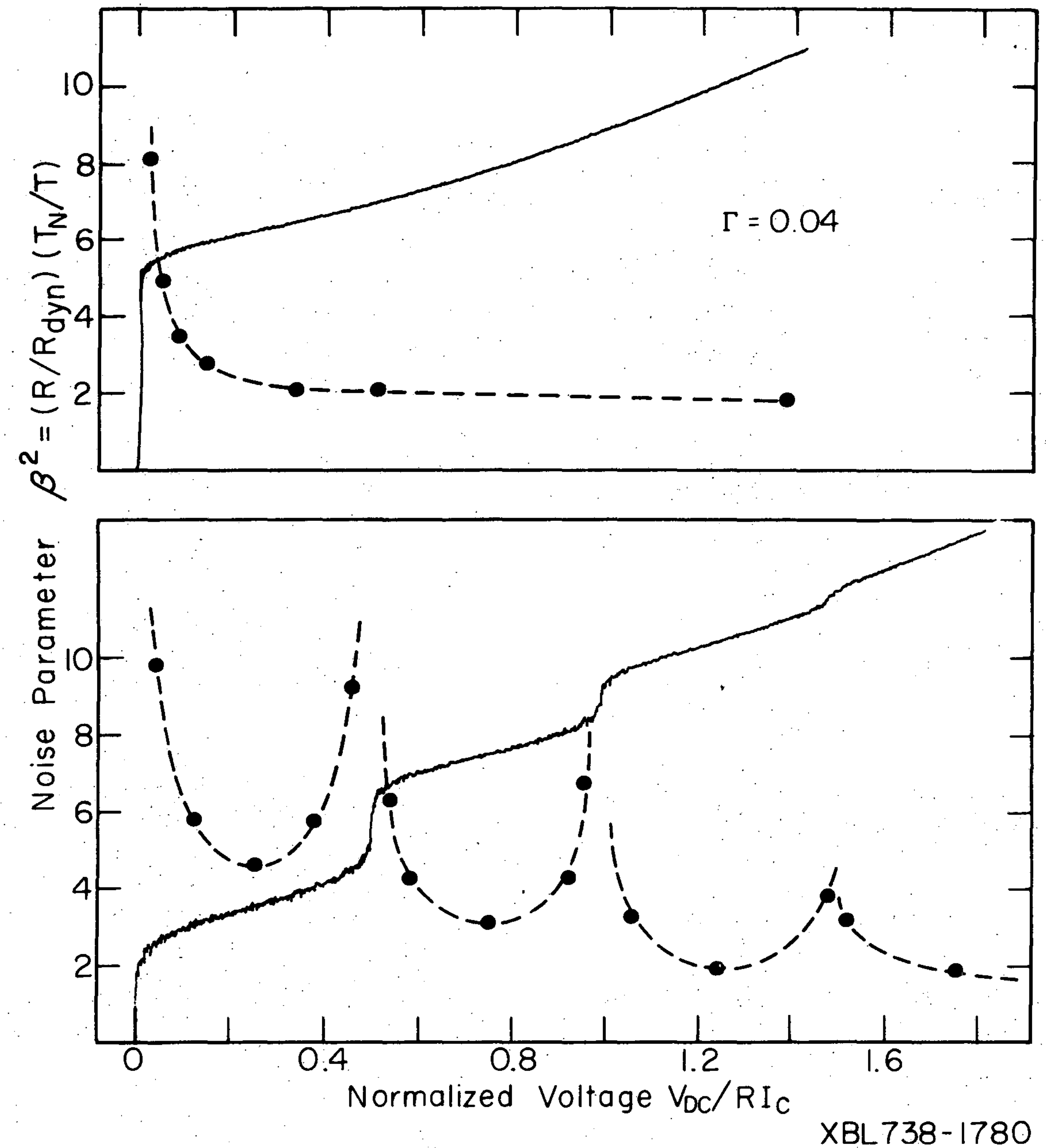

Fig. 32. Noise parameter and I-V curves calculated by the junction simulator for conditions similar to the real junction in Fig. 31.

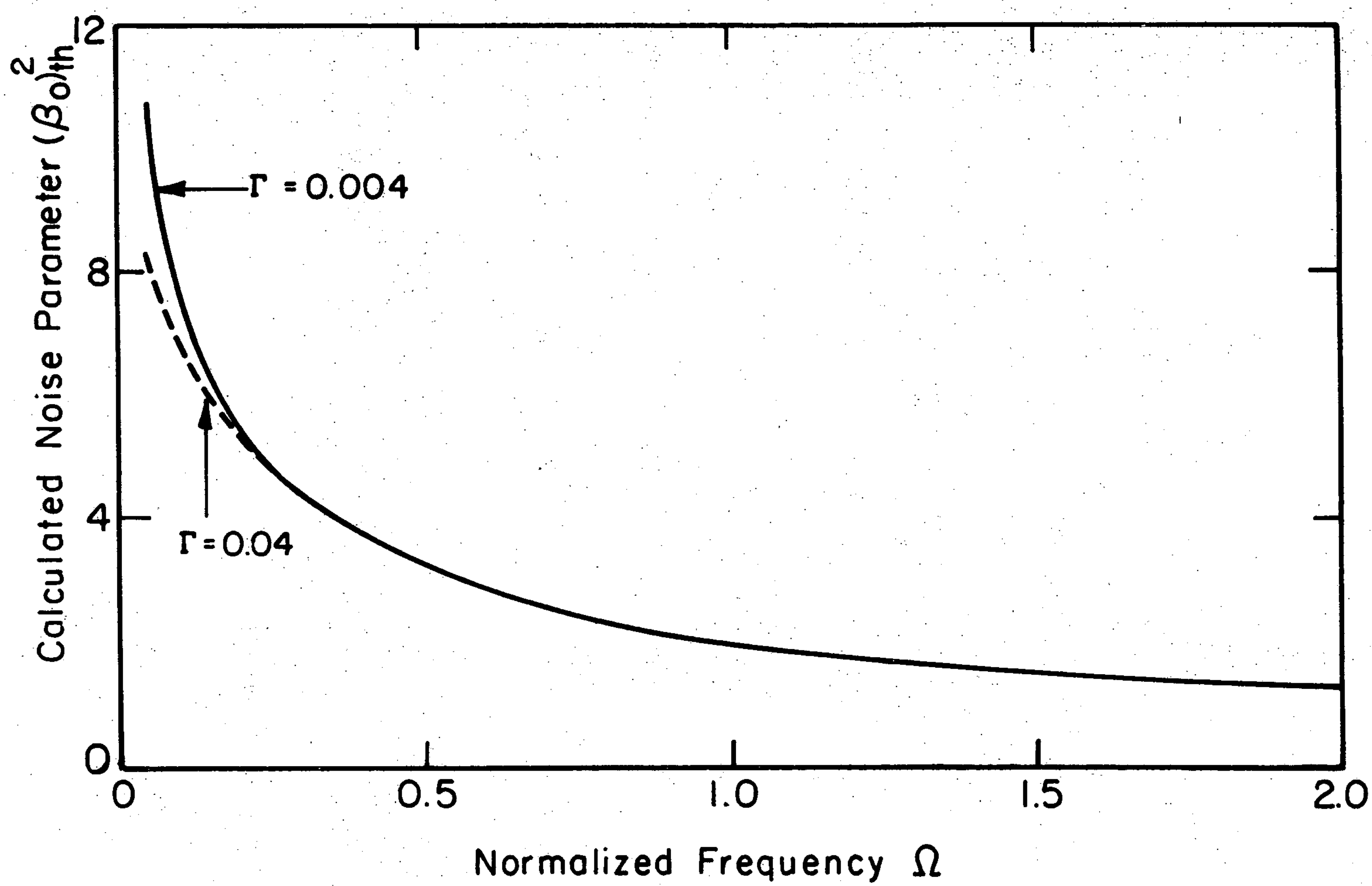

XBL743-5941

Fig. 33. Noise parameter β_o^2 as a function of Ω obtained from the junction simulator.

We have measured β_o^2 in the absence of the matching structure for niobium, tantalum, and vanadium junctions at temperatures between 1.4 K and 4.2 K. It was found that $(\beta_o)^2_{exp}$ is independent of the material of the point contact and the junction temperature, which means $T_N \propto T$. This is a very important result since it implies that we can improve the noise properties of our point contact Josephson junctions by operating at a lower temperature without changing other parameters if pick-up can be avoided. We also found that $(\beta_o)^2_{exp}$ has similar dependence on Ω to that predicted by the simulator, but the measured values at small normalized frequencies are approximately a factor of two larger than the predicted value $(\beta_o)^2_{th}$ at the same normalized frequency. This is shown in Fig. 34 where we plot points of $(\beta_o)^2_{exp}/(\beta_o)^2_{th}$ versus Ω for a number of different junctions.

We tried to explain this discrepancy in terms of the photon shot noise calculated by Stephen,[35-37] which was shown to agree with the experimental results of tunnel junctions by Dahm, et.al.[9] and point contacts by Kanter and Vernon[38,39] (they assumed $\beta^2 \equiv 1$). But the values of β_o^2 obtained by the addition of this extra noise in our experimental limit of $eV_{DC} \ll kT$, eRI_c are larger than the values of $(\beta_o)^2_{exp}$ we observed. We have attempted to include the shunt capacitance and phase dependent quasiparticle current ($\cos\phi$) in our junction model. However, the simulator calculation shows that these terms can only raise $(\beta_o)^2_{th}$ by at most 20 percent without causing hysteresis to appear on the junction I - V curve.[31] Despite this discrepancy of an extra factor of two, we regard the result of our noise measurement to

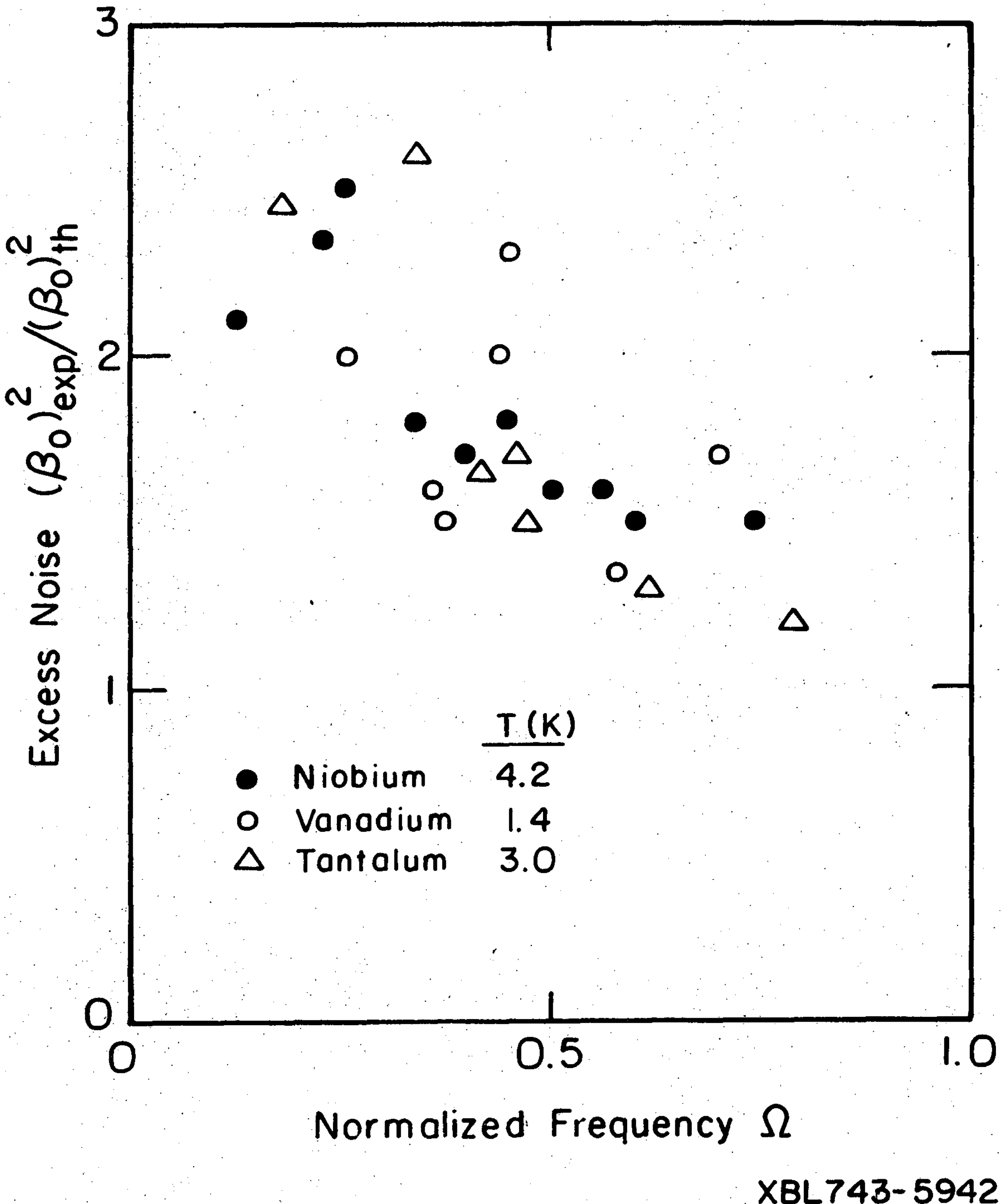

Fig. 34. Observed noise parameters β_o^2 for a number of junctions relative to the calculated value in Fig. 33; the data points obtained from junctions with different materials and temperatures scatter over the same range.

be reasonable considering the fact that the RSJ model is so simple that it does not include effects such as the frequency-dependent Josephson current[40,41] and fluctuations arising from the $\cos\phi$ term[42] into account.

B. Mixer Noise Temperature

1. Definition of Single Side Band (SSB) Mixer Noise Temperature

The sensitivity of a heterodyne receiver can be represented by a temperature T_R which is related to the minimum detectable power P_{min} by[43]

$$P_{min} = k\, T_R \sqrt{B_1\, B_2} \tag{25}$$

Here B_1, B_2 are the predetection and postdetection bandwidths of the IF system. The receiver noise temperature T_R consists of contributions from the IF amplifier and from the mixing element, that is,

$$T_R = T_M + T_{IF}/\eta \tag{26}$$

where T_M is the SSB mixer noise temperature obtained by referring the intrinsic noise of the mixing element to the input of the mixer. Conventionally, the performance of a mixer can be specified by a pair of numbers for η and T_M.

In our system, since $C_{IF}T_N$ is the amount of junction noise coupled to the IF amplifier, we have

$$T_M = C_{IF}\, T_N/\eta \tag{27}$$

Therefore we can calculate T_M from the measured values of η, T_N, and C_{IF}. Using Eqs. (20) and (22), the SSB mixer noise temperature of a Josephson junction is related to its ambient temperature by

$$T_M = (\beta^2/\alpha^2)T \tag{28}$$

This is independent of the IF coupling efficiency as it should be.

2. Experimental Results for T_M

It was observed experimentally that the value of $\beta_o{}^2$ measured for a well-coupled junction is larger than that measured for a junction driven by RF current source by a factor of 1.5 to 2. The same effect was also obtained in the junction simulator[31] with the presence of resonant coupling. Precise comparisons between the data and the simulator result are difficult because of the extra parameters (Q, R_S/R etc.) involved, but the overall trend is that this excess noise is more pronounced in junctions with small normalized frequencies.

For the matched junctions listed in Table 1, we measured T_N under the same conditions that η_{exp} was obtained and calculated T_M from Eq. (27). The best result that we have achieved is a mixer noise temperature of 54 K and $\eta_{exp} = 1.35$ for a vanadium point contact with normalized frequency 0.3 operated at 1.4 K. We have also included in Table 1 values of $(\beta_o)^2_{exp} = (T_N/T)/(R_{dyn}/R)$ and $(\beta_o)^2_{exp}/(\beta_o)^2_{th}$ which is the excess noise factor above the curve in Fig. 33 calculated from the junction simulator in the absence of the resonant circuit.

We learned from Fig. 11 that junctions with smaller normalized frequencies have larger coupling parameters and therefore larger conversion efficiencies. However, it was demonstrated in Fig. 33 that these junctions also have large noise parameters. Furthermore, both the excess noise arising from resonant matching and the discrepancy $(\beta_o)^2_{exp}/(\beta_o)^2_{th}$ in Fig. 34 result in additional noise experimentally at small normalized frequencies. These considerations make it plausible that the experimental value of T_M/T should be rather insensitive to the normalized frequency of the junction, and this is what we actually found by comparing the values of T_M in Table 1 for different junctions operated at the same temperature.

VII. OTHER MODES OF MIXING

A. Fourth Harmonic Mixing

Besides fundamental mixing, we also tried fourth order harmonic mixing in our point contacts with the same apparatus. The local oscillator now has a frequency of 8.99 GHz and its power is coupled to the junction via the coaxial IF cable with filters to isolate the LO power from IF amplifiers. The same technique as described in Section IV was used to couple the small 36 GHz signal to the junction. In this experiment, the junction acts like a harmonic generator as well as a mixer.

The experimental result is shown in Fig. 35 where we plot the conversion efficiency against DC voltage and the corresponding I - V curves for a niobium junction at 7 K. The response peak occurs at zero bias voltage and is obtained with rather large amount of local oscillator power in contrast with the case of fundamental mixing. Unfortunately no simple model is available to explain our data, but we found that the conversion efficiency in our fourth harmonic mixing experiments is also insensitive to the frequency ratio ω_{IF}/ω_S and remains unchanged whether $\omega_S > 4\omega_{LO}$ or $\omega_S < 4\omega_{LO}$.

We also measured the noise temperature of this junction and found that T_N = 230 K at the point where η = 0.5. This yields a mixer noise temperature of 400 K (C_{IF} = 0.87) which is not much worse than the number obtained from the fundamental mixing for junctions operated at the same temperature. If this result remains valid at higher frequencies,

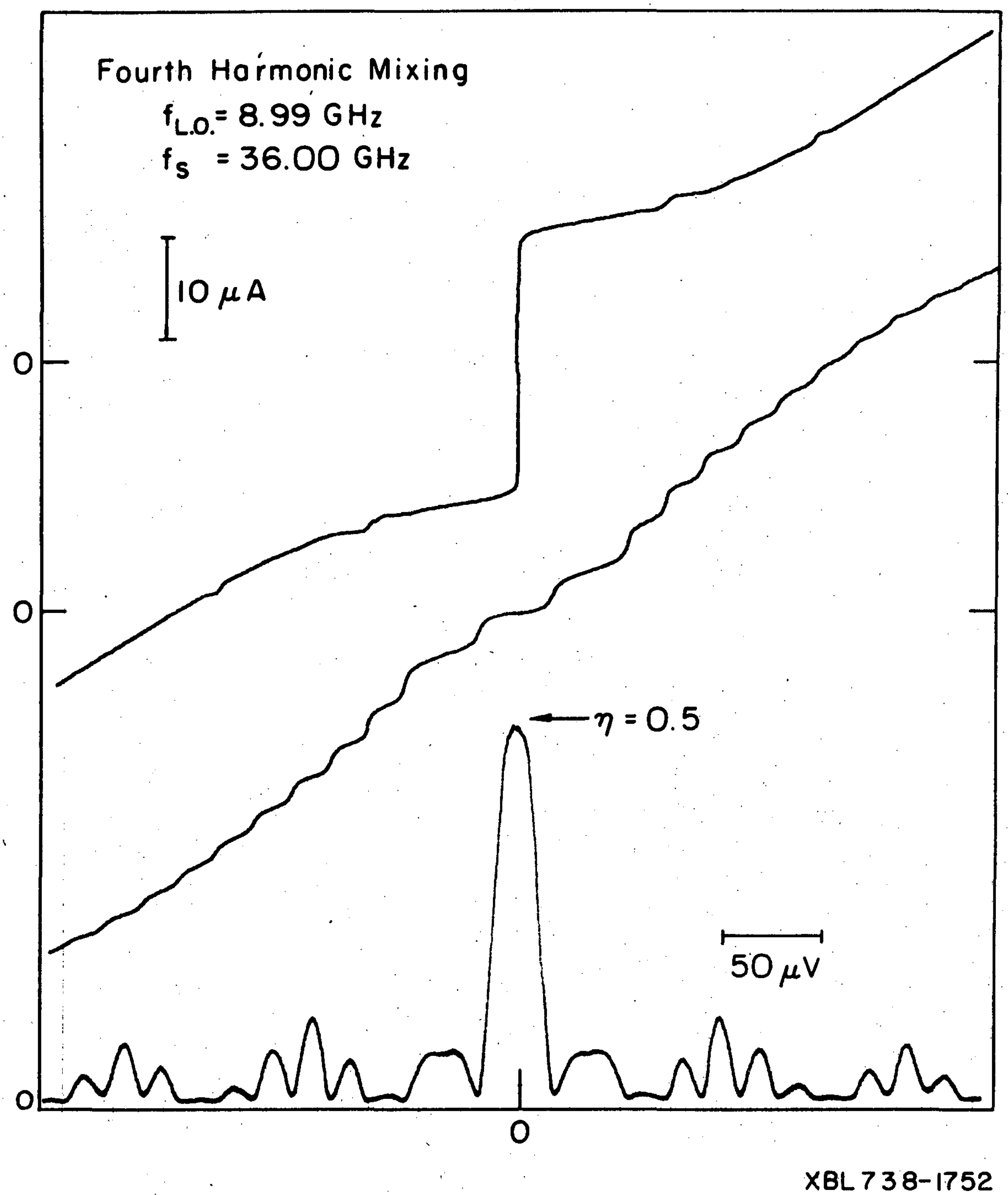

Fig. 35. Conversion efficiency versus bias voltage for fourth harmonic mixing together with I-V curves for $P_{LO}=0$ and $P_{LO}\neq 0$; the maximum value of η occurs when the zero-voltage current is completely suppressed.

it will greatly aleviate the problem of providing local oscillators for heterodyne systems with signal frequencies beyond 100 GHz.

B. Self Local Oscillator Mixing

When a Josephson junction is DC biased near the cavity induced step described in Section IV.C, it can be operated as a heterodyne receiver in which the Josephson oscillation, synchronized by the resonant cavity, serves as the local oscillator. We have observed the response of a point contact operated in this mode. Since the linewidth of the Josephson radiation is always broadened by the junction noise,[9] the IF output was smeared out over a bandwidth of approximately 5 MHz with a center frequency sensitive to both DC bias voltage and plunger position (which determines the resonant frequency of the cavity). We must then integrate the output power over this bandwidth to obtain the conversion efficiency.

In Fig. 36 we plot the junction I - V curve and its response--the latter is proportional to the IF power within a bandwidth of 1 MHz (the predetection bandwidth of the spectrum analyzer) centered around 30, 40, and 50 MHz. These data were taken when the signal frequency and the plunger position were held unchanged. The responses for three different center frequencies occur at slightly different voltages, all below the cavity mode step. The largest output is observed when the IF is set at 40 MHz which we believe is the difference between the signal frequency and the center frequency of the cavity resonance. There is also a large cavity step at a voltage corresponding

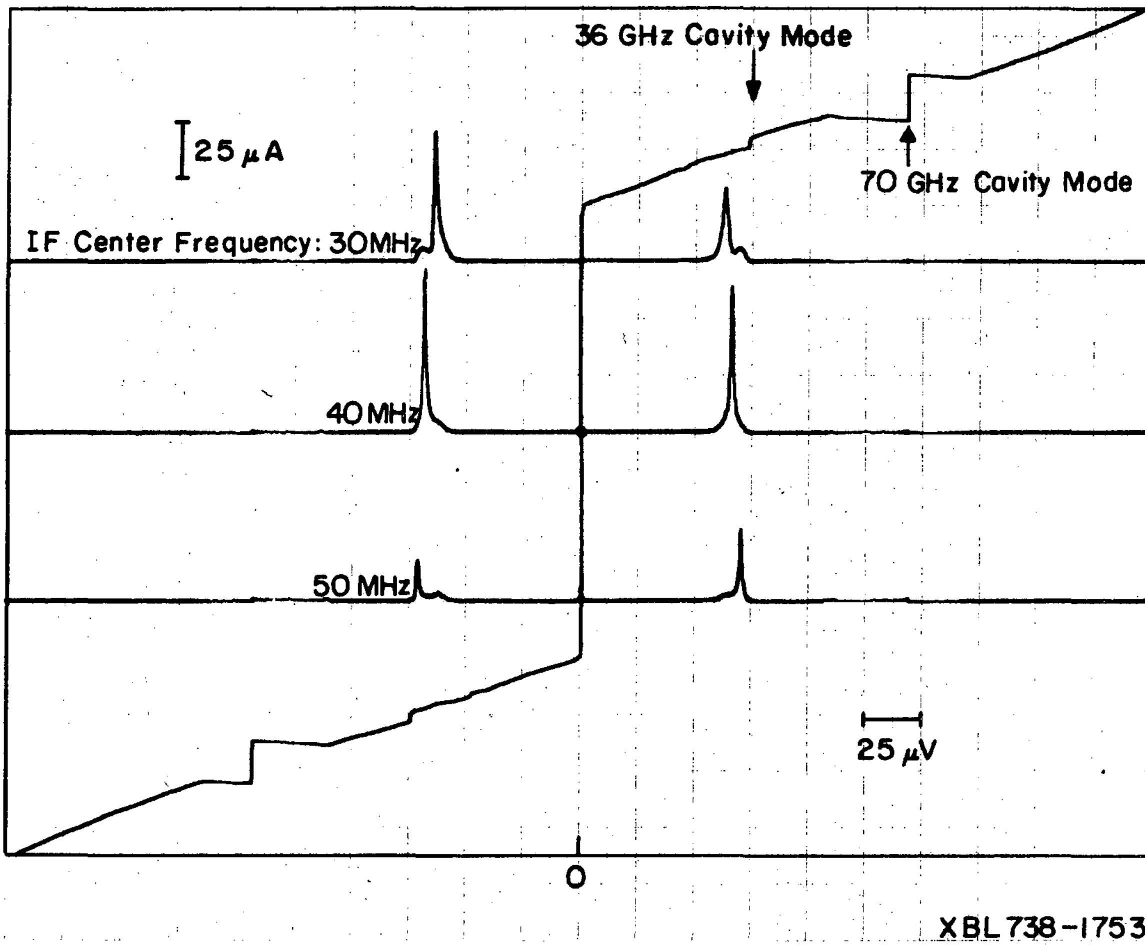

Fig. 36. Frequency conversion using the Josephson oscillation synchronized to a eavity as LO; the junction I-V curve is also shown.

to about 70 GHz caused by higher order modes in the microwave cavity, which does not show response for the 36 GHz signal.

We do not fully understand these complicated effects observed in cavity mode mixing. The measured value of the integrated conversion efficiency $\eta = 0.006$, however, is not very encouraging.

C. An Oscillating Mixer

When a hysteretic junction is DC biased with a low impedance source in the switching region on its I - V characteristic, both the junction current and voltage will oscillate at a frequency determined by the inductance and resistance of the external circuit. This phenomenon is called the "relaxation oscillation" first observed in tunnel junctions by Vernon and Pedersen.[44] We shall develop a simple model in Appendix B for relaxation oscillations in point contacts.

In the presence of such oscillations, the static I - V curve of the junction shows a region of negative resistance. A typical example is given in Fig. 37, where the frequency of the relaxation oscillation varies from 2 to 5 MHz depending on the bias voltage. If such a junction is DC biased in the negative resistance region, it acts as an one-port amplifier for signals introduced into the IF cable at frequencies close to the frequency of relaxation oscillation. Gains of several hundred have been observed in our experiments; however, the gain is highly non-linear and vanishes at a signal level comparable to the power of the relaxation oscillation.

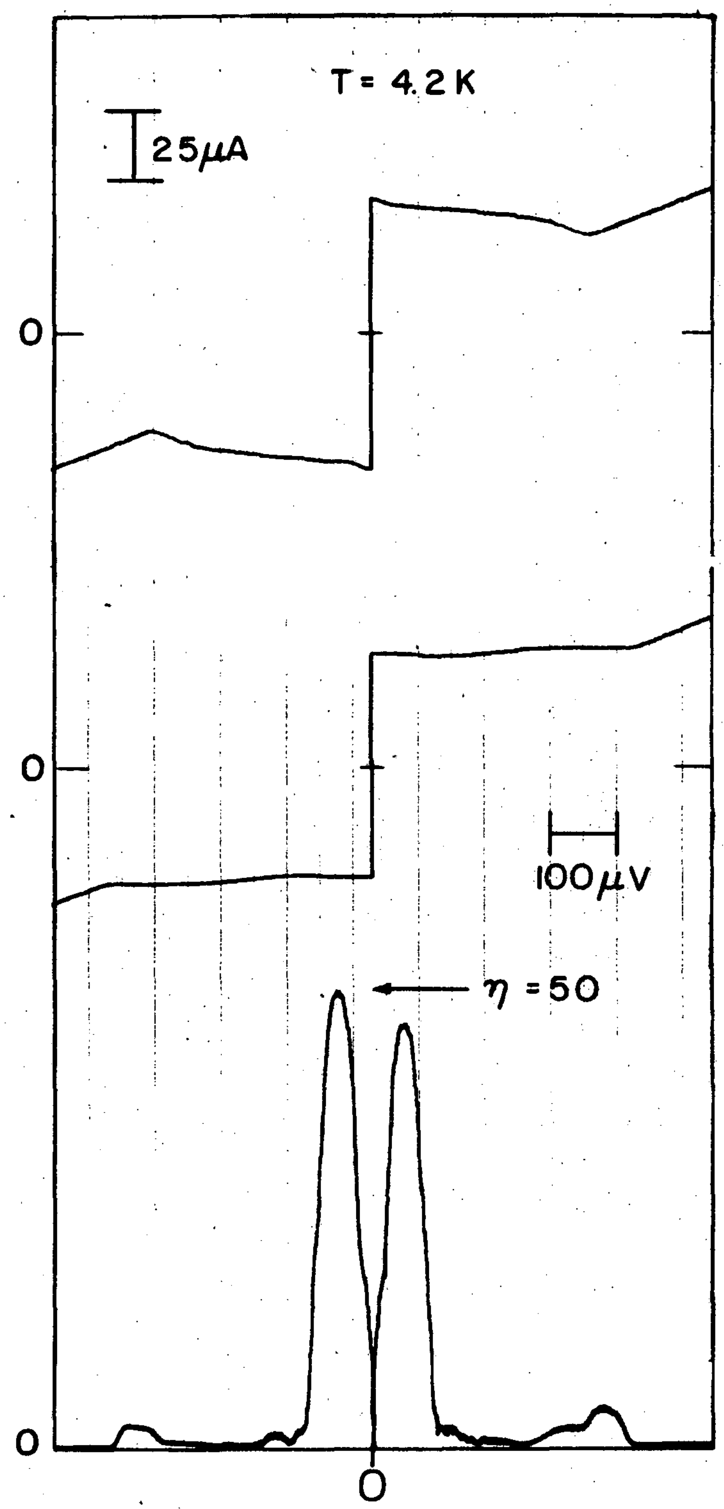

XBL 737-6554A

Fig. 37. Averaged I-V curves for $P_{LO}=0$ and $P_{LO}\neq0$ and conversion efficiency versus junction DC voltage for fundamental mixing in the presence of relaxation oscillation; the junction would be hysteretic if biased with a DC current source.

We have also tried to operate these junctions as mixers with external local oscillator as shown in Fig. 37. They do not show low order LO induced steps, but have given conversion gains as large as $\eta = 50$ at a bias voltage where the relaxation oscillation frequency is equal to the intermediate frequency (which in this case was set at 5 MHz).

Although these oscillating mixers show large conversion gains, the bandwidth in which the gain was observed is very small ($\approx$ 5 MHz). Furthermore, they have an enormous amount of IF noise so that their mixer noise temperature is very large ($T_M \gtrsim 1000$ K for the case in Fig. 37). Therefore, such oscillating mixers are not as useful as our non-hysteretic mixers listed in Table 1. (Similar effects have been found in germanium diodes[33] which also give a large amount of noise and are not suitable for practical uses.)

VIII. CONCLUSION

In this work we have demonstrated that the physical properties of our point contact Josephson junctions can be understood in terms of the RSJ model. In particular, the agreement between our experimental data and the models we developed for RF coupling and IF noise is very useful in estimating the performance of a high frequency Josephson effect device.

For signal frequencies at 36 GHz, we have achieved a mixer noise temperature of 54 K and a conversion gain of 1.35. These numbers can be consistently obtained by operating vanadium point contacts at 1.4 K. It requires only minor modification of our apparatus to raise the intermediate frequency to 1 GHz where cooled parametric amplifiers with noise temperatures of 15 K are available.[45] A 36 GHz heterodyne system can then be constructed with our mixer and such an IF amplifier to give a receiver noise temperature $T_R = 65$ K. If such a system were used for astronomical observation, it should be able to resolve a source temperature change[43] of $\Delta T_S = T_R\sqrt{B_2/B_1} \approx 2\times10^{-3}$ K for a predetection bandwidth $B_1 = 1$ GHz and a postdetection bandwidth $B_2 = 1$ Hz. This is a substantial improvement over existing systems in this frequency range.

If we compare our mixer with other mixing devices operated at similar signal frequencies, the noise temperature of our Josephson mixer is a factor of 20 lower than conventional room temperature resistive mixers and a factor of 4 lower than recently developed cooled Schottky-barrier diode mixers.[45] Moreover, the noise in a

Schottky-barrier diode at low temperatures ($T < 30$ K) is dominated by temperature-independent shot noise,[46] while the noise in our mixer is proportional to the ambient temperature and can be further improved by operating the junction at temperatures even lower than 1.4 K.

The single sideband conversion efficiency of conventional resistive mixers is limited to be less than one-half. Even with careful designs to reject the image response at $2\omega_{LO}-\omega_S$, its conversion efficiency can not be larger than one.[33] However, Josephson mixers may have conversion gain which reduces the contribution to T_R from the IF amplifier noise. Furthermore, since only a small amount of LO power is required for optimum operation of a Josephson mixer ($\approx$ 1 nW compared with $\approx$ 1 mW for resistive mixers), the problem of LO noise is eliminated and a balanced mixer is not required. This is especially important for heterodyne systems at higher signal frequencies where a coherent LO with large power is very difficult to build.

The theoretical model described in Section V.A predicts that the conversion efficiency of a Josephson effect mixer is a strong function of its normalized frequency Ω. However, since there is excess noise associated with small normalized frequencies, the noise temperature of a Josephson effect mixer is not very sensitive to Ω in the range $0.1 \lesssim \Omega \lesssim 1$. Therefore, we believe that our method can be extended to higher signal frequencies without too much change in the noise performance.

To extrapolate our results to a higher frequency range, we consider the case where a nonhysteretic Josephson junction with $RI_c = 600\ \mu V$ (this number is experimentally achievable for our point contacts) is operated as a 300 GHz mixer at 1.4 K. This corresponds to $\Omega = 1$ and we know from Figs. 11 and 33 that in this case, $\alpha^2_{opt} = 0.06$ and $\beta^2_o = 2$. Since it is very difficult to make good quality microwave plungers and chokes at such high frequencies, we assume that the RF coupling efficiency is only 40 percent, which means that $\alpha^2_{exp} \approx 0.025$. These numbers predict a mixer noise temperature of approximately 120 K and a conversion efficiency slightly less than 0.1, which are significantly better than resistive mixers operated in this frequency range.[47]

For signal frequencies much higher than 300 GHz however, the performance of Josephson effect mixers degrades very rapidly not only because the coupling parameter α^2 decreases as $(1/\omega_{RF})^2$ but also because the capacitance of the junction is not negligible even if it does not cause hysteresis.

IX. ADDITIONAL TOPIC I

A. Josephson Effect Homodyne Detectors

1. Detection Principle

It is well known that if an RF signal is applied to a Josephson junction, current steps appear at voltages given by the Josephson relation $V_{DC} = n\hbar\omega_{RF}/2e$ on the static I - V curve. This occurs when the Josephson oscillator is phase-locked to the n-th harmonic of the external signal. The magnitudes of these radiation-induced steps are related to the strength of the RF fields in a fundamental way.[48] We are interested in measuring the height of the first order (n = 1) step to provide a homodyne or lock-in detector for the applied signal.

In the absence of RF matching circuits, the external signal appears to be a constant current source to the junction. According to the noise-free RSJ model, the full height of the first order step ΔI_1 is related to the amplitude of the RF current I_{RF} by[49]

$$\Delta I_1 = I_{RF}/\sqrt{1 + \Omega^2} \tag{29}$$

in the small signal limit ($I_{RF} \ll I_c$). Here $\Omega \equiv \hbar\omega_{RF}/2eRI_c$ is the normalized frequency of the junction. This shows that ΔI_1 is proportional to the square-root of the RF power and its measurement yields linear detection.

In order to obtain zero-frequency output, the applied RF signal must be strong enough to overcome the influence of noise and synchronize Josephson oscillation. This condition can be derived from Stephen's calculation[37] for the shape of a noise-rounded step.[50] Under the assumption that noise is not too large to affect[34,37] the dynamic resistance R_{dyn} at the step voltage in the absence of RF signal, he showed that the slope at the center of an induced step can be written as

$$R_c^{-1} = R_{dyn}^{-1} I_o^2 (\gamma) \tag{30}$$

Here I_o is a Bessel function of the second kind and $\gamma = (\hbar \Delta I_1/4ekT)\times(R/R_{dyn})$ is a dimensionless measure of the radiation strength relative to the junction noise (this expression has been modified so that the only source of noise under consideration is the thermal noise generated in the shunt resistor R at temperature T). If $\gamma \gg 1$, Eq. (30) indicates that R_c^{-1} varies exponentially with γ and the step is exceedingly steep with a height given by Eq. (29). However, if $\gamma \lesssim 1$ (very small RF signal), Eq. (30) can be expanded to give

$$R_c^{-1} = R_{dyn}^{-1} (1 + \gamma^2/2) \tag{31}$$

In this case the output of the Josephson detector is proportional to $(R_c^{-1} - R_{dyn}^{-1})/R_{dyn}^{-1} = \gamma^2/2 \propto P_{RF}$. This implies that the junction is no longer synchronized and becomes a square-law detector.[51] Therefore, the condition for linear homodyne detection is set by $\gamma \gtrsim 1$ to be

$$\Delta I_1 \geqslant \frac{4ekT}{\hbar} \frac{R_{dyn}}{R} \tag{32}$$

Using Eq. (29) and the equality $R_{dyn}/R = \sqrt{1 + \Omega^2}/\Omega$ from the RSJ model, this becomes

$$I_{RF} \geqslant \frac{4ekT}{\hbar} \frac{1 + \Omega^2}{\Omega} \tag{33}$$

If the RF source resistance R_S is much larger than both the junction resistance R and the equivalent resistance due to other losses, the power criterion for synchronization is

$$P_{RF} \geqslant \frac{R_S}{8} \left(\frac{1 + \Omega^2}{\Omega}\right)^2 \left(\frac{4ekT}{\hbar}\right)^2 \tag{34}$$

which has a minimum value of $(R_S/2)(ekT/\hbar)^2$ at $\Omega = 1$. The amount of RF power which equalizes the influence of noise is related to T^2 since the step rounding is a quadratic effect of noise.

2. Experimental Results

We have investigated the properties of Josephson junctions operated in the homodyne mode using preset-type niobium point contacts and a 37 GHz RF source. In this experiment no attempt has been made to resonantly reduce the impedance of the microwave source. The point contact is DC voltage biased with a circuit shown in Fig. 38(a), where the resistance of the bias resistor is chosen to be much smaller than the junction resistance. This resistor has no effect in shorting out AC currents above 10 kHz because of the large inductance of the loop.

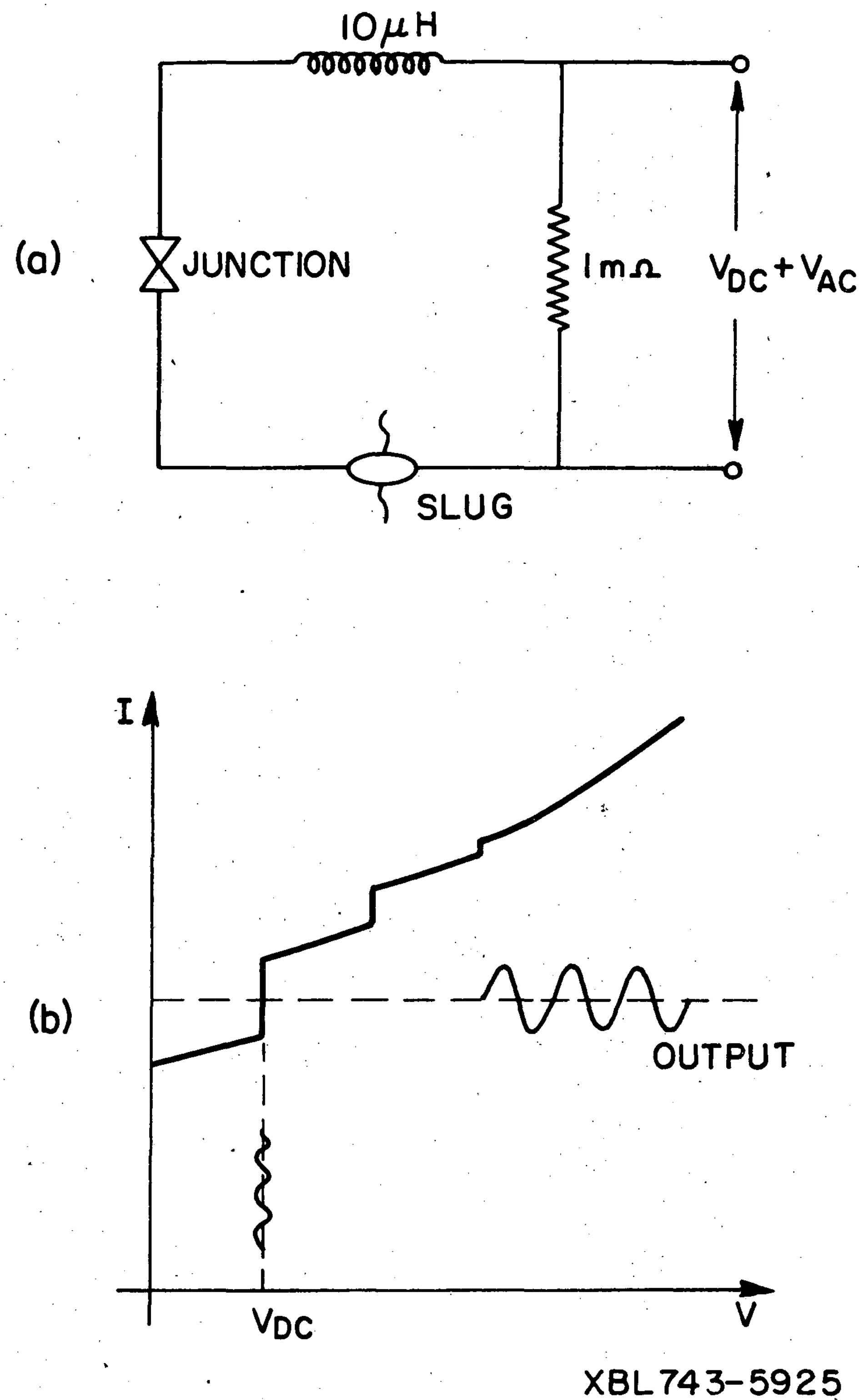

Fig. 38. Bias circuit and schematic step height measurement for a Josephson homodyne detector.

The height of the first step is measured by superimposing a small modulation (~ 100Hz) on the DC voltage and reading the junction current with a superconducting quantum interference galvanometer (SLUG[52]) followed by a lock-in detector. This method is shown schematically in Fig. 38(b).

When the junction is synchronized by the applied RF signal, its response shows a peak proportional to the step height at a bias voltage corresponding to the RF frequency as is shown in Fig. 39. However, if the RF power is too weak to synchronize the junction, the response is reduced and smeared out as shown in Fig. 40. For a point contact with R = 0.3 ohm and I_c = 1.8 mA operated at 4.2 K, we found that the minimum RF current required to synchronize the junction is approximately 15 μA (calibrated by the first zero of the zero-voltage step). This result was obtained without any matching structure and the power limit for synchronization is 10^{-8} W (R_S = 450 ohms). According to Eq. (34), this number corresponds to an equivalent junction temperature five times higher than the ambient temperature, which indicates that our detector is external noise limited. (This measurement was done with rather rudimentary shielding.) If this experiment were repeated with our present shielding system and coupling structure, one should be able to achieve ambient temperature noise limit and reduce the RF source resistance to $R_S \approx 1$ ohm. Then the junction mentioned above can be synchronized with incident power approximately 10^{-12} W.

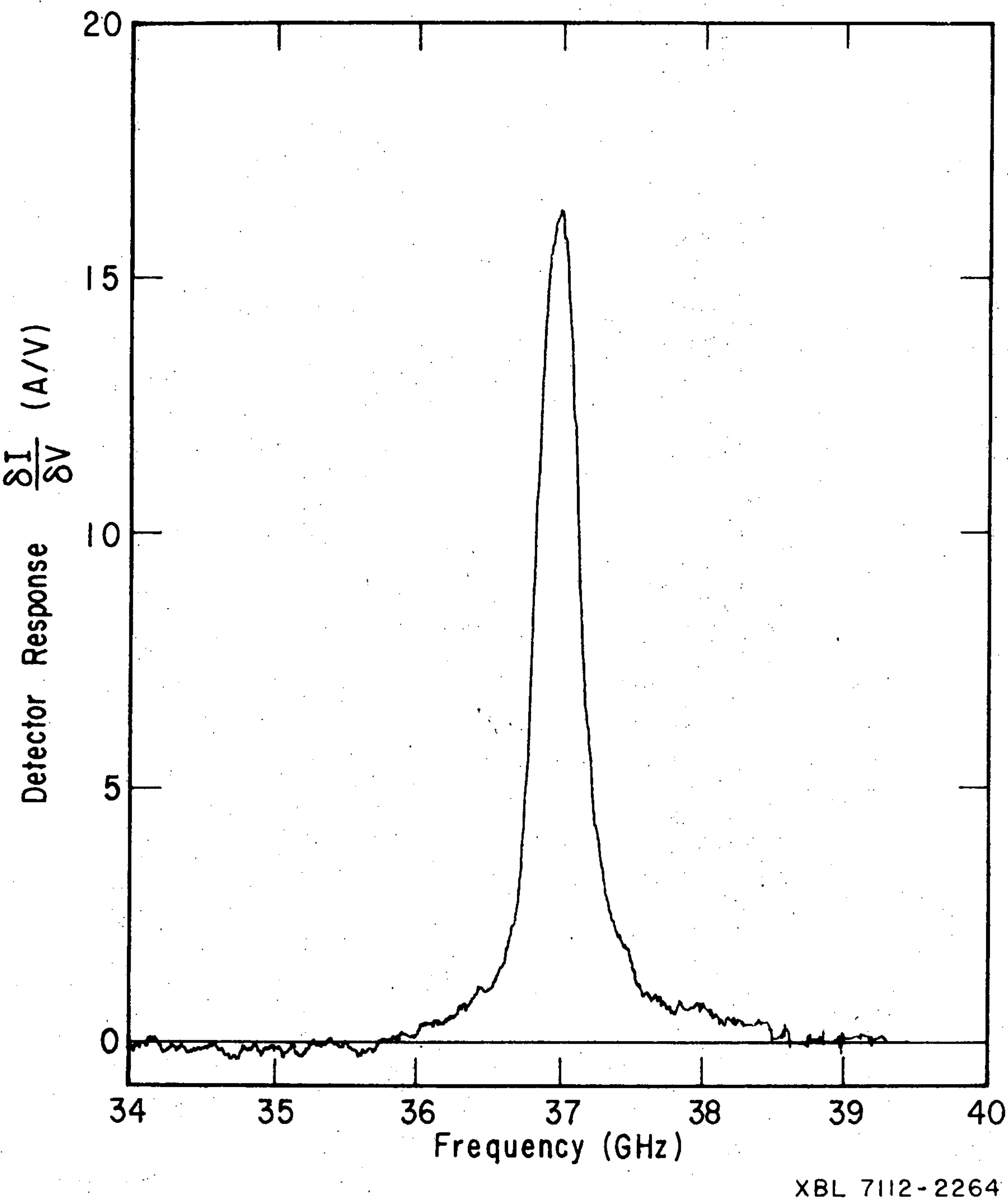

Fig. 39. Output of the SLUG against bias voltage in frequency units; the peak indicates a well-defined step at the signal frequency.

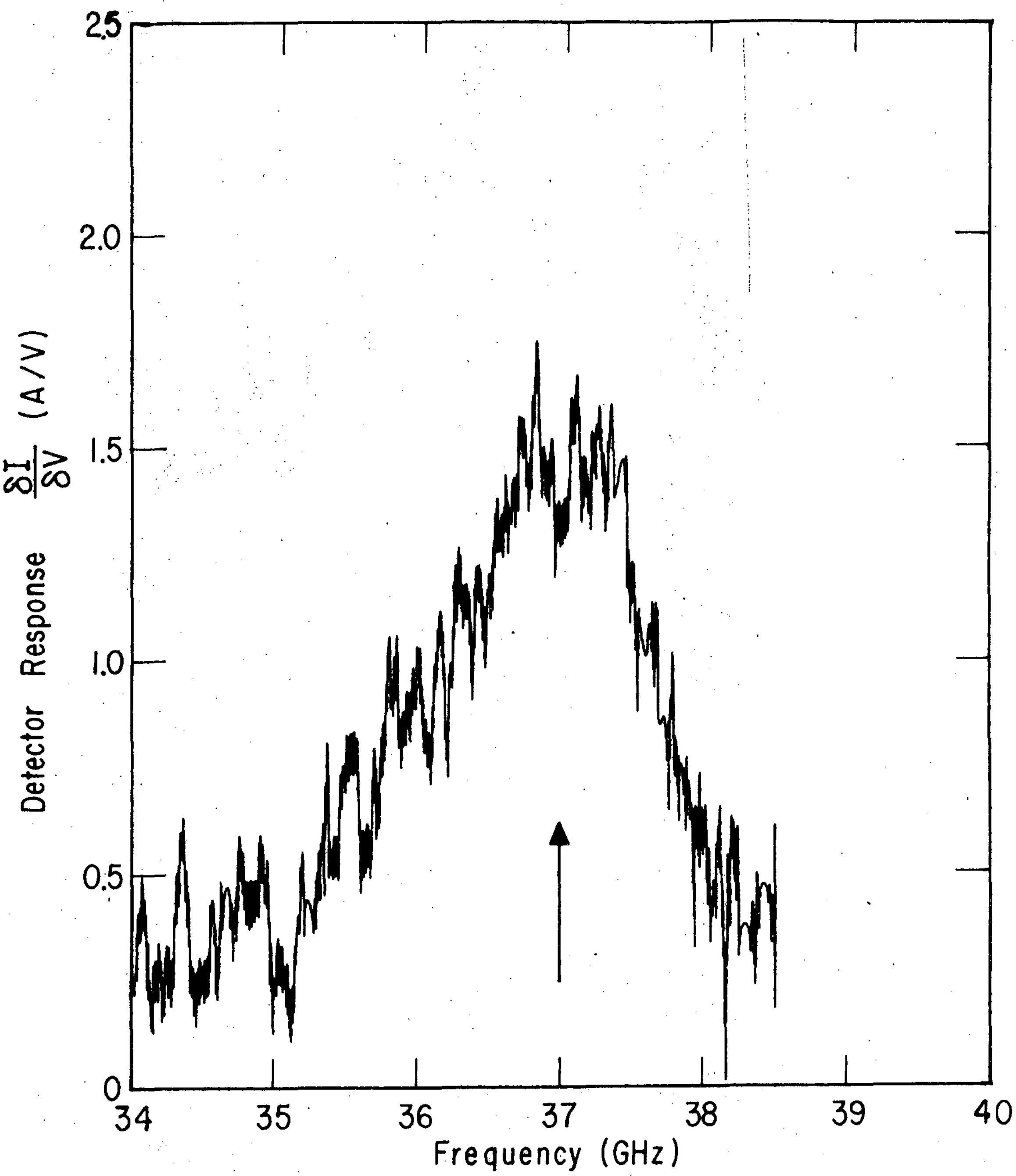

XBL 7112-2265

Fig. 40. A plot similar to Fig. 39 except that the RF signal is so weak that the step is severely rounded by noise.

Such a homodyne detector has an important feature of being frequency-selective, in that its operating frequency can be easily tuned by varying the DC bias voltage of the junction. At a fixed bias voltage, the junction is sensitive to RF signals within a bandwidth determined by the amplitude of the voltage modulation (apart from higher-order harmonic response to frequencies $2eV_{DC}/n\hbar$). Since Josephson junctions must be synchronized to show linear homodyne response, the application of such a device is limited to the detection of coherent signals.

X. ADDITIONAL TOPIC II

A New Design of Superconducting Bolometers

Superconducting bolometers[53-60] are not as widely used as semiconducting bolometers[61-64] for detecting electromagnetic radiation. Among the reasons for the neglect of the superconducting bolometer is its low impedance compared with conventional voltage amplifiers. In most applications, superconducting bolometers are seriously limited by amplifier noise. Recently superconducting quantum interference devices (SLUG,[52] SQUID[65-66]) were developed with excellent current sensitivity and zero resistance. Therefore we consider the situation in which a SLUG or SQUID is used to read the current from a low impedance bolometer as shown in Fig. 41. This design permits the operation of a superconducting bolometer with slow response in a regime where amplifier noise is negligible compared with the helium temperature Johnson noise in the bolometer element.

1. Responsivity

In this section we consider the responsivity of an idealized isothermal bolometer: the bolometer element has a finite heat capacity C and infinite thermal conductance, while the mounting has zero heat capacity, but a finite heat conductance G. The basic equation which governs the behavior of a superconducting bolometer can be derived from energy conservation in the bolometer element to be

$$C \frac{dT}{dt} = Ri^2 + aW_o e^{j\omega t} - G(T - T_S) \tag{35}$$

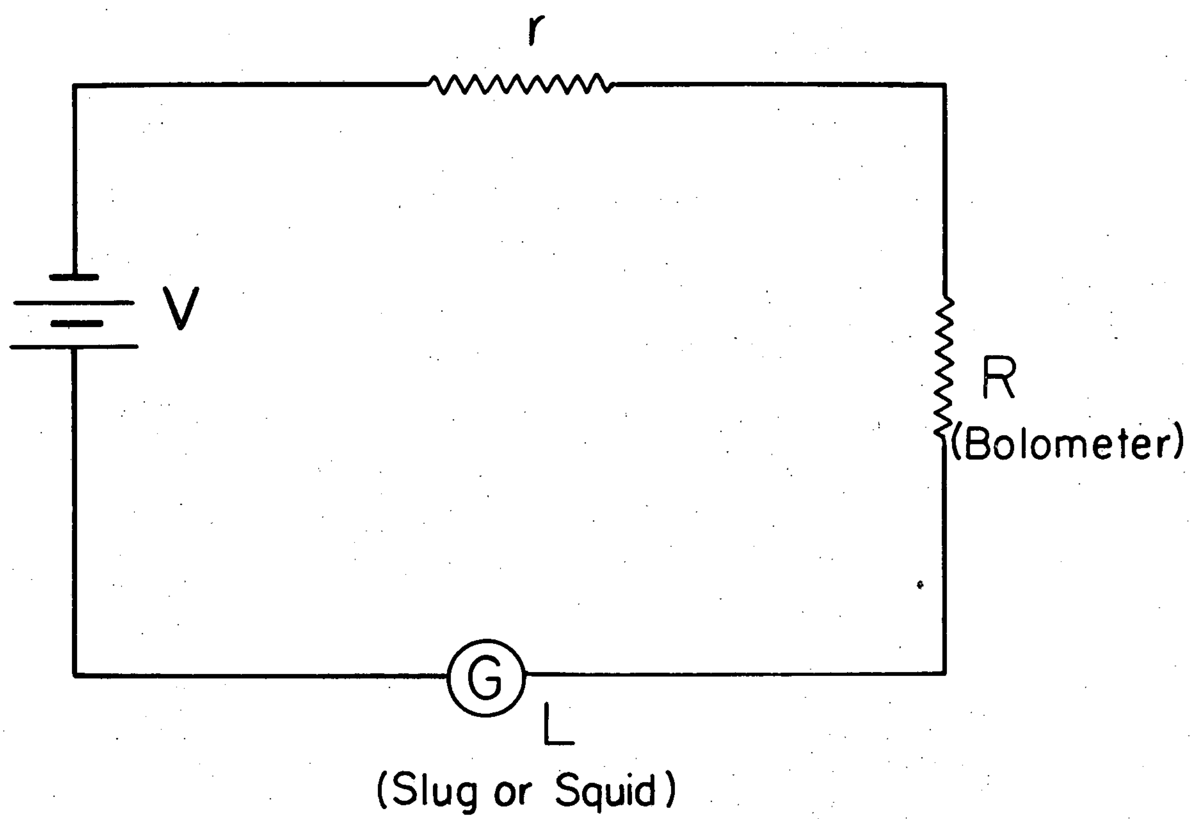

XBL709-3867

Fig. 41. Equivalent circuit for measurement of bolometer response with a superconducting quantum interference galvanometer which has zero resistance but finite inductance.

Here R is the resistance of the bolometer element (approximately half the resistance in the normal state); i is the current flowing through it and T is its operating temperature. The left side of Eq. (35) represents energy storage, while the terms on the right side include Joule heating, the absorbed radiation signal power chopped at frequency ω, and the heat conducted to the thermal bath. We assume a constant absorption coefficient, a, for signal power and lump all steady state radiation heating (from unchopped room temperature radiation or the steady state component of the chopped signal) into an effective sink temperature T_S. If we let

$$\begin{aligned} T(t) &= T_o + \Delta T_o\, e^{j\omega t} \\ R(t) &= R_o + \Delta R_o\, e^{j\omega t} \\ i(t) &= i_o + \Delta i_o\, e^{j\omega t} \end{aligned} \tag{36}$$

then the steady state part of Eq. (35) gives the operating condition

$$R_o i_o^{\,2} = G(T_o - T_S) \tag{37}$$

and the time-varying part becomes

$$j\omega C \Delta T_o e^{j\omega t} = \Delta(Ri^2) + aW_o e^{j\omega t} - G\Delta T_o e^{j\omega t} \tag{38}$$

where $\Delta(Ri^2) = R(t)i^2(t) - R_o i_o^{\,2}$.

We now consider DC biasing the bolometer with an arbitrary resistor r shown in Fig. 41 and measuring its response with a lock-in detector, referenced by the chopping signal, following the superconducting galvanometer. To first order in ΔR, the current responsivity of the bolometer is

$$S_i \equiv |\Delta i_o/\sqrt{2}\, W_o|$$

$$= \frac{a i_o(\partial R/\partial T)}{\sqrt{2}\, GR_o(1+\alpha+r/R_o)\left\{\omega^2\tau^2 + \left[1 + \frac{(R_o-r)i_o^{\,2}\,(\partial R/\partial T)}{GR_o(1+\alpha+r/R_o)}\right]^2\right\}^{1/2}} \tag{39}$$

Here $\tau \equiv C/G$ is the thermal time constant of the bolometer mount and $\alpha \equiv (i_o/R_o)(\partial R/\partial i)$ is a dimensionless parameter peculiar to superconducting bolometers which measures the change of resistance due to current. In most cases of interest, $\alpha \lesssim 1$.

In order to maximize S_i, we must consider various values of the bias circuit parameters. For thermal stability[67] we require

$$1 + (R_o-r)\; i_o^{\,2}\; (\partial R/\partial T)/GR_o(1+\alpha+r/R_o) > 0 \tag{40}$$

Since $\partial R/\partial T > 0$ for superconductors, thermal runaway is avoided for all values of i_o if $R_o \geqslant r$. From Eq. (39), if $R_o = r$, S_i will increase linearly with i_o until i_o is limited by the heating power. For other values of r, S_i has a maximum at a particular i_o but the height of this peak is less than the absolute maximum which occurs for $r = R_o$. A given cryogenic system provides a minimum value of T_S; a given superconductor, a specific critical temperature $T_c \approx T_o$. Thus the circuit bias condition should be $r = R_o$ and $i_o^{\,2} = G(T_c - T_S)/R_o$, then Eq. (39) becomes

$$S_i = \frac{a(\partial R/\partial T)}{3R_o}\sqrt{\frac{T_c-T_S}{2GR_o(1+\omega^2\tau^2)}} \tag{41}$$

This mathematical approach corresponds closely with experimental practice.

2. Noise

There are four sources of noise which limit the performance of a superconducting bolometer. These are Johnson noise, thermal fluctuation noise, amplifier noise, and extra noise arising from the superconducting transition itself. Background fluctuation noise is not included since any detector limited by this noise[68] (BLIP condition) clearly needs no improvement. It has been reported that the extra noise associated with the superconducting resistive transition is important for certain materials.[55] However, recent experiments[59] demonstrate that it can be eliminated in at least some experimentally useful cases. We shall neglect this extra noise contribution in the following discussion.

In our bolometer configuration, amplifier noise is determined by the sensitivity of the superconducting quantum interference device. The performance of such a device can be specified by a figure of merit[69] F in units of K/Hz, which is related to its current sensitivity i_A by $i_A{}^2 = 4kFB/2\pi L$. Here L is the inductance of the device presented to the bolometer circuit and B is the bandwidth of the measurement which, in our case, is much smaller than the chopping frequency ω. In order to compare amplifier noise with the Johnson noise generated in the bolometer element, we consider $i_A{}^2/i_J{}^2 = (4kFB/2\pi L)/(4kT_oB/R_o) = (R_o/2\pi L)(F/T_o)$. This ratio can be reduced by using superconducting transformers[70] to bring L up until the circuit cut-off frequency $R_o/2\pi L$ is equal to the signal frequency $\omega/2\pi$. Under this condition we have $i_A{}^2/i_J{}^2 = (\omega/2\pi)(F/T_o)$. The figure of merit F of a SQUID has been reported[71] to be 10^{-4} K/Hz. Therefore for a chopping frequency of 10 Hz, amplifier noise is small compared with Johnson noise as long as $T_o > 10^{-3}$ K. This general result is independent of the value of R_o. (For fast bolometers with $\omega/2\pi \approx 10^8$ Hz,[58-60] amplifier noise is not negligible.)

Now we shall minimize the effect of Johnson noise and thermal fluctuation noise arising from heat exchange between the bolometer element and the sink via a finite conductance G.[72] It is convenient to express noise contributions in terms of the square of a noise power entering the detector.[68] Since the noise sources are independent, the sum of these contributions gives the square of the noise equivalent power $(NEP)^2$. For comparison, we need approximate expressions for the responsivity and various noise contributions. If we take $\partial R/\partial T = 6R_o/\delta T$ where R_o is half the normal state resistance and δT is the full width of the superconducting transition, then we have from Eq. (41)

$$\langle W_J^2 \rangle = 4kT_o B/R_o S_i^2 = \frac{2kT_c(\delta T)^2 G(1 + \omega^2\tau^2)B}{a^2(T_c - T_s)} \tag{42}$$

for Johnson noise, and

$$\langle W_T^2 \rangle = 4kT_c^2 GB/a^2 \tag{43}$$

for thermal fluctuation noise.

If $\omega\tau \lesssim 1$, $\langle W_J^2 \rangle / \langle W_T^2 \rangle \approx (\delta T)^2/T_c(T_c - T_S) \ll 1$, and the responsivity is high enough that Johnson noise is much smaller than thermal fluctuation noise. Since we have shown that amplifier noise is negligible compared with Johnson noise, the dominant noise will be thermal fluctuation noise if we take $\omega\tau \lesssim 1$. Thermal fluctuation noise can only be reduced by decreasing G. Since there exist lower practical limits for C in any configuration, $\omega\tau = \omega C/G$ will increase as we decrease G and $\langle W_J^2 \rangle \propto G\tau^2 \propto G^{-1}$ in the limit $\omega\tau \gg 1$. If we choose a value of G such that $\langle W_J^2 \rangle = \langle W_T^2 \rangle$, we have

$$G = \omega C\delta T/\sqrt{2T_c(T_c - T_S)} \tag{44}$$

and then the combined Johnson and thermal fluctuation noise has the minimum value

$$\langle W_J^2 \rangle + \langle W_T^2 \rangle = \frac{8kT_c^2\omega C\delta TB}{a^2\sqrt{2T_c(T_c - T_S)}} \tag{45}$$

Thus we can reduce the detector NEP if we sacrifice some responsivity and let $\omega\tau$ exceed unity.

3. Discussion

In order to make specific predictions for the performance of superconducting bolometers we consider several practical configurations. The maximum static current responsivity is achieved in a high purity single crystal slab of superconductor which has the small transition width δT associated with bulk material and a resistance R_o, small compared with a thin film. One such configuration (100μ thick Sn) is considered in Table 2. We also include in Table 2 a practical example of a low frequency thin film Sn bolometer on a 3-μ thick mica substrate (similar to that used by Martin and Bloor[56]). In this configuration the heat capacity of the substrate cannot be neglected. Although the bulk bolometer has a slightly larger NEP, it is easier to blacken without raising its heat capacity significantly. Since the transition temperature T_c plays an important role in the NEP, we also include in Table 2 an example of a thin film Al bolometer which has a lower transition temperature than the Sn film. It should be noted that the 10 Hz operating frequency for slow bolometers in Table 2 was selected arbitrarily as the lowest convenient frequency for experimental work. In order to compare detectors with different area or chopping frequency, we must use a figure of merit. From Eq. (45) we see that the NEP varies as $(\omega C)^{1/2}$ or, for a given ω as the square root of the detector area A. The concept of a specific detectivity $D^* = \sqrt{A}/\mathrm{NEP}$ is therefore useful for the superconducting bolometer. The figure of merit $m = \sqrt{\omega A}/\mathrm{NEP}$ is also useful if we wish to compare bolometers with different response times.

We believe that the predicted performance described in Table 2 can be achieved in practice. Care must be taken to regulate the sink temperature T_S adequately. Existing feedback temperature regulators are more than adequate for this purpose.[12] If T_S is above the superfluid transition temperature T_λ, the bolometer must be isolated from the bath by a thermal filter with response slow compared with ω to avoid He bubbling noise.[59] Finally, care must be taken to avoid noise from the superconducting transition. The choice between the otherwise nearly equivalent bulk and thin-film bolometers may be made on the basis of such noise.

Our theoretical model requires isothermal conditions in the bolometer element and negligible heat capacity associated with the thermal link. This can be achieved over a wide range of response times by minimizing the heat capacity of the mechanical support by the technique of Martin and Bloor[56] and then surrounding the bolometer element with He exchange gas at the appropriate pressure.

It is useful to compare the slow superconducting bolometers described above with the He temperature doped Ge bolometer.[61-64] Such bolometers are usually operated in a regime such that some responsivity-dependent source of noise (amplifier noise, Johnson noise in the bolometer element or bias circuit) is at least comparable to the thermal fluctuation noise when $\omega\tau = 1$. Unlike the superconducting bolometer discussed here, therefore, the doped Ge bolometer cannot be improved by operating with $\omega\tau > 1$. The best Ge bolometers operated in the He^4 range at $\omega = 10$ Hz have $D^* \approx 10^{12}$ cm$\sqrt{Hz}$/W. This is several orders of magnitude less than the predicted values for the superconducting bolometers shown in Table 2. Both types of bolometer can be improved by going to lower bath temperatures.[63] Superconductors such as Cd or Zn are suitable for operation in the He^3 region.

APPENDIX A

Microwave Circuit Analysis

1. Impedance Transformation

In this section we shall discuss how the plunger and stub provide the proper impedance transformation required for optimum microwave coupling. The total microwave impedance seen by the junction can be calculated from the equivalent circuit in Fig. 14(b) to be

$$Z_T \equiv R_T + jX_T$$

$$= \frac{Z_o}{(B_1B_2Z_o^2 - 1)^2 + (B_1Z_o)^2} + j\left[X_L - \frac{B_1Z_o^2 + B_2Z_o^2(B_1B_2Z_o^2 - 1)}{(B_1B_2Z_o^2 - 1)^2 + (B_1Z_o)^2}\right] \qquad \text{(A-1)}$$

where B_1 and B_2 represent the susceptances of the plunger and stub respectively, which can be adjusted to any positive values.[26,27] It was shown in Section IV that in order to achieve optimum coupling to a Josephson junction, values of B_1 and B_2 must be chosen such that $X_T=0$ and $R_T=(R_S)_{opt}$. These two conditions can be solved to give B_1, B_2 in terms of Z_o, X_L, and $(R_S)_{opt}$. In general, there are two sets of solutions, we shall only consider the case in which B_2 is positive:

$$B_1 = \frac{X_L + \sqrt{(R_S)_{opt}\,[X_L^2 + (R_S)_{opt}^2]/Z_o - (R_S)_{opt}^2}}{(R_S)_{opt}^2 + X_L^2} \qquad \text{(A-2)}$$

$$B_2 = \frac{\sqrt{(R_S)_{opt}\,[X_L^2 + (R_S)_{opt}^2]/Z_o - (R_S)_{opt}^2}}{(R_S)_{opt}\,Z_o} \qquad \text{(A-3)}$$

Typical values of $(R_S)_{opt}$ for our point contacts vary between 5 and 10 ohms, much smaller than the inductive reactance $X_L \approx 0.25 \times Z_o \approx 100$ ohms obtained from waveguide handbook.[26] Therefore, Eqs. (A-2), (A-3) can be simplified to the form

$$B_1 = X_L^{-1}\left[1 + \frac{\sqrt{(R_S)_{opt}}}{X_L}\sqrt{X_L^{\,2}/Z_o-(R_S)_{opt}}\right] \approx X_L^{-1} \qquad \text{(A-4)}$$

$$B_2 = \frac{1}{Z_o\sqrt{(R_S)_{opt}}}\sqrt{X_L^{\,2}/Z_o - (R_S)_{opt}} \qquad \text{(A-5)}$$

Since $X_L^2/Z_o \approx 30$ ohms $> (R_S)_{opt}$, optimum coupling at a given signal frequency can be achieved by adjusting B_1 and B_2 to these values. Equations (A-4) and (A-5) do not set any lower limit for $(R_S)_{opt}$, but in order to neglect the effect of microwave leakage, $(R_S)_{opt}$ must be larger than 2 ohms. If a junction happens to have $(R_S)_{opt} \approx X_L^{\,2}/Z_o$, it can be optimally coupled when $B_2=0$, that is, without the stub tuner. (For junctions having $(R_S)_{opt} > X_L^{\,2}/Z_o$, the distance between the stub and junction has to be changed to achieve optimum coupling, but this never occurred in our experiments.)

The analysis presented above can be illustrated on a Smith chart[27] as is shown in Fig. A-1. Every point with polar coordinates ρ, θ inside the unit circle C_o corresponds to a particular impedance Z_L with voltage reflection coefficient $\Gamma_v \equiv (Z_L-Z_o)/(Z_L+Z_o) = \rho e^{i\theta}$. Conventionally, one starts with the point corresponding to the load impedance and brings it to the origin where $\Gamma_v = 0$ by various matching

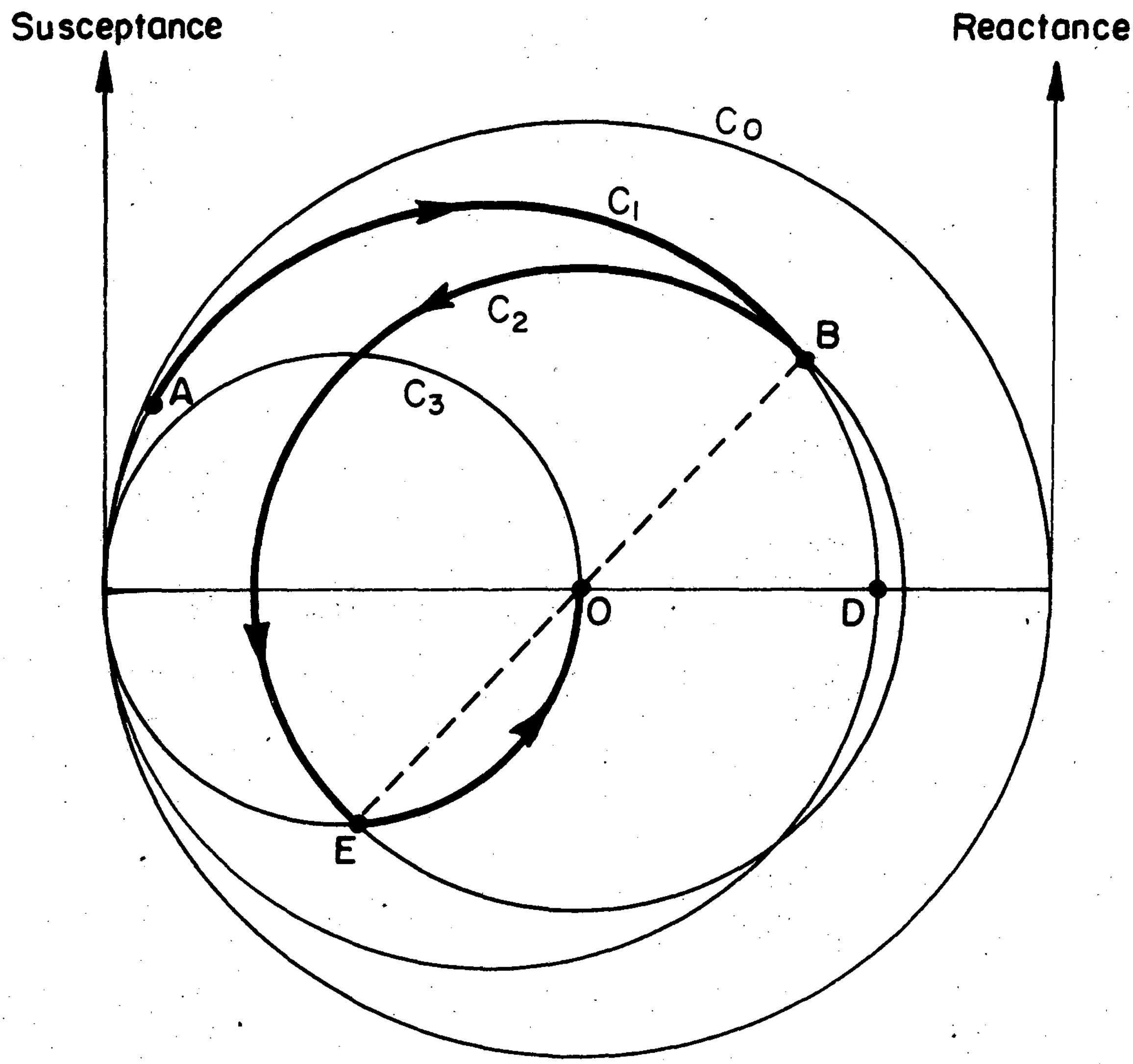

XBL743-5929

Fig. A-1. Smith chart for impedance transformation from point A with Z_L/Z_o = 0.01+0.2 j to the origin.

techniques. The order of the impedance transformation is thus reversed from that of the preceding analysis.

Suppose we have a junction with $(R_S)_{opt} = 5$ ohms and $X_L = 100$ ohms. This can be represented by a point A on the Smith chart ($Z_o = 450$ ohms). Without any matching arrangement, the microwave power absorption $1-|\Gamma_v|^2$ at A is only 5 percent. Adjustment of the plunger is equivalent to adding shunt susceptance to the junction, which brings point A along a circle C_1 of constant conductance ($G \approx (R_S)_{opt}/X_L^2 \approx 0.23/Z_o$) to B (or D, the best point which can be reached with the plunger alone, where the power absorption is approximately 50 percent for this particular junction). Transformation of the $3\lambda_g/4$ section corresponds to a rotation of 540° along a circle C_2 concentric with C_o. This moves point B to point E where C_2 intersects with another circle C_3 of constant conductance $G' = 1/Z_o$. Now we can adjust the susceptance of the stub tuner to bring point E along C_3 to the origin, which completes the impedance transformation.

2. <u>The Bandwidth of the Matching Circuit</u>

In order to estimate the bandwidth of our matching circuit, we consider the unloaded $Q \equiv (\omega/2R_T)|\partial X_T/\partial\omega|$, where R_T and X_T are given by Eq. (A-1). Carrying out the differentiation and using Eqs. (A-4), (A-5) for B_1 and B_2, we obtain

$$\frac{\partial X_T}{\partial\omega} = \frac{\partial X_L}{\partial\omega} + X_L^{\,2}\,\frac{\partial B_1}{\partial\omega} - Z_o(R_s)_{opt}\,\frac{\partial B_2}{\partial\omega} \approx X_L^{\,2}\,\frac{\partial B_1}{\partial\omega} \qquad \text{(A-6)}$$

We neglected terms $\partial X_L/\partial\omega$ and $Z_o(R_S)_{opt}(\partial B_2/\partial\omega)$ since X_L is not very sensitive to ω and $Z_o(R_S)_{opt}$ is smaller than X_L^2. The susceptance B_1 can be expressed in terms of the distance ℓ between the plunger and junction as $B_1 = - Z_o^{-1} \cot (2\pi\ell/\lambda_g)$. Therefore we have

$$Q \approx \frac{X_L^2}{2(R_S)_{opt}} \lambda_g \left|\frac{\partial B_1}{\partial \lambda_g}\right| = \frac{X_L^2}{2Z_o(R_S)_{opt}} (2\pi\ell/\lambda_g) \csc^2 \frac{2\pi\ell}{\lambda_g} \qquad \text{(A-7)}$$

At resonance $\cot (2\pi\ell/\lambda_g) = - Z_o/X_L \ll - 1$, its first root occurs at $2\pi\ell/\lambda_g \lesssim \pi$. (This agrees with the experimental fact shown in Fig. 15 that when optimum coupling was achieved, the distance between the plunger and junction is slightly less than $\lambda_g/2$). Then Eq. (A-7) becomes

$$Q \approx (\pi/2) \frac{Z_o}{(R_S)_{opt}} \qquad \text{(A-8)}$$

This equation states the general result that the bandwidth of the matching circuit is proportional to the junction resistance. In particular, for the junctions shown in Fig. 16, Eq. (A-8) predicts that $Q \approx 250$ and 30 respectively. These numbers are in reasonable agreement with the coupling bandwidths that we observed.

3. The Design of the Choke Flange

In Fig. A-2 we show the design of the niobium flange which reduces the microwave leakage mentioned in Section IV.B. A circular choke groove was cut in the flange to form quarter-wavelength sections in the radial transmission line so that the microwave impedance is a minimum at plane B. In order to have a short circuit at plane A, the distance between A and B was made to be $\lambda/2 \approx 4.17$ mm for a signal

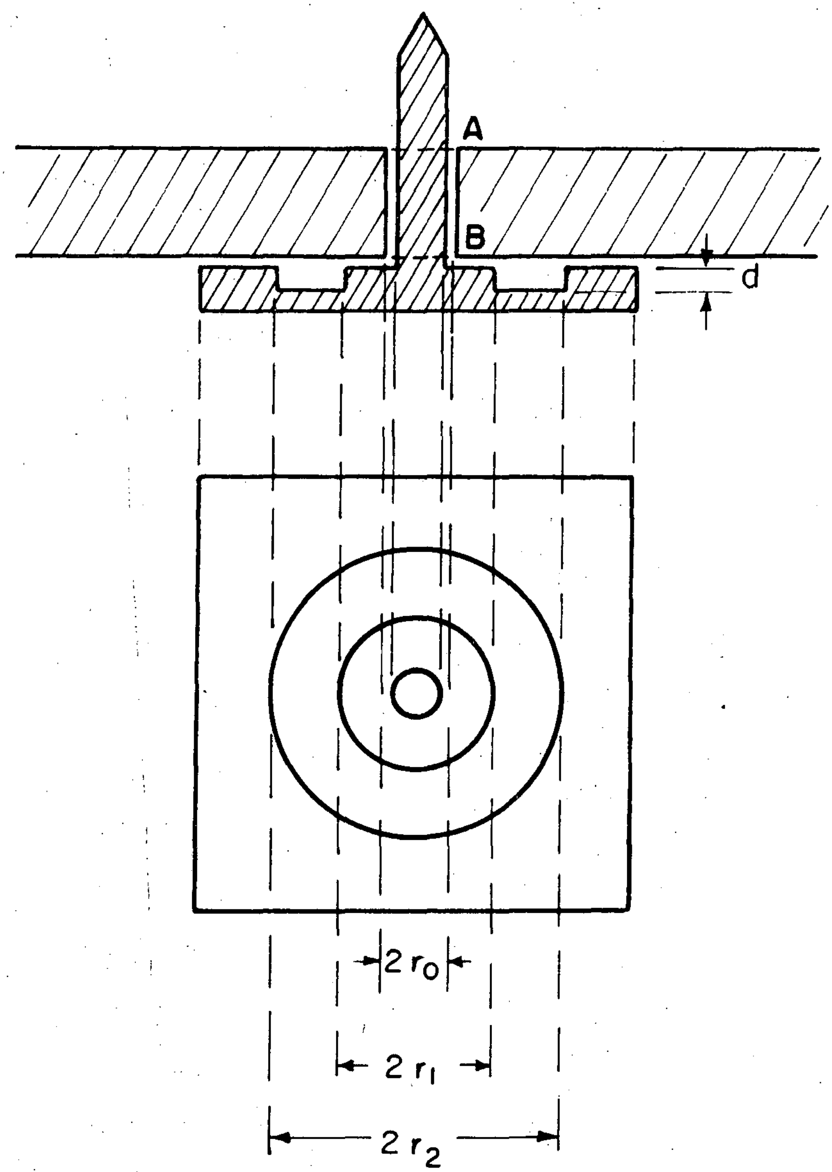

XBL 743-5928

Fig. A-2. Design of the choke flange in the niobium waveguide assembly.

frequency at 36 GHz.

The radii r_1 and r_2 were calculated in the following way:[73] The radius r_o of the hole containing the superconducting wire is 0.66 mm, therefore $X_o = kr_o = 2\pi r_o/\lambda = 0.5$. To reflect a short circuit to the plane B, we need a high impedance at $X_1 = kr_1$, which is related to X_o by

$$\eta_1(X_1) = \pi/2 + \eta_o(X_o) \tag{A-9}$$

where η_1 and η_o are the phases of Hankel functions $H_1^{(1)}$ and $H_o^{(1)}$ respectively. We obtain $X_1 = 1.7$ or $r_1 = 2.26$ mm from Eq. (A-9). In order for the microwave to see an open circuit at r_1, we must have a low impedance at r_2 and a high impedance section, which is the radial groove, between r_1 and r_2. Similarly, $X_2 = kr_2$ can be calculated from

$$\eta_1(X_2) = \pi/2 + \eta_o(X_1) \tag{A-10}$$

which gives $X_2 = 3.1$, i.e. $r_2 = 4.11$ mm. The depth d of the groove was chosen to be 1.98 mm $\lesssim \lambda/4$ to take care of the coaxial mode and fringing effects.

This choke flange has been tested by measuring the microwave coupling efficiency of very low impedance junctions ($R \lesssim 2$ ohms). The result shows that the microwave leakage is reduced below its value without choke grooves by a factor of 20 and can therefore be neglected for junctions with $R \gtrsim 5$ ohms.

APPENDIX B

A Model for Relaxation Oscillation in Point Contact Josephson Junctions

It was mentioned in Section VII. C that when a hysteretic junction is DC biased with a low impedance source, regions of negative resistance appear on its I - V curve. A similar effect has been observed in tunnel junctions by Vernon and Pedersen.[44] They explained this phenomenon successfully in terms of relaxation oscillations. We shall now develop a model to describe relaxation oscillations in point contacts and compare our experimental results with its predictions.

The basic assumption in our model is that the hysteretic junction acts either like a superconductor with zero resistance or like a resistor with resistance R depending on its bias current as illustrated in Fig. B-1(a). The AC Josephson effect is not important in the discussion of relaxation oscillation.

The bias circuit of the junction is shown in Fig. B-1(b), where L_o represents the inductance of the leads. It is clear that for bias voltage V_o less than R_oI_c, the junction stays in the zero-resistance state with current $I = V_o/R_o < I_c$; while for V_o larger than $(R + R_o)I_m$, the junction stays in the resistive state with $I = V_o/(R_o + R) > I_m$. However, if V_o lies in between these values, i.e. $(R_o + R)I_m > V_o > R_oI_c$, the junction must make alternate transitions between the superconducting and resistive states, which causes the junction current and voltage to oscillate. The criterion for this relaxation oscillation to occur is

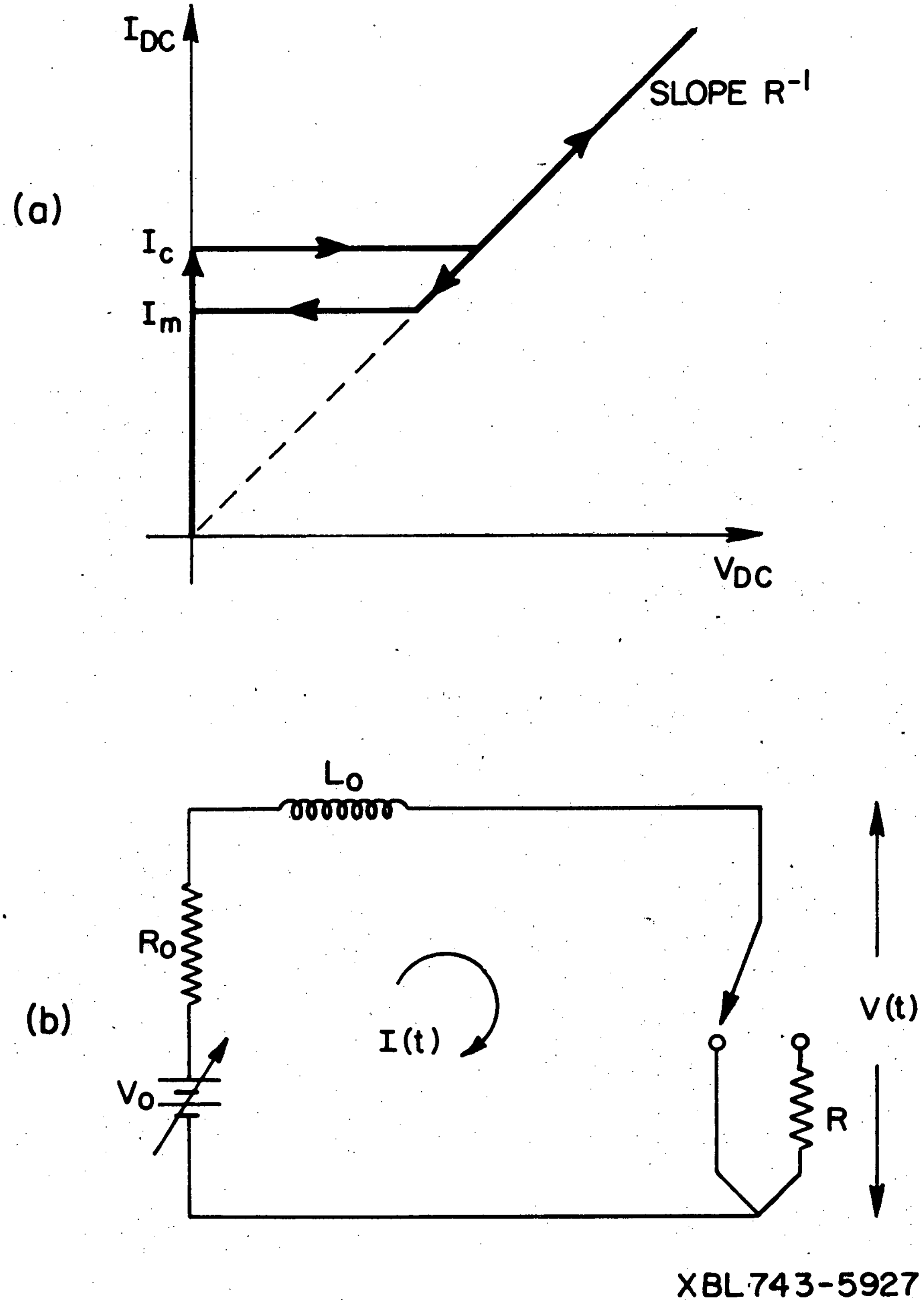

Fig. B-1. A model for the I-V curve of a hysteretic junction with current source bias (a), and equivalent circuit of the junction with external biasing elements (b), used to calculate relaxation oscillations.

$$(R_o + R)I_m > R_o\, I_c \tag{B-1}$$

which is usually met if $R_o \lesssim R$.

In the presence of relaxation oscillation, both the junction current and voltage are periodic functions of time, which can be calculated from the circuit shown in Fig.B-1(b) to be:

$$I(t) = \begin{cases} I_m + \left(\dfrac{V_o}{R_o} - I_m\right)\left(1 - e^{-\frac{R_o t}{L_o}}\right) & \text{if} \quad 0 < t < T_1 \\ I_c - \left(I_c - \dfrac{V_o}{R_o+R}\right)\left[1 - e^{-\frac{(R_o+R)(t-T_1)}{L_o}}\right] & \text{if} \quad T_1 < t < T_1 + T_2 \end{cases} \tag{B-2}$$

$$V(t) = \begin{cases} 0 & \text{if} \quad 0 < t < T_1 \\ RI(t) & \text{if} \quad T_1 < t < T_1 + T_2 \end{cases} \tag{B-3}$$

where transient effects were neglected and T_1, T_2 are given by

$$T_1 = \frac{L_o}{R_o} \quad \ell n \left(\frac{V_o - R_o I_m}{V_o - R_o I_c}\right) \tag{B-4}$$

$$T_2 = \frac{L_o}{R_o+R} \; \ell n \left[\frac{(R_o+R)I_c - V_o}{(R_o+R)I_m - V_o}\right] \tag{B-5}$$

We sketched I(t) and V(t) in Fig. B-2, where the frequency of the oscillation $f = 1/(T_1+T_2)$ depends upon DC voltage V_o. Equations (B-4) and (B-5) predict that f is a maximum in the middle

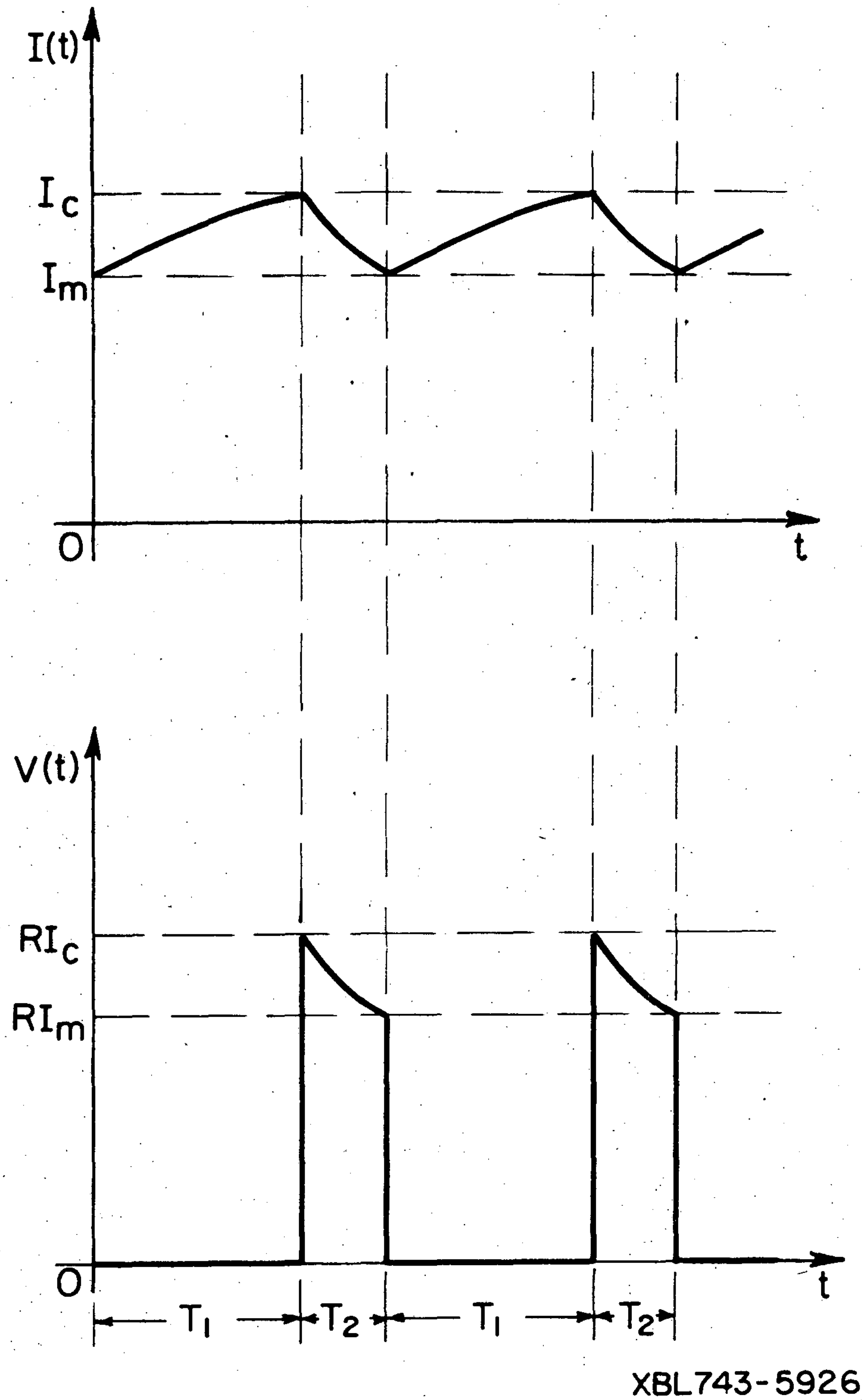

Fig. B-2. Current and voltage waveforms for the model of Fig. B-1.

of the oscillating region and tends to zero when V_o approaches $R_o I_c$ or $(R_o + R)I_m$. Typically we have $R_o \approx 10$ ohms, $R \approx 20$ ohms, $L_o \approx 10$ μH, and $I_m/I_c \approx 0.8$, which give $f_{max} \approx 5$ MHz.

In order to find the static I - V curve predicted by the model, we evaluated $I_{DC} \equiv \overline{I(t)}$ and $V_{DC} \equiv \overline{V(t)}$ from Eqs. (B-2) and (B-3) in terms of the parameter V_o. Assuming $I_m/I_c = 0.8$, we obtain two static I - V curves plotted in Fig. B-3 for $R_o/R = 0.2$ and 2 respectively. As expected, they show negative resistance regions where relaxation oscillations take place and the curve with $R_o/R = 2$ is very similar to the experimental curve without RF shown in Fig. 37.

Besides the qualitative agreement of static I - V curves, direct evidence of the existence of relaxation oscillations was also observed with a spectrum analyzer. We found that, as the model predicts, the oscillation contains a large amount of harmonics and is thus very non-sinusoidal. Furthermore, the fundamental frequency of the oscillations has its largest value in the middle of the negative resistance region, which also agrees with the model. Noise, of course, tends to broaden the linewidths of these oscillations.

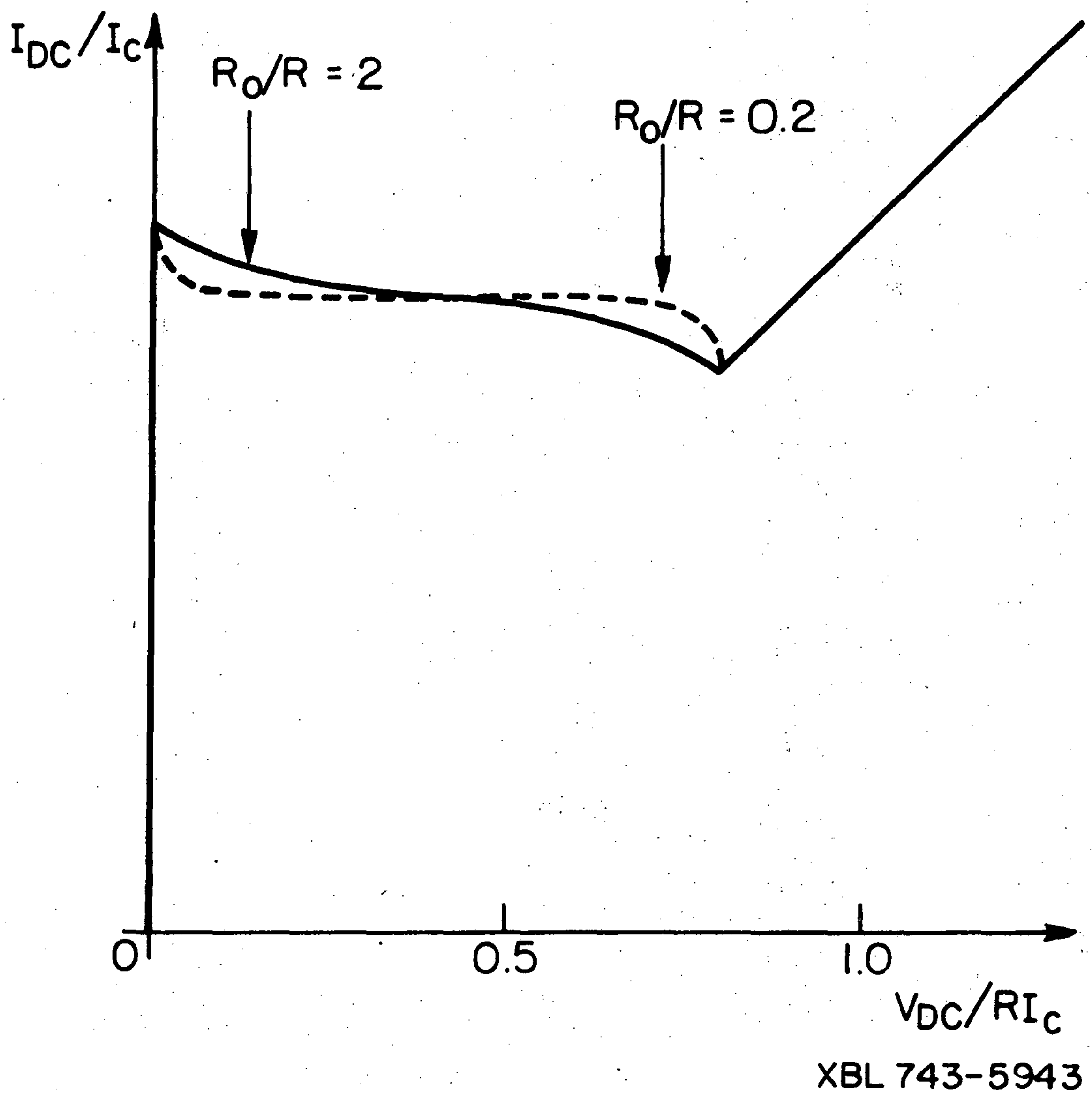

Fig. B-3. Averaged I-V curves (reversible) with relaxation oscillations calculated for two representative values of R_o/R; the hysteresis parameter I_m/I_c was assumed to be 0.8 in both cases.

ACKNOWLEDGEMENTS

I would like to thank Professor P. L. Richards for his support of this research project and his continued guidance and encouragement throughout the work. I also thank Professors J. Clarke and T. Van Duzer for many fruitful discussions and Dr. J. H. Claassen for his invaluable suggestions during the course of this work and his friendly help with the writing of this thesis. I want to express my special gratitude to Grace Chu for the preliminary typing of this thesis. At last, I would like to thank my fiancée, Betty Chu, and my parents, to whom this work must be dedicated, for their emotional support in these years.

This work was done under the auspices of the U.S. Atomic Energy Commission and was supported in part by the U.S. Office of Naval Research.

Table 1. Representative Data of Non-hysteretic Josephson Junction Fundamental Mixers at 36 GHz.

JUNCTION				RF COUPLING		CONVERSION EFFICIENCY				JUNCTION NOISE			
Material	T (K)	R (ohm)	Ω	α^2_{exp}	C_{RF}	η_{exp}	R_{dyn} (ohm)	C_{IF}	$\frac{\eta_{exp}}{\eta_{th}}$	T_N (K)	$(\beta_o)^2_{exp}$	$\frac{(\beta_o)^2_{exp}}{(\beta_o)^2_{th}}$	T_M (K)
Nb	8	28	0.48	0.22	99%	0.34	60	0.88	0.82	80	4.7	1.5	210
Nb	8	5	0.50	0.18	82%	4.05	150	0.69	1.09	1500	6.3	1.9	260
Nb	4.2	19	0.21	0.74	90%	0.47	16	0.74	1.02	76	21.5	4.1	120
Nb	4.2	16	0.36	0.27	75%	0.55	37	0.90	0.98	85	8.8	2.2	140
V	1.4	17	0.33	0.34	81%	0.66	40	0.90	0.92	40	12.1	2.9	55
V	1.4	25	0.30	0.36	75%	1.35	110	0.75	1.14	97	15.7	3.6	54

Remark: $C_{RF} \equiv \alpha^2_{exp}/\alpha^2_{opt}$, RF coupling efficiency

$\eta_{th} = C_{IF}(R_{dyn}/R)\alpha^2_{exp}$, conversion efficiency (gain) predicted by Eq. (20)

$(\beta_o)^2_{exp}/(\beta_o)^2_{th}$, excess noise compared with the calculated results in Fig. 33

Table 2. Calculated properties of various superconducting bolometers with area $A=0.06\ cm^2$, bandwidth $B=1$ Hz, modulation frequency $\omega/2\pi=10$ Hz and sink temperature $T_s=1$ K. We assume perfect blackening, but include a realistic substrate (3 μ thick mica) heat capacity for the film bolometers.

	Bulk Sn	Film Sn	Film Al
Critical Temperature T_c (K)	3.7	3.7	1.2
Thickness t (Å)	10^6	10^2	10^2
Resistance R_o (Ω)	2×10^{-7}	5	3
Transition Width δT (K)	10^{-3}	3×10^{-2}	3×10^{-2}
Heat Capacity (J/K)	2.4×10^{-7}	3×10^{-9}	10^{-10}
Thermal Conductance G(W/K)	5×10^{-9}	2×10^{-9}	4×10^{-10}
Johnson Noise or Thermal Fluctuation Noise $W_J=W_T$ ($W/\sqrt{Hz}$)	2×10^{-15}	10^{-15}	2×10^{-16}
NEP ($W/\sqrt{Hz}$)	3×10^{-15}	2×10^{-15}	3×10^{-16}
$D^* = \sqrt{A}/NEP$ (cm $\sqrt{Hz}$/W)	8×10^{13}	1.4×10^{14}	8×10^{14}
$m = \sqrt{\omega A}/NEP$ (cm Hz/W)	2.4×10^{14}	4.2×10^{14}	2.4×10^{15}

REFERENCES

1. B. D. Josephson, Phys. Lett. 1, 251 (1962).
2. P. W. Anderson and J. M. Rowell, Phys. Rev. Lett. 10, 230 (1963).
3. J. E. Zimmerman, P. Thiene, and J. I. Harding, J. Appl. Phys. 41, 1572 (1970).
4. P. W. Anderson and A. H. Dayem, Phys. Rev. Lett. 13, 195 (1964).
5. A. H. Dayem and J. J. Wiegand, Phys. Rev. 155, 419 (1967).
6. C. C. Grimes, P. L. Richards, and S. Shapiro, Phys. Rev. Lett. 17, 431 (1966).
7. P. L. Richards and S. A. Sterling, Appl. Phys. Lett. 14, 394 (1969).
8. C. C. Grimes and S. Shapiro, Phys. Rev. 169, 397 (1968).
9. A. J. Dahm, A. Denenstein, D. N. Langenberg, W. H. Parker, D. Rogovin, and D. J. Scalapino, Phys. Rev. Lett. 22, 1416 (1969).
10. J. E. Zimmerman and A. H. Silver, Phys. Rev. 141, 367 (1966).
11. R. A. Buhrman, S. F. Strait, and W. W. Webb, Technical Report #1555 The Material Science Center, Cornell University (1971).
12. G. I. Rochlin, Rev. Sci. Instr. 41, 73 (1970).
13. D. E. McCumber, J. Appl. Phys. 39, 3113 (1968).
14. N. F. Pedersen, T. F. Finnegan, and D. N. Langenberg, Phys. Rev. B6, 4151 (1972).
15. F. Auracher, P. L. Richards, and G. I. Rochlin, Phys. Rev. B8, 4182 (1973).
16. H. Kanter and F. L. Vernon, J. Appl. Phys. 43, 3174 (1972).
17. P. Russer, J. Appl. Phys. 43, 2008 (1972).

18. P. E. Gregers-Hansen and M. T. Levinsen, Phys. Rev. Lett. 27, 847 (1971).

19. Y. Song and G. I. Rochlin, Phys. Rev. Lett. 29, 416 (1972).

20. A. Dayem and R. J. Martin, Phys. Rev. Lett. 8, 246 (1962).

21. F. Auracher and T. Van Duzer, J. Appl. Phys. 44, 848 (1973).

22. F. Auracher, Ph. D. thesis, University of California, Berkeley (1973).

23. C. A. Hamilton, J. Appl. Phys. 44, 2371 (1973).

24. Y. Taur, J. H. Claassen, and P. L. Richards, Appl. Phys. Lett. 24, 101 (1974).

25. C. A. Hamilton, Rev. Sci. Instr. 43, 445 (1972).

26. N. Marcuvitz, Waveguide Handbook (Volume 10 of MIT Rad. Lab. Series), Chap. 5. (McGraw-Hill Book Company, Inc. 1951).

27. C. G. Montgomery, Principles of Microwave Circuits (Volume 8 of MIT Rad. Lab. Series), Chap. 6, 7. (McGraw-Hill Book Company, Inc. 1948).

28. M. D. Fiske, Rev. Mod. Phys. 36, 221 (1964).

29. A. H. Dayem and C. C. Grimes, Appl. Phys. Lett. 9, 49 (1966).

30. F. Auracher and T. Van Duzer, Report in the Applied Superconductivity Conference, Annapolis, Md. (1972).

31. J. H. Claassen, private communication.

32. J. M. Manley and H. E. Rowe, Proc. IRE 44, 904 (1956).

33. H. C. Torrey and C. A. Whitmer, Crystal Rectifiers (Volume 15 of MIT Rad. Lab. Series), Chap. 5. (McGraw-Hill Book Company, Inc. 1948).

34. V. Ambegaokar and B. I. Halperin, Phys. Rev. Lett. 22, 1364 (1969).

35. M. J. Stephen, Phys. Rev. Lett. 21, 1629 (1968).

36. M. J. Stephen, Phys. Rev. 182, 531 (1969).

37. M. J. Stephen, Phys. Rev. 186, 393 (1969).

38. H. Kanter and F. L. Vernon, Jr., Appl. Phys. Lett. 16, 115 (1970).

39. H. Kanter and F. L. Vernon, Jr., Phys. Rev. Lett. 25, 588 (1970).

40. E. Riedel, Z. Naturforsch 19a, 1634 (1964).

41. N. R. Werthamer, Phys. Rev. 147, 255 (1966).

42. M. J. Stephen, preprint.

43. A. van der Ziel, Noise: Sources, Characterization, Measurement (Prentice-Hall, Inc., New Jersey 1970).

44. F. L. Vernon, Jr. and R. J. Pedersen, J. Appl. Phys. 39, 2661 (1968).

45. S. Weinreb and A. R. Kerr, J. Solid-State Circuits SC-8, 58 (1973).

46. T. J. Viola, Jr. and R. J. Mattauch, J. Appl. Phys. 44, 2805 (1973).

47. P. Goldsmith, private communication.

48. P. L. Richards, F. Auracher, and T. Van Duzer, Proc. IEEE 61, 36 (1973).

49. L. G. Aslamazov and A. I. Larkin, JETP Letters 9, 87 (1969).

50. W. H. Henkels and W. W. Webb, Phys. Rev. Lett. 26, 1164 (1971).

51. H. Ohta, J. Appl. Phys. 43, 5161 (1972).

52. J. Clarke, Phil. Mag. 13, 115 (1966).

53. T. J. Dean, G. O. Jones, D. H. Martin, P. A. Mawer and C. H. Perry, Physica 24, S151 (1958).

54. T. J. Dean, G. O. Jones, D. H. Martin, P. A. Mawer, and C. H. Perry, Optica Acta 7, 185 (1960).

55. B. Lalevic, J. Appl. Phys. 31, 1234 (1960).

56. D. H. Martin and D. Bloor, Cryogenic 1, 159 (1961).

57. W. Franzen, J. Opt. Soc. Am. 53, 596 (1963).

58. C. L. Bertin and K. Rose, J. Appl. Phys. 39, 2561 (1968).

59. M. K. Maul, M. W. P. Strandberg, and R. L. Kyhl, Phys. Rev. 182, 522 (1969).

60. M. K. Maul and M. W. P. Strandberg, J. Appl. Phys. 40, 2822 (1969).

61. F. J. Low, J. Opt. Soc. Am. 51, 1300 (1961).

62. F. J. Low, Proc. IEEE 54, 477 (1965).

63. H. D. Drew and A. J. Sievers, Appl. Opt. 8, 2067 (1969).

64. P. L. Richards, Far Infrared Properties of Solids, S. Mitra, Ed. (Plenum, New York, 1970).

65. J. E. Zimmerman and A. H. Silver, Phys. Rev. 141, 367 (1966).

66. J. E. Zimmerman and A. H. Silver, Phys. Letters 10, 47 (1964).

67. R. C. Jones, J. Opt. Soc. Am. 43, 1 (1953).

68. F. J. Low and A. R. Hoffman, Appl. Opt. 2, 649 (1963).

69. V. Radhakrishnan and V. L. Newhouse, J. Appl. Phys. 42, 129 (1971).

70. J. Clarke, W. E. Tennant, and D. Woody, J. Appl. Phys. 42, 3859 (1971).

71. R. P. Giffard, R. A. Webb, and J. C. Wheatley, J. Low Temp. Phys. 6, 533 (1972).

72. J. M. W. Milatz and H. A. van der Velden, Physica 10, 369 (1943).

73. S. Ramo and J. R. Whinnery, Fields and Waves in Modern Radio (J. Wiley and sons, Inc. 1944).

TECHNICAL INFORMATION DIVISION
LAWRENCE BERKELEY LABORATORY
UNIVERSITY OF CALIFORNIA
BERKELEY, CALIFORNIA 94720